Propagation, reflection and transmission of plane waves in pre-stressed elastic solids

by

WASIQ HUSSAIN

A thesis submitted to the Faculty of Science, University of Glasgow, for the degree of Doctor of Philosophy.

Department of Mathematics,
University of Glasgow,
October 1999

ProQuest LLC.
789 East Eisenhower Parkway
P.O. Box 1346
Ann Arbor, MI 48106 – 1346

To my parents, brother and his family, sister and her family and especially my father who always encouraged me at every stage.

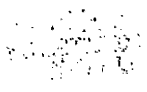

Contents

Preface vi

Summary ix

1 Introduction 1

2 Basic equations of non-linear elasticity 9

2.1 Kinematics 9

2.2 Simple shear 14

2.3 Stress and the equations of motion 15

2.4 Incremental equations of motion 18

2.4.1 Homogeneous plane waves 22

3 Propagation and reflection of plane waves in an incompressible elastic half-space 24

3.1 Mathematical background 25

3.2 Homogeneous plane waves 26

3.2.1 Case A: $2\beta = \alpha + \gamma$ 27

3.2.2 Case B: $\alpha + \gamma \neq 2\beta$ 27

3.3 The slowness curve 28

3.4 Reflection from a plane boundary 30

3.4.1 Case A: $2\beta = \alpha + \gamma$ 32

3.4.2 Case B: $\alpha + \gamma \neq 2\beta$ 33

4 The effect of pre-strain on the reflection and transmission of plane waves at an elastic interface 36

4.1 Basic equations 36

4.2 Plane waves 38

4.2.1 Case A: $2\beta = \alpha + \gamma,\ 2\beta^* = \alpha^* + \gamma^*$ 39

4.2.2 Case B: $2\beta \neq \alpha + \gamma,\ 2\beta^* \neq \alpha^* + \gamma^*$ 41

4.3 Reflection and transmission at the interface 43

4.3.1 Case A: $2\beta = \alpha + \gamma,\ 2\beta^* = \alpha^* + \gamma^*$ 46

4.3.2 Case B: $\beta = \sqrt{\alpha\gamma},\ \beta^* = \sqrt{\alpha^*\gamma^*}$ 50

4.4 Numerical results 56

4.4.1 Case A: $2\beta = \alpha + \gamma,\ 2\beta^* = \alpha^* + \gamma^*$ 56

4.4.2 Case B: $\beta = \sqrt{\alpha\gamma},\ \beta^* = \sqrt{\alpha^*\gamma^*}$ 63

5 Reflection of plane waves at the boundary of an elastic half-space subject to simple shear 69

5.1 Basic equations 70

5.2 Plane waves 72

5.3 Reflection from a plane boundary 81

5.3.1 Case A: $2\beta = \alpha + \gamma$ 83

5.3.2 Case B: $\beta = \sqrt{\alpha\gamma}$ 86

5.4 Numerical results 88

5.4.1 Case A: $2\beta = \alpha + \gamma$ 88

5.4.2 Case B: $\beta = \sqrt{\alpha\gamma}$ 98

6 Reflection and transmission of plane waves at a shear-twin interface 110

6.1 Basic equations 111

6.2 Superimposed incremental motions 113

6.3 Plane waves 114

6.4 Reflection and transmission at the interface 119

6.4.1 Case A: $2\beta = \alpha + \gamma$ 122

6.4.2 Case B: $\beta = \sqrt{\alpha\gamma}$ 125

6.5 Numerical results 129

6.5.1 Case A: $2\beta = \alpha + \gamma$ 129

6.5.2 Case B: $\beta = \sqrt{\alpha\gamma}$ 135

Preface

This thesis is submitted to the University of Glasgow in accordance with the requirements for the degree of Doctor of Philosophy.

I would like to take this opportunity to thank my good natured and devoted supervisor, Professor Ray Ogden, for his advice, encouragement and support throughout the period of my research and also helping me a lot with my financial problems.

My research has been funded by the Department of Mathematics, University of Glasgow scholarship, UK government ORS award, The Charles Wallace Pakistan trust, Student hardship fund of the University of Glasgow and Mountbatten memorial grants to commonwealth students by the Sir Ernest Cassel educational trust. I am extremely grateful to each of these award giving bodies for their financial help.

I am also thankful to Professor David Fearn for every type of help especially arranging funds in collaboration with Professor Ken Brown. In addition I am grateful to Dr. Ken Lindsay and Dr. John Nimmo for their kindness and helping me with Latex.

Finally it would be unfair if I do not mention my mother for her special prayers for my success.

Summary

This thesis is concerned with the effect of pure homogeneous strain, pre-stress and simple shear deformation on the propagation of homogeneous, surface and interfacial waves in elastic materials. Following a review of previous work regarding the propagation of infinitesimal plane waves in a half-space of incompressible material subject to pure homogeneous strain, the analysis is extended to the influence of pure homogeneous strain on the reflection and transmission of plane waves at the boundary between two half-spaces of incompressible isotropic elastic material. In general, the half-spaces consist of different material and are subjected to different deformations.

For a certain class of constitutive laws it is shown that a homogeneous plane (SV) wave incident on the boundary from one half-space gives rise to a reflected wave (with angle of reflection equal to the angle of incidence) together with an interfacial wave in the same half-space, while in the other half-space two possibilities arise depending on the angle of incidence, the material properties and the magnitudes of the deformations in the two half-spaces. *Either* (a) there is a transmitted (homogeneous plane) wave accompanied by an interfacial wave, *or* (b) there are two interfacial waves with equal speeds of propagation but different rates of (spa-

tial) decay away from the boundary.

For a second class of constitutive laws similar behaviour is found for certain combinations of angle of incidence, material properties and deformations, but additional possibilities also arise. In particular, there may be two reflected waves instead of one reflected wave and an interfacial wave, coupled with either possibility (a) or (b) in the second half-space. Equally, there may be two transmitted waves for each of the possible combinations of reflected and interfacial waves in the first half-space.

The effect of finite strain principal axis orientation on the reflection from a plane boundary of infinitesimal plane waves propagating in a half-space of incompressible isotropic elastic material is then examined. Attention is focussed on waves propagating in a principal plane of the deformation corresponding to simple shear.

For a special class of constitutive laws it is shown that an incident plane harmonic wave propagating in the considered plane gives rise to a surface wave in addition to a reflected wave for *every* angle of incidence although its amplitude may vanish at certain discrete angles depending on the state of stress and deformation. Unlike the situation in which the underlying deformation is a pure homogeneous strain, however, the amplitude ratio of the reflected (plane harmonic) wave does not in general have unit magnitude, but its magnitude is independent of the pre-stress. Moreover, the angle of reflection differs from the angle of incidence.

For materials not in this special class, on the other hand, it is shown that two plane harmonic waves may be reflected when the angle of incidence lies within certain ranges of values (which depend on the shear deformation). Outside this range there is in general a single reflected wave, and a surface wave is generated.

This analysis is further used to study the effect of *simple shear* on the reflection

and transmission of plane waves at the boundary between two half-spaces of incompressible elastic material, and, in particular, two half-spaces which form a twin in the sense that equal and opposite simple shears are applied to the two half-spaces.

For a special class of constitutive laws it is shown that an incident plane harmonic (shear) wave propagating in the plane of shear in one half-space gives rise to an interfacial wave in each half-space in addition to a reflected and a transmitted plane wave in the respective half-spaces for *every* angle of incidence, although the amplitudes of the waves may vanish at certain discrete angles (different for each type of wave) depending on the state of deformation.

For a specific material not in this special class, corresponding calculations for a particular value of shear show that the nature of the resulting waves is similar to that for the special class of materials. On the other hand, we note that for values of the shear beyond a certain critical value there are certain ranges of angles of incidence for which, instead, two homogeneous plane (shear) waves are reflected and also two transmitted.

The dependence of the amplitudes of the reflected, transmitted and interfacial waves on the angle of incidence, the states of deformation and the material properties is illustrated graphically.

Chapter 1

Introduction

In this chapter, we shall discuss briefly the main results contained in the thesis and mention some references regarding related work which has been done already.

The study of infinitesimal waves propagating in a pre-stressed finitely-deformed elastic material was initiated in a series of papers by Biot, summarized in his monograph [1], and by Hayes and Rivlin [9], who studied surface waves in a half-space subject to pure homogeneous strain. The latter topic was examined in detail for compressible elastic materials by Chadwick and Jarvis [4]. More recently, Dowaikh and Ogden [7,8], for incompressible and compressible isotropic elastic materials respectively, have investigated surface waves and deformations of a half-space, again for a finite deformation corresponding to pure homogeneous strain. See also [3]. Related work concerned with waves and deformations in pre-stressed plates and in a layered half-space has been provided by Ogden and Roxburgh [14], Roxburgh and Ogden [21] and Ogden and Sotiropoulos [15,16] for both incompressible and compressible materials. Discussion of Flexural waves in incompressible pre-stressed

elastic composites and small amplitude vibrations of pre-stressed laminates is done by Rogerson and Sandiford in [19] and [20] respectively. These papers contain references to work on interfacial waves and deformations.

In each of the papers cited above, the considered finite deformation is a pure homogeneous strain so that the orientation of the principal axes of strain is fixed whatever the magnitude of the strain. The effect of principal axis orientation on waves and deformations in a plate or half-space has been exemplified in the case of simple shear by Connor and Ogden [5,6] and Ogden and Connor [13]. See also the recent paper by Boulanger and Hayes [2].

Relatively little attention has been devoted to the study of wave reflections from a boundary in a finitely-deformed elastic solid. References to the very limited literature on this topic are contained in the recent papers by Ogden and Sotiropoulos [17,18] in which, for incompressible and compressible isotropic elastic materials respectively, the reflection of infinitesimal plane waves from the plane boundary of a half-space subject to pure homogeneous strain was investigated.

In this thesis we have extended the work done in [17] to reflection and transmission at an interface of two half-spaces made up of *incompressible* isotropic elastic material with different material properties. Also we study the effect of finite strain on wave reflections by considering a half-space of incompressible isotropic elastic material subject to simple shear and then extend this problem to reflection and transmission of plane waves at a shear-twin interface.

In Chapter 2, the basic equations of non-linear elasticity are summerized, which will be used in later chapters.

We introduce in Section 2.1 the notations required for the description of the

deformation of an elastic body and incompressible elastic material. In Section 2.2 we note the simple shear deformation and in Section 2.3 we discuss stress and the equations of motion. Constitutive laws for both compressible and incompressible elastic materials are also discussed here. In Section 2.4 we establish the incremental equations of motion for incompressible materials. In Section 2.4.1 we consider time harmonic plane waves, the associated propagation condition and the strong ellipticity condition.

Chapter 3 is concerned with the summary of [17] for the effect of pure homogeneous strain on the propagation of plane waves in the half-space occupied by incompressible isotropic elastic material. In Section 3.1, the shear and normal components of traction are given. In Section 3.2, the discussion is started with the description of plane harmonic waves and the propagation condition. It is assumed that the deformed half-space occupies the region $x_2 \leq 0$ and the waves are propagating at an angle θ to the x_1 axis. Further, it is assumed that the incremental displacement associated with the wave has no component normal to the $(x_1, x_2)-$plane and that the x_1 and x_2 components are independent of x_3. The propagation conditions for two distinct classes of strain-energy functions are derived. The propagation conditions are then used in Section 3.3 to derive the slowness curves. The shape of the slowness curves helps in analysing the nature of plane waves and this analysis is also given in Section 3.3.

In Section 3.4 the reflection of plane harmonic waves is discussed with reference to the transitional angle which can be seen from the pictures of the slowness curves. Reflection of plane waves is then extended to two different classes of strain-energy functions. For a particular class of the strain-energy functions it is shown that

there will be always one reflected wave along with a surface wave for every angle of incidence, but for the materials not in this particular class, two reflected waves may exist for a certain range of angles of incidence. Results are discussed for both classes of strain-energy functions without giving the mathematical detail. For the mathematical detail we refer to [17].

Chapter 4 illustrates the influence of pure homogeneous strain on the reflection and transmission of plane waves at the boundary between two half-spaces of incompressible isotropic elastic material. In general, the half-spaces consist of different material and are subjected to different deformations.

In Section 4.1 some basic equations are recalled. In Section 4.2 the propagation of plane harmonic waves is discussed with reference to the slowness curves for the two materials in respect of two distinct classes of strain-energy functions, exemplified by the neo-Hookean and Varga forms of strain-energy function.

For the case in which the two half-spaces correspond to (different) neo-Hookean materials, the amplitudes of the reflected, transmitted and interfacial waves are calculated explicitly in Section 4.3.1. For each angle of incidence a single reflected wave, with angle of reflection equal to the angle of incidence, is generated when a homogeneous plane (SV) wave is incident on the boundary from one half-space, and it is accompanied by an interfacial wave (whose amplitude may vanish for certain discrete angles of incidence, which depend on the material parameters and the deformations in the two half-spaces). It is shown that under a certain restriction on the material parameters and deformations a transmitted (homogeneous plane SV) wave and an interfacial wave are generated for *all* angles of incidence. When this restriction does not hold there exists a critical angle (measured from parallel

to the interface) above which there is again a transmitted and an interfacial wave but below which there are two interfacial waves (and no transmitted wave). The interfacial waves have the same speed but decay at different rates with distance from the interface.

When the half-spaces consist of (different) Varga materials corresponding results are given in Section 4.3.2. In this case additional possibilities may arise for certain combinations of angle of incidence, material parameters and deformations. Specifically, two reflected (homogeneous plane SV) waves may be generated instead of one reflected and one interfacial wave and (not in general for the same angles of incidence, material parameters and deformations) two transmitted (homogeneous plane SV) waves may emerge. The ranges of values of the material parameters, deformations and angles of incidence for which the various possibilities arise are identified in Section 4.3.2.

The theory in Section 4.3 is illustrated in Section 4.4 using graphical results to show the dependence of the amplitudes of the waves on the angle of incidence for representative values of the material and deformation parameters.

Chapter 5 is concerned with the effect of finite strain principal axis orientation on the reflection from a plane boundary of infinitesimal plane waves propagating in a half-space of incompressible isotropic elastic material. The work included in this chapter has been published (for details see [10]). Attention is focussed on waves propagating in a principal plane of the deformation corresponding to simple shear. The direction of shear is taken to be parallel to the half-space boundary and the plane of shear normal to that boundary, and we consider waves with direction of propagation and polarization in the latter plane.

In Section 5.1 the basic equations are modified when there is an orientation between the Cartesian axes and the principal axes of strain. In Section 5.2 the propagation of plane harmonic waves is discussed with reference to the relevant (in-plane) *slowness curves* in respect of two distinct classes of strain-energy function. For a special class of strain-energy functions it is noted that, for *any* angle of incidence (within the considered plane), an incident SV wave yields a single reflected wave (with angle of reflection in general *different* from the angle of incidence). This is generally accompanied by a surface wave, whose amplitude may vanish at particular angles of incidence. For materials *not* in this special class similar behaviour is observed except that for angles of incidence within certain ranges (which depend on the magnitude of the shear strain and the material properties) there may exist *two* reflected SV waves and no surface wave.

In Section 5.3 the reflection coefficients (or amplitude in the case of a surface wave) for the two categories of strain-energy functions are calculated. An important difference from previous work that emerges is that the magnitude of the reflection coefficient, in circumstances when a surface wave is generated, is not in general equal to unity. However, for the special class of strain-energy functions the magnitude of the reflection coefficient is found to be independent of the pre-stress whereas the amplitude of the surface wave depends on the pre-stress. This is also the case for the second class of strain-energy functions when a surface wave is generated, but not when there are two reflected waves.

For both classes of strain-energy functions, as the angle of incidence approaches normal incidence the amplitude of the surface wave reduces to zero. It also vanishes at certain other points which depend on the amount of shear and pre-stress. The

symmetry about normal incidence which is apparent in the classical theory or in the case of pure homogeneous strain is removed by the simple shear deformation.

Graphical results are provided in Section 5.4 in order to illustrate the dependence of the reflection coefficients and surface wave amplitudes on the angle of incidence, the amount of shear and the pre-stress with reference to the stability of the underlying configuration. The detailed features of the results are described for the two classes of strain-energy functions in Sections 5.4.1 and 5.4.2.

Chapter 6 is concerned with the effect of *simple shear* on the reflection and transmission of plane waves at the boundary between two half-spaces of incompressible elastic material, and, in particular, two half-spaces which form a *twin* in the sense that equal and opposite simple shears are applied to the two half-spaces. This configuration simulates the finite deformation associated with a crystal twin, but we note that the shear component of traction is discontinuous across the boundary. The work included in this chapter has been accepted for publication [11].

The required equations and notations are summarized in Section 6.1 and Section 6.2. In Section 6.3 the propagation of plane harmonic waves is discussed with reference to the *slowness curves* appropriate for the two half-spaces for two distinct classes of strain-energy functions.

For the two categories of strain-energy functions the amplitudes of the reflected, transmitted and interfacial waves are calculated in Section 6.4 when a given homogeneous plane (shear) wave is incident on the boundary. For each class of strain-energy functions, the amplitude of the reflected wave reduces to zero as the angle of incidence approaches normal incidence. In contrast to the classical theory and to the case of pure homogeneous strain, there is no symmetry about normal incidence, as

discussed in Chapter 5 for the problem of reflection from the boundary of a half-space.

Graphical results are provided in Section 6.5 to show the dependence of the amplitudes of the reflected, transmitted and interfacial waves on the angle of incidence and the magnitude of the shear for the materials in the special class of strain-energy functions. For materials not in the special class, results are calculated for one illustrative value of the shear, for which there is again only one reflected and one transmitted plane wave along with two interfacial waves. We note, however, that for sufficiently large values of the shear two reflected plane waves and two transmitted plane waves may be generated for certain ranges of values of the angle of incidence. This is analogous to the situation discussed in [10] for reflection from a simply sheared half-space in isolation. The graphical results are discussed in detail for the two classes of strain-energy functions in Section 6.5.1 and 6.5.2.

Chapter 2

Basic equations of non-linear elasticity

In this chapter we summarize the basic equations of non-linear elasticity that will be used frequently in the subsequent Chapters. Detailed derivations are not given because these can be found in standard texts. We refer to [12], for example, for full details.

2.1 Kinematics

We consider a continuous body and identify its undeformed (reference) configuration by $\mathcal{B}_0$ say. After time t let the deformed (current) configuration of the body be denoted by $\mathcal{B}$.

Let $\mathbf{X}$ and $\mathbf{x}$ respectively be the position vectors of a typical material particle in the configurations $\mathcal{B}_0$ and $\mathcal{B}$ of the material. Since $\mathcal{B}_0$ and $\mathcal{B}$ are configurations of

the body there exists a bijection mapping

$$\chi : \mathcal{B}_0 \to \mathcal{B}$$

such that

$$\mathbf{x} = \chi(\mathbf{X}, t), \ \mathbf{X} \in \mathcal{B}_0,$$

$$\mathbf{X} = \chi^{-1}(\mathbf{x}, t), \ \mathbf{x} \in \mathcal{B}. \tag{2.1}$$

The mapping χ is called the *deformation* of the body from $\mathcal{B}_0$ to $\mathcal{B}$. It is assumed that $\chi(\mathbf{X}, t)$ is twice-continuously differentiable with respect to position and time.

The *deformation gradient* $\mathbf{A}$ is defined by

$$\mathbf{A} = \mathrm{Grad}\chi(\mathbf{X}, t), \tag{2.2}$$

where the gradient operator Grad is with respect to $\mathcal{B}_0$. With reference to Cartesian basis vectors $\{\mathbf{E}_\alpha\}$ and $\{\mathbf{e}_i\}$ associated with $\mathcal{B}_0$ and $\mathcal{B}$ respectively, we may write

$$\mathbf{A} = A_{i\alpha}\mathbf{e}_i \otimes \mathbf{E}_\alpha, \quad A_{i\alpha} = \frac{\partial x_i}{\partial X_\alpha}, \tag{2.3}$$

with summation over i and α from 1 to 3 implied in the first equation in (2.3), where $A_{i\alpha}$ are the Cartesian components of $\mathbf{A}$. It follows from (2.3) that

$$\dot{\mathbf{A}} = \mathbf{L}\mathbf{A}, \tag{2.4}$$

where the superposed dot denotes $\partial/\partial t$ at fixed $\mathbf{X}$ and

$$\mathbf{L} = \mathrm{grad}\mathbf{v} \tag{2.5}$$

is the *velocity gradient tensor*. Here the gradient operator grad is with respect to $\mathcal{B}$.

We assume that $\det \mathbf{A} \neq 0$ so that $\mathbf{A}$ has an inverse $\mathbf{A}^{-1}$ given by

$$\mathbf{A}^{-1} = \mathrm{grad}\,\mathbf{X}. \tag{2.6}$$

The components of $\mathbf{A}^{-1}$ are given by

$$(\mathbf{A}^{-1})_{ij} = \frac{\partial X_i}{\partial x_j} \tag{2.7}$$

with $x_i = \chi_i(\mathbf{X}, t)$. From (2.3) we have

$$A_{ij} dX_j = \frac{\partial x_i}{\partial X_j} dX_j = dx_i, \tag{2.8}$$

i.e.

$$d\mathbf{x} = \mathbf{A} d\mathbf{X}, \tag{2.9}$$

which has inverse

$$d\mathbf{X} = \mathbf{A}^{-1} d\mathbf{x}. \tag{2.10}$$

Equation (2.9) describes how infinitesimal *line elements* $d\mathbf{X}$ of material at $\mathbf{X}$ transform under the deformation into $d\mathbf{x}$ at $\mathbf{x}$. If $\mathbf{A}$ is independent of $\mathbf{X}$ then the deformation is said to be *homogeneous*.

We take $\mathbf{A}$ to be non-singular ($\det\mathbf{A} \neq 0$) by noting that

$$\mathbf{A} d\mathbf{X} \neq \mathbf{0} \quad \text{if} \quad d\mathbf{X} \neq \mathbf{0}.$$

Next, consider a parallelepiped in $\mathcal{B}_0$ formed by line elements $d\mathbf{X}$, $d\mathbf{X}'$, $d\mathbf{X}''$ at $\mathbf{X}$. Its volume dV is given by

$$dV = d\mathbf{X}.(d\mathbf{X}' \times d\mathbf{X}'') = |d\mathbf{X} \;\; d\mathbf{X}' \;\; d\mathbf{X}''|. \tag{2.11}$$

The corresponding volume dv in $\mathcal{B}$ is

$$dv = d\mathbf{x}.(d\mathbf{x}' \times d\mathbf{x}'') = |d\mathbf{x} \;\; d\mathbf{x}' \;\; d\mathbf{x}''|$$

$$= |\mathbf{A}d\mathbf{X} \;\; \mathbf{A}d\mathbf{X}' \;\; \mathbf{A}d\mathbf{X}''| = |\mathbf{A}||d\mathbf{X} \;\; d\mathbf{X}' \;\; d\mathbf{X}''|, \tag{2.12}$$

i.e.

$$dv = JdV, \quad \text{where} \quad J = \det\mathbf{A}. \tag{2.13}$$

For the volume to be positive, we must have

$$J = \det\mathbf{A} > 0. \tag{2.14}$$

From (2.13) we see that J is a measure of the change in volume under the deformation. If the deformation is such that there is no change in volume then the deformation is said to be *isochoric,* and then

$$J = \det\mathbf{A} = 1. \tag{2.15}$$

A material for which (2.15) holds for all deformations is called an *incompressible material.*

From the polar decomposition theorem we have

$$\mathbf{A} = \mathbf{RU} = \mathbf{VR}, \tag{2.16}$$

where $\mathbf{R}$ is proper orthogonal and $\mathbf{U}$ and $\mathbf{V}$ are positive definite and symmetric, and are called the *right* and *left stretch tensors* respectively.

The spectral decompositions of $\mathbf{U}$ and $\mathbf{V}$ have the forms

$$\mathbf{U} = \sum_{i=1}^{3} \lambda_i \mathbf{u}^{(i)} \otimes \mathbf{u}^{(i)},$$

$$\mathbf{V} = \sum_{i=1}^{3} \lambda_i \mathbf{v}^{(i)} \otimes \mathbf{v}^{(i)}, \tag{2.17}$$

where $\lambda_i\,(>0)\,(i = 1, 2, 3)$ are the *principal stretches* of the deformation, and $\mathbf{u}^{(i)}$ and $\mathbf{v}^{(i)}$, $(i = 1, 2, 3)$ respectively are the unit eigenvectors of $\mathbf{U}$ and $\mathbf{V}$. We shall refer to $\mathbf{u}^{(i)}$ and $\mathbf{v}^{(i)}$ as the *Lagrangian* and *Eulerian* principal axes respectively.

We note that

$$\mathbf{v}^{(i)} = \mathbf{R}\mathbf{u}^{(i)}, \qquad i \in \{1, 2, 3\}, \tag{2.18}$$

follows from (2.16) and (2.17).

The *right* and *left* Cauchy-Green deformation tensors are given by

$$\mathbf{A}^T\mathbf{A} = \mathbf{U}^2 = \sum_{i=1}^{3} \lambda_i^2 \mathbf{u}^{(i)} \otimes \mathbf{u}^{(i)},$$

and

$$\mathbf{A}\mathbf{A}^T = \mathbf{V}^2 = \sum_{i=1}^{3} \lambda_i^2 \mathbf{v}^{(i)} \otimes \mathbf{v}^{(i)}, \tag{2.19}$$

respectively, where $\mathbf{A}^T$ denotes the transpose.

We further see from (2.16) and (2.17) that

$$\det\mathbf{A} = \det\mathbf{V} = \lambda_1\lambda_2\lambda_3, \tag{2.20}$$

and hence from (2.15) and (2.20) for an isochoric deformation we have the *incompressibility condition* given by

$$\lambda_1\lambda_2\lambda_3 = 1. \tag{2.21}$$

We are concerned with a plane strain problem in the plane normal to the basis vectors $\mathbf{E}_3$ and $\mathbf{e}_3$, and, for convenience, we take $\mathbf{e}_1 = \mathbf{E}_1$, $\mathbf{e}_2 = \mathbf{E}_2$, $\mathbf{e}_3 = \mathbf{E}_3$. We consider a homogeneous deformation and associate Cartesian coordinates (x_1', x_2', x_3') with the Eulerian principal axes. Since the considered deformation is confined to the (1,2)-plane, we have $\mathbf{v}^{(3)} = \mathbf{e}_3$, and we may set $\lambda_3 = 1$, so that (2.21) reduces to

$$\lambda_1\lambda_2 = 1. \tag{2.22}$$

2.2 Simple shear

Let ϕ denote the orientation of the Eulerian axes $(\mathbf{v}^{(1)}, \mathbf{v}^{(2)})$ relative to $(\mathbf{e}_1, \mathbf{e}_2)$ so that the coordinates (x_1', x_2') are related to (x_1, x_2) by

$$x_1' = x_1 \cos\phi + x_2 \sin\phi, \quad x_2' = -x_1 \sin\phi + x_2 \cos\phi. \tag{2.23}$$

From (2.3) and (2.19) we may then deduce that

$$A_{11}^2 + A_{12}^2 = \lambda_1^2 \cos^2\phi + \lambda_2^2 \sin^2\phi,$$

$$A_{11}A_{21} + A_{12}A_{22} = (\lambda_1^2 - \lambda_2^2) \sin\phi \cos\phi,$$

$$A_{21}^2 + A_{22}^2 = \lambda_1^2 \sin^2\phi + \lambda_2^2 \cos^2\phi, \tag{2.24}$$

with $A_{\alpha 3} = A_{3\alpha} = \delta_{\alpha 3}$, $\alpha = 1, 2, 3$, $\delta_{\alpha 3}$ being the Kronecker delta.

From (2.24) an expression for the orientation ϕ in terms of the components $A_{i\alpha}$ is obtainable in the form

$$\tan 2\phi = 2(A_{11}A_{21} + A_{12}A_{22})/(A_{11}^2 + A_{12}^2 - A_{21}^2 - A_{22}^2). \tag{2.25}$$

When the considered deformation is *simple shear* we have $A_{11} = 1$, $A_{12} = \epsilon$, $A_{21} = 0$, $A_{22} = 1$, where

$$\epsilon = \lambda - \lambda^{-1} \tag{2.26}$$

and, in accordance with (2.22), we have set

$$\lambda_1 = \lambda, \quad \lambda_2 = \lambda^{-1}. \tag{2.27}$$

Equation (2.25) reduces to

$$\tan 2\phi = 2/\epsilon \tag{2.28}$$

with $0 < \phi \leq \pi/4$ for $\epsilon \geq 0$ and $\pi/4 \leq \phi < \pi/2$ for $\epsilon \leq 0$. From (2.28) we deduce that

$$\cos\phi = \lambda/\sqrt{\lambda^2+1}, \quad \sin\phi = 1/\sqrt{\lambda^2+1}. \tag{2.29}$$

2.3 Stress and the equations of motion

For an *isotropic elastic material*, the *Cauchy stress tensor* denoted by $\boldsymbol{\sigma}$ is *coaxial* with $\mathbf{V}$, i.e. with the Eulerian principal axes, we may write

$$\boldsymbol{\sigma} = \sum_{i=1}^{3} \sigma_i \mathbf{v}^{(i)} \otimes \mathbf{v}^{(i)}, \tag{2.30}$$

where σ_i, $i \in \{1,2,3\}$ are the principal Cauchy stresses.

We now introduce the *elastic stored energy* $W(\mathbf{A})$ per unit volume in the reference configuration such that

$$\frac{\partial}{\partial t} W(\mathbf{A}) = J\mathrm{tr}(\boldsymbol{\sigma}\boldsymbol{L}), \tag{2.31}$$

where $\boldsymbol{L}$ is given by (2.5) and trace $\mathrm{tr}(\boldsymbol{\sigma}\boldsymbol{L})$ is given by

$$\mathrm{tr}(\boldsymbol{\sigma}\boldsymbol{L}) = \sigma_{ij} L_{ji} \tag{2.32}$$

and σ_{ij} are the components of $\boldsymbol{\sigma}$ with respect to basis vectors $\{\mathbf{e_i}\}$.

Since W depends only on $\mathbf{A}$, we have

$$\frac{\partial}{\partial t} W(\mathbf{A}) = \frac{\partial W}{\partial A_{ij}} \frac{\partial A_{ij}}{\partial t} \equiv \mathrm{tr}(\frac{\partial W}{\partial \mathbf{A}} \dot{\mathbf{A}}), \tag{2.33}$$

where $\partial W/\partial \mathbf{A}$ is the second-order tensor with components defined by

$$(\frac{\partial W}{\partial \mathbf{A}})_{ji} = \frac{\partial W}{\partial A_{ij}}. \tag{2.34}$$

From (2.4) we obtain

$$\frac{\partial W}{\partial t} = \mathrm{tr}(\frac{\partial W}{\partial \mathbf{A}}\mathbf{L}\mathbf{A}) = \mathrm{tr}(\mathbf{A}\frac{\partial W}{\partial \mathbf{A}}\mathbf{L}) \tag{2.35}$$

and comparison of this with (2.31) shows that

$$J\boldsymbol{\sigma} = \mathbf{A}\frac{\partial W}{\partial \mathbf{A}}, \tag{2.36}$$

which provides a formula for $\boldsymbol{\sigma}$ in terms of $W(\mathbf{A})$.

It is convenient to introduce the notation

$$\mathbf{S} = \frac{\partial W}{\partial \mathbf{A}}, \quad S_{ji} = \frac{\partial W}{\partial A_{ij}}, \tag{2.37}$$

where $\mathbf{S}$ is called *nominal stress tensor.*

For an isotropic elastic material with strain-energy function W per unit volume, W depends symmetrically on $\lambda_1, \lambda_2, \lambda_3$. It follows that

$$\dot{W} = \sum_{i=1}^{3} \frac{\partial W}{\partial \lambda_i}\dot{\lambda}_i. \tag{2.38}$$

But, from (2.31),

$$\dot{W} = J\mathrm{tr}(\boldsymbol{\sigma}\boldsymbol{D}), \tag{2.39}$$

where $\boldsymbol{D}$ is the symmetric part of $\boldsymbol{L}$. Now, referred to the principal axes of $\boldsymbol{\sigma}$ (2.39) can be expressed as

$$\dot{W} = J\sum_{i=1}^{3} \sigma_i D_{ii}, \tag{2.40}$$

where D_{ii} are the normal components of $\boldsymbol{D}$ referred to those axes.

Note that $\boldsymbol{D}$ may be written in the form

$$\mathbf{D} = \tfrac{1}{2}\mathbf{R}(\dot{\mathbf{U}}\mathbf{U}^{-1} + \mathbf{U}^{-1}\dot{\mathbf{U}})\mathbf{R}^T, \tag{2.41}$$

and from (2.17) it follows that

$$\dot{\mathbf{U}} = \sum_{i=1}^{3} \dot{\lambda}_i \mathbf{u}^{(i)} \otimes \mathbf{u}^{(i)} + \lambda_i \mathbf{u}^{(i)} \otimes \dot{\mathbf{u}}^{(i)} + \lambda_i \dot{\mathbf{u}}^{(i)} \otimes \mathbf{u}^{(i)}. \tag{2.42}$$

Using (2.18), (2.41) and (2.42) we calculate the components

$$D_{ii} \equiv \mathbf{v}^{(i)}.(\mathbf{D}\mathbf{v}^{(i)}) = \lambda_i^{-1}\dot{\lambda}_i \tag{2.43}$$

noting that, since $\mathbf{u}^{(i)}$ is a unit vector, $\mathbf{u}^{(i)}.\dot{\mathbf{u}}^{(i)} = 0$.

From (2.38), (2.40) and (2.43) we get

$$\dot{W} = \sum_{i=1}^{3} \frac{\partial W}{\partial \lambda_i}\dot{\lambda}_i = \sum_{i=1}^{3} J\sigma_i \lambda_i^{-1}\dot{\lambda}_i, \tag{2.44}$$

and hence

$$\sigma_i = J^{-1}\lambda_i \frac{\partial W}{\partial \lambda_i} \qquad i \in \{1,2,3\}. \tag{2.45}$$

If the considered material is incompressible then (2.21) holds, so we replace W by $W - p(\lambda_1\lambda_2\lambda_3 - 1)$, where p is a Lagrange multiplier. Thus, (2.45) becomes

$$\sigma_i = \lambda_i \frac{\partial W}{\partial \lambda_i} - p, \qquad i \in \{1,2,3\}. \tag{2.46}$$

Equation (2.46) gives the expressions for the principal stresses σ_i in terms of the derivatives of W with respect to the stretches.

For an incompressible material (2.37) will be replaced by

$$\mathbf{S} = \frac{\partial W}{\partial \mathbf{A}} - p\mathbf{A}^{-1}. \tag{2.47}$$

In terms of nominal stress the equation of motion has the form

$$\mathrm{Div}\,\mathbf{S} = \rho_0 \ddot{\boldsymbol{\chi}}, \tag{2.48}$$

where ρ_0 is the reference density, Div denotes the divergence operator with respect to $\mathbf{X}$, a superposed dot indicates the material time derivative and body forces are assumed to be absent. Furthermore, if we take the reference configuration to coincide with the current configuration at any stage of the deformation then (2.48) is replaced by

$$\operatorname{div} \boldsymbol{\sigma} = \rho \ddot{\boldsymbol{\chi}}, \tag{2.49}$$

where, again div denotes the divergence operator with respect to $\mathbf{x}$, $\boldsymbol{\sigma}$ is Cauchy stress tensor and ρ is the current mass density of the material.

2.4 Incremental equations of motion

We now consider an incremental motion superimposed on the finite deformation with a small time dependent displacement $\mathbf{u}$ defined by

$$\mathbf{u} = \delta\mathbf{x} = \delta\boldsymbol{\chi}(\mathbf{X}, t) = \boldsymbol{\chi}'(\mathbf{X}, t) - \boldsymbol{\chi}(\mathbf{X}, t), \tag{2.50}$$

where $\boldsymbol{\chi}$ and $\boldsymbol{\chi}'$ are two deformations of the elastic body.

Corresponding to an incremental deformation, the deformation gradient $\mathbf{A}$ changes to

$$\delta\mathbf{A} = \operatorname{Grad} \delta\boldsymbol{\chi}(\mathbf{X}, t), \tag{2.51}$$

where Grad again refers to $\mathcal{B}_0$. If the current configuration is now chosen as the reference configuration then the right-hand side of (2.51) becomes $(\delta\mathbf{A}_0)\mathbf{A}$, where $\delta\mathbf{A}_0$ is the value of $\delta\mathbf{A}$ in this configuration. We obtain

$$\delta\mathbf{A} = (\delta\mathbf{A}_0)\mathbf{A}, \tag{2.52}$$

where

$$\delta \mathbf{A}_0 = \operatorname{grad} \mathbf{u} \tag{2.53}$$

and the grad operator refers to $\mathcal{B}$.

The nominal stress increment for (2.37) can be written as

$$\delta \mathbf{S} = \boldsymbol{\mathcal{A}}(\delta \mathbf{A}), \tag{2.54}$$

where

$$\boldsymbol{\mathcal{A}} = \frac{\partial^2 W}{\partial \mathbf{A} \partial \mathbf{A}}, \tag{2.55}$$

or, in components,

$$(\delta \mathbf{S})_{ji} = \mathcal{A}_{jilk}(\delta \mathbf{A})_{kl} \tag{2.56}$$

with

$$\mathcal{A}_{jilk} = \frac{\partial^2 W}{\partial A_{ij} \partial A_{kl}}. \tag{2.57}$$

We refer to $\boldsymbol{\mathcal{A}}$ as the tensor of *first-order elastic moduli.*

If the reference configuration is now updated to coincide with the current configuration $\mathcal{B}$, (2.54) gives the increment in nominal stress $\boldsymbol{\Sigma}$ (say) by

$$\boldsymbol{\Sigma} = \boldsymbol{\mathcal{A}}_0(\delta \mathbf{A}_0), \tag{2.58}$$

where the subscript zero indicates evaluation in $\mathcal{B}$. The tensor $\boldsymbol{\mathcal{A}}_0$ is called the tensor of first-order *instantaneous* elastic moduli and its components are related to the components of $\boldsymbol{\mathcal{A}}$ by

$$\mathcal{A}_{0ijkl} = J^{-1} A_{i\alpha} A_{k\beta} \mathcal{A}_{\alpha j \beta l}. \tag{2.59}$$

From (2.54), (2.58) and (2.59) we obtain

$$\boldsymbol{\Sigma} = J^{-1}\mathbf{A}\,\delta\mathbf{S}, \tag{2.60}$$

In the case of (2.47), (2.58) will be replaced by

$$\boldsymbol{\Sigma} = \boldsymbol{\mathcal{A}}_0(\delta\mathbf{A}_0) + p(\delta\mathbf{A}_0) - \pi\mathbf{I}, \tag{2.61}$$

where π is the time-dependent increment in p and $\mathbf{I}$ is the identity tensor. Equation (2.53) is accompanied by the incompressibility constraint

$$\mathrm{tr}(\delta\mathbf{A}_0) = \mathrm{tr}(\mathrm{grad}\,\delta\boldsymbol{\chi}) = \mathrm{tr}(\mathrm{grad}\,\mathbf{u}) = 0. \tag{2.62}$$

where $\mathbf{u}$ is given by (2.50).

The component form of (2.61) is given by

$$\Sigma_{ji} = \mathcal{A}_{0jilk}u_{k,l} + pu_{j,i} - \pi\delta_{ij}, \tag{2.63}$$

where δ_{ij} is the Kronecker delta and $,i$ signifies differentiation with respect to x_i.

The corresponding incremental form of the incompressibility condition is

$$u_{i,i} = 0. \tag{2.64}$$

The components of $\boldsymbol{\mathcal{A}}_0$ referred to Eulerian principal axes of the underlying deformation are derived in [12], for example; we refer to this book for full details. In terms of the derivatives of the strain-energy function, the non-zero components are given by

$$\mathcal{A}_{0iijj} = \lambda_i\lambda_j W_{ij},$$

$$\mathcal{A}_{0ijij} = \frac{(\lambda_i W_i - \lambda_j W_j)\lambda_i^2}{(\lambda_i^2 - \lambda_j^2)} \qquad i \neq j, \quad \lambda_i \neq \lambda_j,$$

$$\mathcal{A}_{0ijij} = \frac{1}{2}(\mathcal{A}_{0iiii} - \mathcal{A}_{0iijj} + \lambda_i W_i) \qquad i \neq j, \quad \lambda_i = \lambda_j,$$

$$\mathcal{A}_{0ijji} = \mathcal{A}_{0jiij} = \mathcal{A}_{0ijij} - \lambda_i W_i \qquad i \neq j, \tag{2.65}$$

where $W_i = \partial W/\partial \lambda_i$, $W_{ij} = \partial^2 W/\partial \lambda_i \partial \lambda_j$ and there is no summation over repeated indices.

From (2.48) the equation governing the *incremental* motion is given by

$$\mathrm{Div}(\delta \mathbf{S}) = \rho_0 \, \ddot{\mathbf{u}}, \tag{2.66}$$

where Div is with respect to $\mathcal{B}_0$ and when the reference configuration is updated to coincide with the current configuration then (2.66) is replaced by

$$\mathrm{div}\, \mathbf{\Sigma} = \rho \, \ddot{\mathbf{u}}, \tag{2.67}$$

where div is with respect to $\mathcal{B}$.

The component form of (2.67) is given by

$$\Sigma_{ji,j} = \rho \, \ddot{u}_i. \tag{2.68}$$

On substitution of (2.63) into (2.68) and using (2.64), we obtain (for the case when $\mathcal{A}_0$ is constant)

$$\mathcal{A}_{0jilk} u_{k,jl} - \pi_{,i} = \rho \ddot{u}_i, \tag{2.69}$$

where $\mathbf{u}$ is an incremental displacement superimposed on the finite deformation.

When specialized to a plane motion in the (1,2)-plane equation (2.69) applies for $i = 1, 2$ and summations run over indices in $\{1, 2\}$ and then the components of $\mathbf{u}$ referred to $\{\mathbf{e}_i\}$ will be given by

$$u_1 = u_1(x_1, x_2, t), \quad u_2 = u_2(x_1, x_2, t), \quad u_3 = 0, \tag{2.70}$$

where t is time.

Elimination of π between these two equations (given by (2.69)) by cross differentiation and subtraction yields

$$\mathcal{A}_{0j1lk}u_{k,2jl} - \mathcal{A}_{0j2lk}u_{k,1jl} = \rho\,(\ddot{u}_{1,2} - \ddot{u}_{2,1}). \tag{2.71}$$

From the incompressibility condition (2.64) in terms of these components we deduce the existence of a function $\psi = \psi(x_1, x_2, t)$ such that

$$u_1 = \psi_{,2}, \quad u_2 = -\psi_{,1}, \tag{2.72}$$

wherein the indicated differentiations are with respect to (x_1, x_2).

When referred to the Eulerian principal axes equation (2.71), after substitution from (2.72), yields an equation for ψ, namely

$$\alpha\psi_{,1111} + 2\beta\psi_{,1122} + \gamma\psi_{,2222} = \rho(\ddot{\psi}_{,11} + \ddot{\psi}_{,22}), \tag{2.73}$$

as in [5,6], where the material parameters α, β, γ are defined by

$$\alpha = \mathcal{A}_{01212}, \quad \gamma = \mathcal{A}_{02121}, \quad 2\beta = \mathcal{A}_{01111} + \mathcal{A}_{02222} - 2\mathcal{A}_{01122} - 2\mathcal{A}_{01221}. \tag{2.74}$$

2.4.1 Homogeneous plane waves

We consider time harmonic plane waves in the (1,2)-plane of the form

$$\psi = A\exp[ik(x_1\cos\theta + x_2\sin\theta - ct)], \tag{2.75}$$

where A is a constant, c and k are the wave speed and the wave number respectively and both are taken to be positive. Also, θ is the angle that the direction of propagation of the wave $(\cos\theta, \sin\theta)$ in the (x_1, x_2)-plane makes with the x_1 direction.

Substitution of (2.75) into (2.73) yields

$$\alpha \cos^4 \theta + 2\beta \sin^2 \theta \cos^2 \theta + \gamma \sin^4 \theta = \rho c^2. \tag{2.76}$$

Equation (2.76) is the *propagation condition*, which identifies the wave speed associated with any given angle θ.

For $\rho c^2 > 0$, it is necessary and sufficient that α, β and γ satisfy the *strong ellipticity* inequalities

$$\alpha > 0,\ \gamma > 0,\ \beta > -\sqrt{\alpha\gamma}. \tag{2.77}$$

For detailed discussion of strong ellipticity see [12].

Chapter 3

Propagation and reflection of plane waves in an incompressible elastic half-space

In this chapter we shall give a summary of the paper by Ogden and Sotiropoulos [17]. This paper describes the effect of pre-stress and finite strain on the propagation of homogeneous plane waves and their reflection at the boundary of an *incompressible* isotropic elastic half-space.

For a special class of materials an incident SV wave gives rise to a surface wave in addition to a reflected SV wave for every angle of incidence but the surface wave amplitude vanishes at some discrete angles.

For materials not in this class an incident SV wave gives rise to *two* reflected SV waves in general when the angle of incidence is less than a critical value. The angle of reflection of one wave is equal to the angle of incidence, but for the second wave the angle of reflection may be greater than, equal to or less than the angle of

incidence. When the angle of incidence is *greater* than the critical angle the situation is similar to that for the special class of materials. This is opposite to the situation in the (compressible) classical theory when a surface wave is generated for angles of incidence *less* than a critical value.

3.1 Mathematical background

A homogeneous pure strain is considered with principal stretches λ_1, λ_2, λ_3 associated with Cartesian axes corresponding to coordinates x_1, x_2, x_3 in the current configuration of the incompressible elastic material so that (2.21) holds.

As discussed in Chapter 2 the associated principal Cauchy stresses σ_1, σ_2, σ_3 are given by (2.46). The components of the displacement vector $\mathbf{u}$ for the superimposed incremental motion in the (x_1, x_2)-plane are given by (2.70).

The incompressibility condition in terms of the scalar function $\psi(x_1, x_2, t)$ is (2.72).

The equation of motion (after eliminating the incremental hydrostatic pressure) is given by (2.73). It is assumed that the strong ellipticity condition (2.77) holds as well.

From (2.63) in terms of ψ the shear component of the incremental nominal stress $\mathbf{\Sigma}$ on a plane $x_2 =$ constant can be written as

$$\Sigma_{21} \equiv \gamma(\psi_{,22} - \psi_{,11}) + \sigma_2\psi_{,11}. \tag{3.1}$$

While from (2.63) the normal component of $\mathbf{\Sigma}$ is written as

$$\Sigma_{22} = \mathcal{A}_{02211}u_{1,1} + (\mathcal{A}_{02222} + p)u_{2,2} - \pi. \tag{3.2}$$

We can eliminate the incremental hydrostatic stress π from (3.2) by differentiating it with respect to x_1 to get

$$\Sigma_{22,1} = \mathcal{A}_{02211}u_{1,11} + (\mathcal{A}_{02222} + p)u_{2,21} - \pi_{,1} \tag{3.3}$$

and then using

$$\pi_{,1} = \mathcal{A}_{01111}u_{1,11} + (\mathcal{A}_{01122} + \mathcal{A}_{02112})u_{2,21} + \mathcal{A}_{02121}u_{1,22} - \rho\ddot{u}_1, \tag{3.4}$$

which can be obtained from (2.69).

By substituting (3.4) into (3.3) and using (2.46), (2.65), (2.72) and (2.74) we can write (3.3) in terms of ψ as

$$-\Sigma_{22,1} \equiv (2\beta + \gamma - \sigma_2)\psi_{,112} + \gamma\psi_{,222} - \rho\ddot{\psi}_{,2}. \tag{3.5}$$

3.2 Homogeneous plane waves

Time harmonic waves are considered in the form (2.75). The propagation condition (2.76) can be rewritten as

$$\rho c^2 = (\alpha + \gamma - 2\beta)\cos^4\theta + 2(\beta - \gamma)\cos^2\theta + \gamma. \tag{3.6}$$

From the strong ellipticity condition (2.77) it can be seen that $\rho c^2 > 0$ for any propagation angle θ in (3.6). On the other hand, if the wave speed is given along with the material properties α, β and γ then provided strong ellipticity holds the possible wave propagation directions can be calculated from (3.6).

Two cases with different relative values of α, β, γ will be discussed now.

3.2.1 Case A: $2\beta = \alpha + \gamma$

First we see a special case when $\alpha = \beta = \gamma$ so that from (2.74) and (2.65) we get $\lambda_1 = \lambda_2$. The wave speed for this case will be independent of the direction of propagation and is given by $\rho c^2 = \gamma$.

For $\alpha \neq \gamma$ the propagation condition gives the direction of propagation as

$$\cos^2\theta = \frac{\gamma - \rho c^2}{\gamma - \alpha}, \tag{3.7}$$

which gives real θ if

$$\text{either} \quad \alpha \leq \rho c^2 \leq \gamma \quad \text{or} \quad \gamma \leq \rho c^2 \leq \alpha. \tag{3.8}$$

For $\rho c^2 = \alpha$ the wave will propagate along the x_1-axis and for $\rho c^2 = \gamma$ the wave will propagate along the x_2-axis.

Subject to (3.8), for a given wave speed, two different directions of propagation in the plane of deformation are then possible. Let these be denoted by $(\cos\theta, \pm\sin\theta)$. Then (3.7) may be written as

$$\tan^2\theta = \frac{\rho c^2 - \alpha}{\gamma - \rho c^2}. \tag{3.9}$$

3.2.2 Case B: $\alpha + \gamma \neq 2\beta$

For a given wave speed the solutions of (3.6) are given by

$$\cos^2\theta = \frac{\gamma - \beta \pm [\beta^2 - \alpha\gamma + \rho c^2(\alpha + \gamma - 2\beta)]^{1/2}}{\alpha + \gamma - 2\beta}, \tag{3.10}$$

which gives real solutions for θ if either

$$\beta \leq \min\{\alpha, \gamma\}, \qquad \frac{\alpha\gamma - \beta^2}{\alpha + \gamma - 2\beta} \leq \rho c^2 \leq \min\{\alpha, \gamma\} \tag{3.11}$$

or

$$\beta \geq \max\{\alpha, \gamma\}, \qquad \max\{\alpha, \gamma\} \leq \rho c^2 \leq \frac{\alpha\gamma - \beta^2}{\alpha + \gamma - 2\beta}. \tag{3.12}$$

For the transitional case in which there are repeated solutions we have

$$\cos^2\theta = \frac{\gamma - \beta}{\alpha + \gamma - 2\beta}, \qquad \rho c^2 = \frac{\alpha\gamma - \beta^2}{\alpha + \gamma - 2\beta}. \tag{3.13}$$

Therefore, there are four possible directions of wave propagation for a given wave speed but for the transitional case they reduce to two.

3.3 The slowness curve

Slowness curves play an important role in the interpretation of the nature of the resulting waves. *Slowness curves* are defined in terms of the *slowness vector,* with components (s_1, s_2) given by $(s_1, s_2) = (\cos\theta, \sin\theta)/c$. The equation of the slowness curve can be obtained from the propagation condition (3.6) and is given by

$$\overline{\alpha} s_1^4 + 2\overline{\beta} s_1^2 s_2^2 + \overline{\gamma} s_2^4 - s_1^2 - s_2^2 = 0, \tag{3.14}$$

where $\overline{\alpha}$, $\overline{\beta}$, $\overline{\gamma}$ are defined by

$$(\overline{\alpha}, \overline{\beta}, \overline{\gamma}) = (\alpha, \beta, \gamma)/\rho. \tag{3.15}$$

For Case A in Section 3.2.1 the slowness curve (3.14) becomes an ellipse, given by

$$\overline{\alpha} s_1^2 + \overline{\gamma} s_2^2 = 1. \tag{3.16}$$

For the material constants satisfying the inequality $2\beta < \alpha$, provided the strong ellipticity condition holds, the slowness curve for Case B has the shape shown in Fig. 3.1.

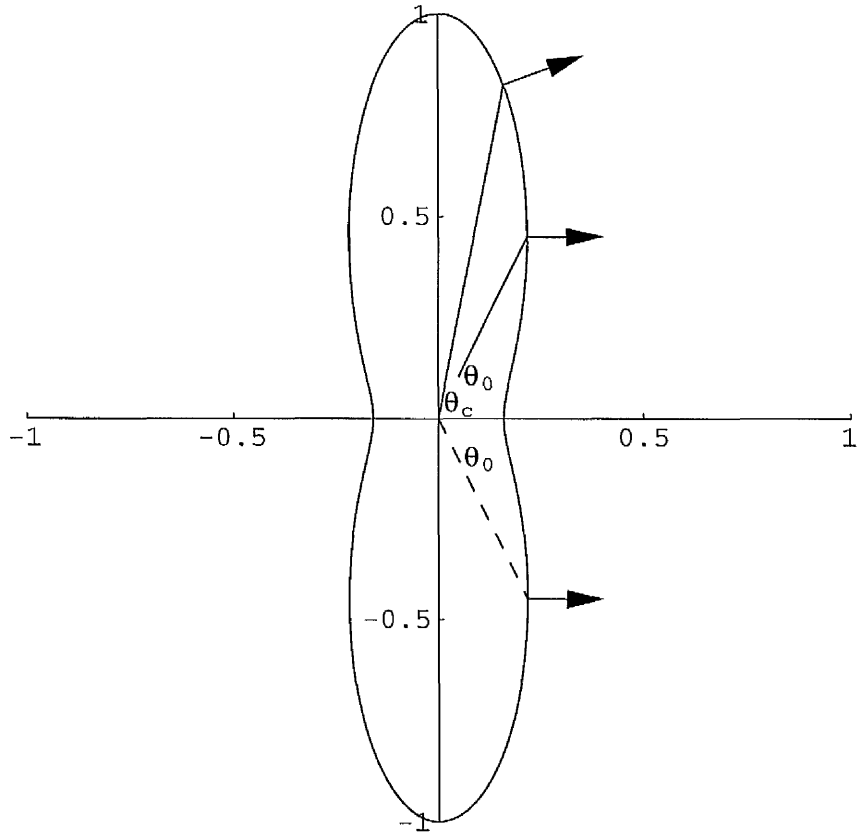

Figure 3.1: Shape of the slowness curve for a material with $2\beta < \alpha$ showing the transitional angle θ_0 and the critical angle θ_c. The arrows normal to the curve indicate the directions of the time-averaged energy flux.

The transitional angle θ_0 and the critical angle θ_c shown in the Fig. 3.1 will be discussed explicitly in Section 3.4.2.

3.4 Reflection from a plane boundary

Here an incident wave of the form (2.75) is considered (in $x_2 < 0$) on the boundary $x_2 = 0$ with wave speed c and the unit direction vector $(\cos\theta, \sin\theta)$. Two separate waves may be reflected at the boundary $x_2 = 0$, one wave having the same speed c as the incident wave with unit direction vector $(\cos\theta, -\sin\theta)$. The second reflected wave is assumed to have speed c' and unit direction vector $(\cos\theta', \sin\theta')$. The wave numbers of the two waves satisfy

$$kc = k'c'. \tag{3.17}$$

From (3.1) and (3.5), the boundary conditions corresponding to zero incremental traction take the form

$$\gamma(\psi_{,22} - \psi_{,11}) + \sigma_2\psi_{,11} = 0 \qquad \text{on} \quad x_2 = 0 \tag{3.18}$$

$$(2\beta + \gamma - \sigma_2)\psi_{,112} + \gamma\psi_{,222} - \rho\ddot{\psi}_{,2} = 0 \qquad \text{on} \quad x_2 = 0. \tag{3.19}$$

The solution comprising the incident wave and the two reflected waves has the form

$$\psi = A\exp[ik(x_1\cos\theta + x_2\sin\theta - ct)] + AR\exp[ik(x_1\cos\theta - x_2\sin\theta - ct)]$$

$$+AR'\exp[ik'(x_1\cos\theta' + x_2\sin\theta' - c't)], \tag{3.20}$$

where R and R' are the reflection coefficients. The solution (3.20) holds when the angle of incidence is less than the critical angle θ_c, as shown in the Fig. 3.1, where θ_c is defined formally in Section 3.4.2. For the time-averaged energy flux (which is normal to the slowness curve) to be directed towards the boundary $x_2 = 0$ (for an incident wave from $x_2 < 0$) and for the time-averaged energy flux to be directed

away from the boundary (for a reflected wave), in (3.20) we must have θ to satisfy (a)

$$\theta_0 \leq \theta \leq \theta_c \quad \text{in} \quad (\cos\theta, \sin\theta)$$

and θ' to satisfy

$$0 \leq \theta' \leq \theta_0 \quad \text{in} \quad (\cos\theta', \sin\theta')$$

or (b)

$$0 \leq \theta \leq \theta_0 \quad \text{in} \quad (\cos\theta, -\sin\theta)$$

and

$$\theta_0 \leq \theta' \leq \theta_c \quad \text{in} \quad (\cos\theta', -\sin\theta'),$$

where θ_0 is the transitional angle as shown in Fig. 3.1. At $\theta = \theta_0$ the energy flux is parallel to the boundary. In the first quadrant, as the angle of incidence θ decreases from θ_c the wave directions are given by (a) above, but after the transitional angle θ_0 they are given by (b), where the wave normal is directed away from the boundary but the energy flux associated with the incident wave is directed towards the boundary.

For $\theta > \theta_c$ the second reflected wave is replaced by a surface wave, with ψ given by

$$\psi = A\exp[ik(x_1\cos\theta + x_2\sin\theta - ct)] + AR\exp[ik(x_1\cos\theta - x_2\sin\theta - ct)]$$

$$+AR'\exp[ik'(x_1 - imx_2 - c't)], \tag{3.21}$$

so that the latter term decays as $x_2 \to -\infty$ provided $\mathrm{Re}(m) > 0$. From (3.20) and (3.21) respectively, by applying the boundary conditions, Snell's law takes the forms

$$k\cos\theta = k'\cos\theta', \qquad k\cos\theta = k'. \tag{3.22}$$

Now we shall discuss two different cases of strain-energy functions regarding the wave propagation without going into the mathematical detail. For the mathematical details we refer to [17].

3.4.1 Case A: $2\beta = \alpha + \gamma$

In this case we refer to the slowness curve (3.16), which is an ellipse, so that the wave solution is (3.21). For the third term in (3.21) to decay we deduce from the equation of motion that $m = 1$. It is calculated in [17] that $|R| = 1$ for all angles of incidence. Now the following three possibilities arise in which $R' = 0$.

Case A(i): $R' = 0,\ R \neq \pm 1$. In this case $\theta = 0$ and the wave speed is given by $\rho c^2 = \alpha$, which corresponds to a plane wave propagating parallel to the boundary.

Case A(ii): $R' = 0,\ R = -1$. In this case θ is arbitrary and the wave speed is given by

$$\rho c^2 = \alpha \cos^2\theta + \gamma \sin^2\theta. \tag{3.23}$$

Case A(iii): $R' = 0,\ R = 1$.

In this case the wave speed is given by

$$\rho c^2 = \frac{\gamma(\alpha + \gamma - \sigma_2)}{2\gamma - \sigma_2}. \tag{3.24}$$

The three cases described above show that a surface wave is generated for all the angles of incidence except when the stress is given by $\sigma_2 = 2\gamma$ or, for $\sigma_2 < \gamma$ and the angle θ given by

$$\cos^2\theta = 1/(2 - \overline{\sigma}_2), \tag{3.25}$$

where $\overline{\sigma}_2 = \sigma_2/\gamma$.

Graphical results show that for $\overline{\sigma}_2 = 0$ $|R'|$ has the same nature as in linear (compressible) theory. For large values of stress the behaviour differs from the classical theory.

The neo-Hookean strain-energy function

$$W = \frac{1}{2}\mu(\lambda_1^2 + \lambda_2^2 + \lambda_3^2 - 3), \tag{3.26}$$

where $\mu\,(>0)$ is the shear modulus and the Mooney-Rivlin strain-energy function

$$W = \frac{1}{2}\mu_1(\lambda_1^2 + \lambda_2^2 + \lambda_3^2 - 3) + \frac{1}{2}\mu_2(\lambda_1^{-2} + \lambda_2^{-2} + \lambda_3^{-2} - 3), \tag{3.27}$$

where the constants μ_1 and μ_2 satisfy $\mu_1+\mu_2 = \mu$ satisfy the condition $2\beta = \alpha+\gamma$. In [17] it was deduced that for values of θ and c obtained from experimental data, information about the deformation, stress and material properties can be obtained.

3.4.2 Case B: $\alpha + \gamma \neq 2\beta$

When the solution (3.20) holds we have a propagation condition similar to (3.6). It is given by

$$(\alpha + \gamma - 2\beta)\cos^4\theta' + 2(\beta - \gamma)\cos^2\theta' + \gamma - \rho c'^2 = 0. \tag{3.28}$$

From (3.28), (3.20) and (3.6) we get $\cos^2\theta' = \cos^2\theta$ or

$$\cos^2\theta\cos^2\theta' = \gamma/(\alpha + \gamma - 2\beta) \tag{3.29}$$

and we have the transitional angle θ_0 when these possibilities occur together, given by

$$\cos^4\theta_0 = \gamma/(\alpha + \gamma - 2\beta). \tag{3.30}$$

Hence, for (3.20) to be applicable, an incident wave gives rise to two reflected waves in general, one with angle of incidence equal to the angle of reflection and the other with the angle of reflection given by (3.29).

Necessary and sufficient conditions for θ' in (3.29) to be real are

$$\alpha > 2\beta \tag{3.31}$$

and

$$\tan^2\theta \leq \frac{\alpha - 2\beta}{\gamma} \equiv \tan^2\theta_c, \tag{3.32}$$

where θ_c is the critical angle which corresponds to $\theta' = 0$, the grazing angle of reflection.

The reflection coefficients R, R' are determined from the boundary conditions. Similarly to Case A, three distinct situations can arise for which R' vanishes. These correspond to $R \neq \pm 1$, $R = 1$ or $R = -1$. It is shown in [17] that the behaviour in this case differs from that in Case A. Further it is proved that $R = 0$ and $R' = -1$ whenever the angle of incidence is equal to the transitional angle θ_0 except for the value of $\overline{\sigma}_2$ given by

$$\cos^2\theta = \frac{\gamma}{2\gamma - \sigma_2} = \frac{2\gamma - \sigma_2}{\alpha + \gamma - 2\beta}, \tag{3.33}$$

which arises when $R \neq \pm 1$. Further, there may be some combinations of the angle of incidence and pre-stress where $R = 0$ so we have a single reflected wave with angle of incidence not equal to the angle of reflection.

For grazing incidence we have $\cos\theta = 1$, $\rho c^2 = \alpha$ and $c' = c\cos\theta'$.

For grazing reflection we have $\cos\theta' = 1$, $\rho c'^2 = \alpha$, $\rho c^2 = \alpha\cos^2\theta$ and

$$\cos^2\theta = \gamma/(\alpha + \gamma - 2\beta). \tag{3.34}$$

For angles greater than that given by (3.34) or for situations in which the conditions (3.31) and (3.32) are not satisfied the grazing homogeneous plane wave is replaced by an inhomogeneous plane wave with amplitude decaying exponentially away from the boundary. This gives rise to the case of one reflected wave so that the solution (3.21) is applicable. As in Case A it is shown in [17] that $|R| = 1$.

Graphical results are given in [17] for a particular form of strain-energy function, namely the Varga strain-energy function, defined by

$$W = 2\mu(\lambda_1 + \lambda_2 + \lambda_3 - 3), \tag{3.35}$$

for which the inequality $\alpha > 2\beta$ can hold. The analysis was done for $\lambda_3 = 1$, and values of $\overline{\sigma}_2$ were selected according to stability conditions which give the upper and lower bounds for the values of pre-stress.

Chapter 4

The effect of pre-strain on the reflection and transmission of plane waves at an elastic interface

In this chapter we extend the discussion of the influence of pure homogeneous strain on the reflection and transmission of plane waves at the boundary between two half-spaces of incompressible isotropic elastic material. In general, the half-spaces consist of different material and are subjected to different deformations. In particular, we recover certain results obtained in [17].

4.1 Basic equations

We consider an incompressible isotropic elastic material subject to pure homogeneous strain. Let λ_1, λ_2, λ_3 denote the principal stretches of the deformation.

Then, the incompressibility condition is expressed as

$$\lambda_1\lambda_2\lambda_3 = 1. \tag{4.1}$$

Since the material is isotropic, the principal Cauchy stresses are given by (2.46).

We consider incremental motions in the $(x_1,\ x_2)$-plane superimposed on the pure homogeneous deformation with displacement vector $\mathbf{u}$ having components given by (2.70). The incremental incompressibility condition $\mathrm{div}\mathbf{u} = 0$ is then used to deduce that (2.72) holds.

Components of the incremental nominal stress tensor referred to the homogeneously deformed configuration are given by (2.63).

Since for the pure homogeneous strain, the Cartesian axes and the Eulerian principal axes are coincident, the components of the fourth-order tensor $\boldsymbol{\mathcal{A}}_0$ of instantaneous elastic moduli in terms of the derivatives of the strain-energy function W from (2.65) are given by

$$\mathcal{A}_{0iijj} = \lambda_i\lambda_j W_{ij},$$

$$\mathcal{A}_{0ijij} = \frac{(\lambda_i W_i - \lambda_j W_j)\lambda_i^2}{(\lambda_i^2 - \lambda_j^2)} \qquad i \neq j, \quad \lambda_i \neq \lambda_j,$$

$$\mathcal{A}_{0ijij} = \frac{1}{2}(\mathcal{A}_{0iiii} - \mathcal{A}_{0iijj} + \lambda_i W_i) \qquad i \neq j, \quad \lambda_i = \lambda_j,$$

$$\mathcal{A}_{0ijji} = \mathcal{A}_{0jiij} = \mathcal{A}_{0ijij} - \lambda_i W_i \qquad i \neq j, \tag{4.2}$$

The components $\mathcal{A}_{0jilk}$ of $\boldsymbol{\mathcal{A}}_0$ are constants since the deformation is homogeneous.

The equation of motion in terms of the scalar function ψ is given by (2.73).

The shear and normal components of the incremental nominal traction Σ_{21}, Σ_{22} on a plane $x_2 =$ constant are expressible in terms of ψ through (3.1) and (3.5).

4.2 Plane waves

We consider time harmonic plane waves of the form given by (2.75). The propagation condition is given by (2.76) and the strong ellipticity condition (2.77) also holds.

Similarly, for an *inhomogeneous* plane wave of the form

$$\psi = A\exp[ik'(x_1 - imx_2 - c't)] \tag{4.3}$$

equation (2.73) gives

$$\alpha - 2\beta m^2 + \gamma m^4 = \rho(1 - m^2)c'^2 \tag{4.4}$$

in place of (2.76). For a given wavespeed c', equation (4.4) determines m. The wave decays exponentially as $x_2 \to -\infty\,(+\infty)$ provided m has positive (negative) real part.

We now consider two half-spaces of *different* incompressible isotropic elastic materials. The half-spaces are subjected to pure homogeneous strain and then bonded along their common (plane) boundary in such a way that the principal directions of strain are aligned, one direction being normal to the interface. In rectangular Cartesian coordinates we take the interface to be $x_2 = 0$.

Let $\lambda_1, \lambda_2, \lambda_3$ be the stretches associated with the half-space $x_2 < 0$, with strain-energy function W, and material constants α, β, γ defined by (2.74) with (4.2). Similarly, let $\lambda_1^*, \lambda_2^*, \lambda_3^*, W^*, \alpha^*, \beta^*, \gamma^*$ be the corresponding quantities for the half-space $x_2 > 0$.

For simplicity, we take the deformation to correspond to plane strain with $\lambda_3 = \lambda_3^* = 1$ so that, with reference to the incompressibility condition (4.1), we introduce

the notations λ, λ^* such that

$$\lambda_1 = \lambda_2^{-1} = \lambda, \quad \lambda_1^* = \lambda_2^{*-1} = \lambda^*. \tag{4.5}$$

We now consider two distinct cases of the strain-energy functions for which $2\beta = \alpha + \gamma$ and $2\beta \neq \alpha + \gamma$ for $x_2 < 0$ and similarly for $x_2 > 0$.

4.2.1 Case A: $2\beta = \alpha + \gamma$, $2\beta^* = \alpha^* + \gamma^*$

For this case (2.76) reduces to (3.7) which can be rewritten as

$$\alpha \cos^2\theta + \gamma \sin^2\theta = \rho c^2 \tag{4.6}$$

and (4.4) reduces to

$$(1 - m^2)\{\alpha - \gamma m^2 - \rho c'^2\} = 0. \tag{4.7}$$

As defined in Section 3.3 the *slowness vector* (s_1, s_2) is given by

$$(s_1, s_2) = (\cos\theta, \sin\theta)/c, \tag{4.8}$$

equation (4.6) becomes the *slowness curve*

$$\lambda^4 s_1^2 + s_2^2 = \overline{\rho}, \qquad x_2 < 0, \tag{4.9}$$

in (s_1, s_2) space, where $\overline{\rho}$ is defined by

$$\overline{\rho} = \rho/\gamma \tag{4.10}$$

and $\alpha/\gamma = \lambda^4$ follows from (4.2) and (2.74).

By using the dimensionless notation $(\overline{s}_1, \overline{s}_2)$ defined by

$$(\overline{s}_1, \overline{s}_2) \equiv (s_1, s_2)/\sqrt{\overline{\rho}}, \tag{4.11}$$

we can write (4.9) as

$$\lambda^4 \overline{s}_1^2 + \overline{s}_2^2 = 1, \quad x_2 < 0. \tag{4.12}$$

Let θ^*, c^*, ρ^* be the counterparts of θ, c, ρ for $x_2 > 0$ and let $\overline{\rho}^*$ be defined by

$$\overline{\rho}^* = \rho^*/\gamma^* \tag{4.13}$$

analogously to (4.10). We use the same non-dimensionalization (4.11) for the slowness vector

$$(s_1^*, s_2^*) = (\cos\theta^*, \sin\theta^*)/c^* \tag{4.14}$$

and define

$$(\overline{s}_1^*, \overline{s}_2^*) \equiv (s_1^*, s_2^*)/\sqrt{\overline{\rho}}. \tag{4.15}$$

The counterpart of (4.12) in $x_2 > 0$ is then written

$$\lambda^{*4} \overline{s}_1^{*2} + \overline{s}_2^{*2} = D, \quad x_2 > 0, \tag{4.16}$$

where D is defined by

$$D = \overline{\rho}^*/\overline{\rho} = \frac{\rho^*\gamma}{\rho\gamma^*}. \tag{4.17}$$

Under the considered plane strain conditions the specialization $2\beta = \alpha + \gamma$ forces the strain-energy function to have the neo-Hookean form given by (3.26), and similarly for $x_2 > 0$ with shear modulus μ^*.

In this case the value of D can be obtained from (4.2), (2.74) and (3.26) and is given by

$$D = d\{\lambda^*/\lambda\}^2, \tag{4.18}$$

where

$$d = \mu\rho^*/\rho\mu^*. \tag{4.19}$$

Slowness curves for $x_2 < 0$ and $x_2 > 0$ are shown superimposed in Fig. 4.1 for illustrative values of d, λ, λ^*.

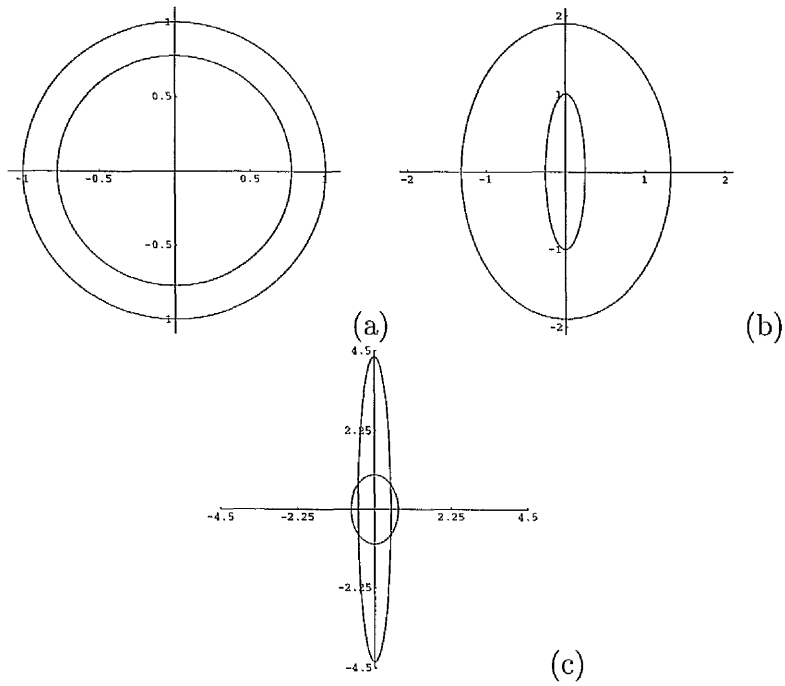

Figure 4.1: Slowness curves for $2\beta = \alpha+\gamma$, $2\beta^* = \alpha^*+\gamma^*$: (a) $\{d, \lambda, \lambda^*\} = \{0.6, 1, 1\}$, inner (outer) circle for $x_2 > 0\,(< 0)$; (b) $\{d, \lambda, \lambda^*\} = \{10, 2, 1.2\}$, inner (outer) ellipse for $x_2 < 0\,(> 0)$; (c) $\{d, \lambda, \lambda^*\} = \{3, 1.2, 3\}$, short (tall) ellipse for $x_2 < 0\,(> 0)$.

4.2.2 Case B: $2\beta \neq \alpha + \gamma,\ 2\beta^* \neq \alpha^* + \gamma^*$

In this case we take the strain-energy functions to satisfy $\beta = \sqrt{\alpha\gamma}$ (as was used by Ogden and Sotiropoulos [17] and by Hussain and Ogden [10]) and similarly $\beta^* = \sqrt{\alpha^*\gamma^*}$. Then (2.76) takes the form

$$\{\sqrt{\alpha}\cos^2\theta + \sqrt{\gamma}\sin^2\theta\}^2 = \rho c^2 \tag{4.20}$$

and (4.4) becomes

$$(\sqrt{\alpha} - \sqrt{\gamma}m^2)^2 = \rho(1 - m^2)c'^2. \tag{4.21}$$

The slowness curve corresponding to (4.20) is given by

$$\{\lambda^2 \overline{s}_1{}^2 + \overline{s}_2{}^2\}^2 = \overline{s}_1{}^2 + \overline{s}_2{}^2, \; x_2 < 0 \tag{4.22}$$

in dimensionless form with the notation (4.11) and $\overline{\rho}$ defined by (4.10). Similarly, for $x_2 > 0$ the corresponding equation of the slowness curve is

$$\{\lambda^{*2}\overline{s}_1^{*2} + \overline{s}_2^{*2}\}^2 = \{\overline{s}_1^{*2} + \overline{s}_2^{*2}\}D, \tag{4.23}$$

where D is again defined by (4.17).

Similarly to Case A we illustrate the slowness curves for particular values of λ and λ^* in the two half-spaces in Fig. 4.2. For this we use the Varga strain-energy function, which is given by (3.35) for $x_2 < 0$, with μ as the shear modulus. Similarly for $x_2 > 0$ with shear modulus μ^*.

In this case the value of D from (2.74), (3.35) and (4.2) is given by

$$D = \frac{d\lambda^*\{\lambda^{*2} + 1\}}{\lambda\{\lambda^2 + 1\}} \tag{4.24}$$

where d is defined by (4.19). Note that D in (4.24) differs from that given by (4.18) for Case A.

Slowness curves for $x_2 < 0$ and $x_2 > 0$ are shown superimposed in Fig. 4.2 for illustrative values of d, λ, λ^*.

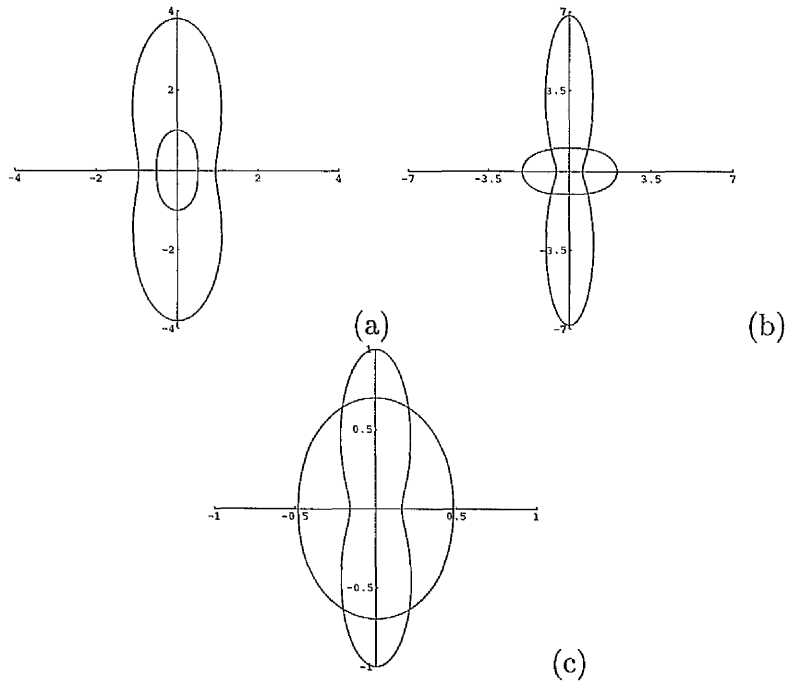

Figure 4.2: Slowness curves for $\beta = \sqrt{\alpha\gamma},\ \beta^* = \sqrt{\alpha^*\gamma^*}$: (a) $\{d, \lambda, \lambda^*\} = \{6, 1.4, 2\}$, inner (outer) curve for $x_2 < 0\,(> 0)$; (b) $\{d, \lambda, \lambda^*\} = \{1.1, 0.7, 3.5\}$, short (tall) curve for $x_2 < 0\,(> 0)$; (c) $\{d, \lambda, \lambda^*\} = \{3, 2.5, 1.2\}$, narrow (wide) curve for $x_2 < 0\,(> 0)$.

4.3 Reflection and transmission at the interface

For continuity of traction at the interface associated with the underlying deformation we require $\sigma_2^* = \sigma_2$.

The boundary conditions corresponding to continuous displacement are

$$u_1 = u_1^*,\ u_2 = u_2^* \quad \text{on} \quad x_2 = 0,$$

where u_1, u_2 are the displacement components in $x_2 < 0$ and u_1^*, u_2^* are those in $x_2 > 0$.

From (2.72) the above boundary conditions can be written in terms of the scalar

functions ψ and ψ^* as

$$\psi_{,1} = \psi^*_{,1}, \ \psi_{,2} = \psi^*_{,2}, \tag{4.25}$$

on $x_2 = 0$, where ψ^* is the counterpart of ψ for $x_2 > 0$.

The boundary conditions for continuous incremental traction on the interface are

$$\Sigma_{21} = \Sigma^*_{21}, \ \Sigma_{22} = \Sigma^*_{22} \quad \text{on} \quad x_2 = 0 \tag{4.26}$$

where Σ_{21}, Σ_{22} are the traction components in $x_2 < 0$ and $\Sigma^*_{21}, \Sigma^*_{22}$ those in $x_2 > 0$.

From (3.1), (3.5) and the continuity condition $\sigma^*_2 = \sigma_2$, the boundary conditions (4.26) take the forms

$$\gamma(\psi_{,22} - \psi_{,11}) = \gamma^*(\psi^*_{,22} - \psi^*_{,11}), \tag{4.27}$$

$$(2\beta + \gamma)\psi_{,112} + \gamma\psi_{,222} - \rho\ddot{\psi}_{,2} = (2\beta^* + \gamma^*)\psi^*_{,112} + \gamma^*\psi^*_{,222} - \rho^*\ddot{\psi}^*_{,2}, \tag{4.28}$$

in term of ψ and ψ^*, where, in order to obtain (4.28), the second equation in (4.26) has been replaced by

$$\Sigma_{22,1} = \Sigma^*_{22,1}$$

and use made of (3.5) and its counterpart for $x_2 > 0$.

Notice that the boundary conditions (4.27) and (4.28) are independent of the pre-stress σ_2.

We now consider a wave incident on the boundary $x_2 = 0$ from the region $x_2 < 0$ with direction of propagation $(\cos\theta, \sin\theta)$ in the (x_1, x_2)-plane and speed

c. We write the solution comprising the incident wave, a reflected wave (with angle of reflection equal to the angle of incidence) and an interfacial wave in $x_2 < 0$ as

$$\psi = A\exp[ik(x_1\cos\theta + x_2\sin\theta - ct)] + AR\exp[ik(x_1\cos\theta - x_2\sin\theta - ct)]$$

$$+AR'\exp[ik'(x_1 - imx_2 - c't)], \tag{4.29}$$

where R is the reflection coefficient and R' measures the amplitude of the interfacial wave. The notation k', m, c' is as used in (4.3).

In the half-space $x_2 > 0$ we write the solution comprising a transmitted and an interfacial wave in the form

$$\psi^* = AR^*\exp[ik^*(x_1\cos\theta^* + x_2\sin\theta^* - c^*t)] + AR^{*'}\exp[ik^{*'}(x_1 + im^*x_2 - c^{*'}t)], \tag{4.30}$$

where R^* is the transmission coefficient and $R^{*'}$ is the analogue of R' for $x_2 > 0$. The transmitted wave has direction of propagation $(\cos\theta^*, \sin\theta^*)$, wave number k^* and speed c^*, while $k^{*'}$, m^*, $c^{*'}$ are the counterparts of k', m, c'. Note that the interfacial wave decays as $x_2 \to \infty$ provided m^* has positive real part.

According to Snell's law we have

$$k\cos\theta = k' = k^*\cos\theta^* = k^{*'}$$

or, equivalently,

$$\cos\theta/c = 1/c' = \cos\theta^*/c^* = 1/c^{*'}. \tag{4.31}$$

Equation (4.31) states, in particular, that the first components of the slowness vectors for each homogeneous plane wave interacting at the boundary $x_2 = 0$ are equal, in this case $s_1 = s_1^*$.

Thus, by reference to the slowness curves for $x_2 < 0$ and $x_2 > 0$, superimposed as exemplified in Fig. 4.1 and Fig. 4.2, the range of angles of incidence for which a transmitted wave exists can be identified. In Fig. 4.1(b), for example, since the inner curve corresponds to $x_2 < 0$ there is, for every angle of incidence (i.e. for every s_1 associated with the curve) a point on the outer curve for which $s_1^* = s_1$, and hence a transmitted wave. In Fig. 4.1(a), on the other hand, there are values of s_1 on the slowness curve for $x_2 < 0$ for which there are no corresponding values of s_1^* on the $x_2 > 0$ slowness curve and therefore there is a range of angles of incidence for which no transmitted wave exists. This will be discussed further in Section 4.3.1. The situation in respect of Fig. 4.2 is less straightforward and will be examined in Section 4.3.2.

We now consider again Case A and Case B separately.

4.3.1 Case A: $2\beta = \alpha + \gamma,\ 2\beta^* = \alpha^* + \gamma^*$

In this case we see from equation (4.7) that $m = \pm 1$, which yields an interfacial wave in the half-space $x_2 < 0$ if $m = 1$. The zeros of the other quadratic factor in (4.7) correspond to $m = i \tan\theta$ and $m = -i \tan\theta$, which are associated respectively with the incident and reflected waves in $x_2 < 0$.

Thus, in $x_2 < 0$, the solution (4.29) applies with $m = 1$.

In $x_2 > 0$ the solution consisting of a transmitted wave and an interfacial wave may be written as (4.30) subject to (4.31) and with $m^* = 1$. The latter arises from the first factor in the analogue of equation (4.7) for $x_2 > 0$, i.e. $m^{*2} - 1$. The second

factor gives

$$m^{*2} = (\alpha^* - \rho^* c^{*\prime 2})/\gamma^*. \tag{4.32}$$

Using the fact that $\alpha^*/\gamma^* = \lambda^{*4}$ together with (4.31) and the definitions (4.10), (4.13) and (4.17) equation (4.32) may be written as

$$m^{*2} = \lambda^{*4} - D(\lambda^4 + \tan^2\theta). \tag{4.33}$$

If this corresponds to a transmitted wave then we must have

$$m^* = -i \tan\theta^*, \tag{4.34}$$

where θ^* is a real angle given by

$$\tan^2\theta^* = D(\lambda^4 + \tan^2\theta) - \lambda^{*4}. \tag{4.35}$$

If $D\lambda^4 > \lambda^{*4}$, i.e., from (4.18), $d\lambda^2 > \lambda^{*2}$, then the right-hand side of (4.35) is positive for all θ. Thus, if $D\lambda^4 > \lambda^{*4}$, a transmitted wave exists for all angles of incidence.

If, on the other hand, $D\lambda^4 < \lambda^{*4}$, then there is a *critical angle*, $\theta = \theta_c$ say, such that

$$\tan^2\theta_c = \lambda^{*4}/D - \lambda^4. \tag{4.36}$$

In this case there is a transmitted wave for angles of incidence such that $\theta_c < \theta \leq \pi/2$, but for $0 \leq \theta < \theta_c$ there is no transmitted wave and there are two interfacial waves, one with $m^* = 1$ and the other with m^* given as the positive solution of (4.33). These interfacial waves have the same speed c' given by (4.31) but in general the value of m^* given by (4.33) is not equal to unity. In fact, it can be unity (for some θ such that $0 \leq \theta < \theta_c$) only if $\lambda^{*4} - D\lambda^4 \geq 1$.

At the transitional angle $\theta = \theta_c$ we have $\theta^* = 0$ and the first term in (4.30) corresponds to a plane shear (body) wave propagating parallel to the boundary in $x_2 > 0$.

Using (4.29) and (4.30) appropriately specialized in the boundary conditions (4.25), we obtain

$$1 + R + R' = R^* + R^{*'}, \tag{4.37}$$

$$t(1 - R) - iR' = t^* R^* + iR^{*'}, \tag{4.38}$$

where we have introduced the notation

$$t = \tan\theta, \qquad t^* = \tan\theta^*,$$

the latter applying when the right-hand side of (4.35) is positive. When (4.35) is replaced by (4.33), t^* is replaced by im^* in (4.38) with m^* real and positive.

With the specialization $2\beta = \alpha + \gamma$, $2\beta^* = \alpha^* + \gamma^*$, the boundary condition (4.28) becomes

$$(\lambda^4 + 2)\psi_{,112} + \psi_{,222} - \overline{\rho}\ddot{\psi}_{,2} = \delta[(\lambda^{*4} + 2)\psi^*_{,112} + \psi^*_{,222} - \overline{\rho}^*\ddot{\psi}^*_{,2}], \tag{4.39}$$

where

$$\delta = \gamma^*/\gamma = \mu^*\lambda^2/\mu\lambda^{*2}. \tag{4.40}$$

Again with appropriate specialization, substitution of ψ and ψ^* from (4.29) and (4.30) into (4.27) and (4.39) leads to

$$(1 - t^2)(1 + R) + 2R' = \delta[(1 - t^{*2})R^* + 2R^{*'}], \tag{4.41}$$

$$2it(R-1)+R'(t^2-1)=\delta[-2it^*R^*+(1-t^{*2})R^{*'}], \tag{4.42}$$

with t^* replaced by im^* where necessary.

Note that when $\delta=0$ equations (4.41) and (4.42) reduce to equations given in [17] for a single half-space with $\sigma_2=0$.

The solution of equations (4.37), (4.38), (4.41) and (4.42) for R, R', R^* and $R^{*'}$ may be written

$$R=\frac{(g+ih)(t+i)}{(a'+ib')(t-i)},\ R'=\frac{e+if}{(a'+ib')(t-i)},$$

$$R^*=\frac{c+id}{(a'+ib')(t^*-i)},\ R^{*'}=\frac{a+ib}{(a'+ib')(t^*-i)}, \tag{4.43}$$

where the coefficients are defined by

$$a=4tt^*(\delta-1)-2t^2\{t^2-1+\delta(1-t^{*2})\},$$

$$b=-2t\{t^2-1+\delta(1-t^{*2})+2(\delta-1)tt^*\},$$

$$a'=\delta t^{*2}(\delta t^*+t)+\delta t^*(1-3\delta+t^2)+(\delta-3)t+t^3,$$

$$b'=(1+\delta)\delta t^{*2}+4tt^*\delta+(\delta-1)^2+(1+\delta)t^2,$$

$$c=td,\ d=2t\{1+t^2+\delta(1+t^{*2})\},$$

$$e=2\delta tt^*\{3(\delta-1)+t^2-\delta t^{*2}\},$$

$$f=2t\{-\delta^2(1+t^{*2})+3\delta-2-(\delta-2)t^2\},$$

$$g=\delta t^{*2}(\delta t^*-t)+\delta t^*(1-3\delta+t^2)-(\delta-3)t-t^3,$$

$$h=\delta t^{*2}(1+\delta)-4\delta t^*t+(\delta-1)^2+(1+\delta)t^2. \tag{4.44}$$

In Section 4.4.1 graphical results for the absolute values of R, R', R^* and $R^{*'}$ are given.

4.3.2 Case B: $\beta = \sqrt{\alpha\gamma},\ \beta^* = \sqrt{\alpha^*\gamma^*}$

In this case, from (4.21), after using $\alpha/\gamma = \lambda^4$ and the Snell's law $\cos\theta/c = 1/c'$, we have

$$(1+t^2)(\lambda^2 - m^2)^2 = (1-m^2)(\lambda^2 + t^2)^2, \tag{4.45}$$

which can be reorganized as

$$m^4(1+t^2) + m^2(\lambda^4 - 2\lambda^2 + t^4) - t^2(t^2 - \lambda^4 + 2\lambda^2) = 0. \tag{4.46}$$

Note that $m = +it$ and $m = -it$ are the solutions of (4.46) corresponding to the incident and reflected waves respectively. By removing the factor $m^2 + t^2$ from (4.46) we get

$$m^2(1+t^2) - t^2 + \lambda^2(\lambda^2 - 2) = 0, \tag{4.47}$$

which gives

$$m = \pm\sqrt{1 - (\lambda^2 - 1)^2/(1+t^2)}. \tag{4.48}$$

If $\lambda \leq \sqrt{2}$ then m is real for all θ and the positive solution of (4.48) corresponds to an interfacial wave in $x_2 < 0$. If $\lambda > \sqrt{2}$ then there is a critical value of θ, θ_c say, for which $m = 0$ and this is given by

$$\tan^2\theta_c = \lambda^2(\lambda^2 - 2). \tag{4.49}$$

It follows that m is real for $\theta_c \leq \theta \leq \pi/2$. For $\theta_c < \theta \leq \pi/2$ there is a reflected wave accompanied by an interfacial wave. For $\theta = \theta_c$ the interfacial wave becomes a plane shear (body) wave propagating parallel to the boundary in $x_2 < 0$. For

$0 < \theta < \theta_c$ the interfacial wave is replaced by a second reflected wave with angle of reflection, θ', say, obtained from (4.48) by replacing m by $-i\tan\theta'$ to give

$$t'^2 = \{\lambda^2(\lambda^2 - 2) - t^2\}/(1 + t^2), \tag{4.50}$$

where

$$t' = \tan\theta'. \tag{4.51}$$

Note that equation (4.50) may be rewritten as

$$\cos^2\theta\cos^2\theta' = 1/(\lambda^2 - 1)^2, \tag{4.52}$$

which is the same as equation (3.29) for $\beta = \sqrt{\alpha\gamma}$ by using $\alpha/\gamma = \lambda^4$, and does not depend on the presence of the half-space $x_2 > 0$ (it requires only the use of Snell's law and the propagation condition).

The wave speed c' of the second reflected wave is obtained from Snell's law in the form $c' = c\cos\theta'/\cos\theta$ together with (4.52).

For the half-space $x_2 > 0$, we obtain a similar equation to (4.45), namely

$$(1 + t^{*2})\{\lambda^{*2} - m^{*2}\}^2 = \{1 - m^{*2}\}\{\lambda^{*2} + t^{*2}\}^2, \tag{4.53}$$

this has solution $m^{*2} + t^{*2} = 0$. The solution $m^* = it^*$ corresponds to a transmitted wave provided t^* is real. The other solutions are

$$m^* = \pm\sqrt{1 - (\lambda^{*2} - 1)^2/(1 + t^{*2})}.$$

An expression for t^* is obtained by using the propagation condition (4.20) and its counterpart for $x_2 > 0$ together with Snell's law (4.31). This gives a quadratic for t^{*2}, which we write as

$$t^{*4} - (D^* - 2\lambda^{*2})t^{*2} + \lambda^{*4} - D^* = 0, \tag{4.54}$$

where D^* is defined by

$$D^* = D(\lambda^2 + t^2)^2/(1 + t^2) \tag{4.55}$$

and D is given by (4.24).

Equation (4.54) may have real, pure imaginary or complex solutions for t^* depending on the values of λ, λ^* and D and on the angle of incidence. We delimit the possibilities as follows.

(a) There are two positive solutions for t^{*2}, and hence two transmitted waves, if

$$\lambda^{*2} > 2, \ \lambda^{*4} > D^* \geq 4(\lambda^{*2} - 1). \tag{4.56}$$

When the equality holds on the right hand side the two solutions (and hence the transmitted waves) coincide. If $\lambda^{*4} = D^* > 4(\lambda^{*2} - 1)$ one of the transmitted waves becomes a plane shear (body) wave propagating parallel to the boundary in $x_2 > 0$.

(b) There is one positive and one negative solution for t^{*2}, and hence one transmitted and one interfacial wave, if

$$D^* > \lambda^{*4}, \tag{4.57}$$

where λ^{*2} may be greater than, equal to or less than 2. If $D^* = \lambda^{*4} < 2\lambda^{*2}$ the transmitted wave becomes a plane shear (body) wave as in (a).

(c) There are two negative solutions for t^{*2}, and hence two interfacial waves, if

$$\lambda^{*2} < 2, \qquad \lambda^{*4} > D^* \geq 4(\lambda^{*2} - 1), \tag{4.58}$$

with the solutions equal when equality holds on the right-hand side.

(d) There are two complex conjugate solutions for t^{*2}, and hence two interfacial waves, if

$$D^* < 4(\lambda^{*2} - 1) \leq \lambda^{*4}. \tag{4.59}$$

As for (b) this can hold for λ^{*2} greater than, equal to or less than 2.

In connection with determination of which of cases (a)–(d) holds it should be observed that if $\lambda^2 \leq 2$ then D^*, regarded as a function of $t\,(\geq 0)$ is monotonically increasing with minimum $D\lambda^4$ at $t = 0$. On the other hand, if $\lambda^2 > 2$ then, as t increases from zero, D^* decreases from $D\lambda^4$ to its minimum $4D(\lambda^2 - 1)$ where $t^2 = \lambda^2 - 2$ and thereafter increases monotonically.

As in Case A, the solutions ψ and ψ^* may be written in the forms (4.29) and (4.30) respectively, with m in (4.29) given by the positive solution of (4.48) when real and replaced by $-i\tan\theta'$ when imaginary. In (4.30), $\tan\theta^*$ and im^* are the relevant solutions of (4.54) for t^* depending on which of the possibilities (a)–(d) applies.

The coefficients R, R', R^* and $R^{*'}$ are determined by using the boundary conditions (4.25), (4.27) and (4.28), with (4.28) taking the form

$$(2\lambda^2 + 1)\psi_{,112} + \psi_{,222} - \overline{\rho}\ddot{\psi}_{,2} = \delta\{(2(\lambda^*)^2 + 1)\psi^*_{,112} + \psi^*_{,222} - \overline{\rho}^*\ddot{\psi}^*_{,2}\} \tag{4.60}$$

in this case, where

$$\delta = \gamma^*/\gamma = \frac{\mu^*\lambda(\lambda^2 + 1)}{\mu\lambda^*(\lambda^{*2} + 1)}. \tag{4.61}$$

By substituting the values of ψ and ψ^* from (4.29) and (4.30) in (4.25), (4.27) and (4.60) we obtain

$$1 + R + R' = R^* + R^{*'}, \tag{4.62}$$

$$t(1-R) - imR' = t^*R^* + im^*R^{*'}, \tag{4.63}$$

$$(1-t^2)R + (1+m^2)R' + 1 - t^2 = \delta(1-t^{*2})R^* + \delta(1+m^{*2})R^{*'} \tag{4.64}$$

and

$$it[D\{t^2+2\lambda^2+1\} - D^*]R + m[D\{m^2-2\lambda^2-1\} + D^*]R'$$

$$-itD\{t^2+2\lambda^2+1\} + itD^* = iDt^*\delta[D^* - 2\lambda^{*2} - 1 - t^{*2}]R^*$$

$$-Dm^*\delta[m^{*2} - 2\lambda^{*2} - 1 + D^*]R^{*'}, \tag{4.65}$$

respectively.

For $\delta = 0$, (4.64) and (4.65) reduce to equations obtained in [17] for $\sigma_2 = 0$ when specialized for the Varga material.

The solutions of (4.62)–(4.65) for R, R', R^* and $R^{*'}$ are obtained in the form

$$R = \frac{(f+ig)(h+iI)}{(t^* - im^*)(c'+id')(e'+if')}, \; R' = \frac{(d+ie)}{(t^*-im^*)(c'+id')},$$

$$R^* = \frac{c}{(t^* - im^*)(c'+id')(e'+if')}, \; R^{*'} = \frac{a+ib}{(a'+ib')}, \tag{4.66}$$

but now the coefficients are defined by

$$a = 2(m^2+t^2)\{A - \delta Dt(L+t^{*2})\}t^*,$$

$$b = 2m[t^3(BD+D^*) - \{A + (BD+D^*)t\}\{1+\delta(t^{*2}-1)\}],$$

$$a' = mm^*\{t^2 - 1 - \delta(t^{*2}-1)\}\{\delta D(m^{*2}-L) - BD - D^*\} + t^*\{\delta(m^{*2}+1) - m^2 - 1\}$$

$$\{\delta Dt(L+t^{*2}) - A\},$$

$$b' = (BD+D^*)m\{m^2(t+t^*)-tm(t+\delta t^*)t^*-(m+\delta m^*)m^*mt-mt^*\{\delta-1+m^*(m+\delta m^*)\}$$

$$-\delta Dm^*(m^{*2}-L)\{m^2(t+t^*)+tt^*(t+\delta t^*)\}-m\{-1+\delta+m^*(m+\delta m^*)\}\{A+\delta Dt^*(L+t^{*2})\}$$

$$-(m^*+m)\delta\{t^2D(L+t^{*2})+t^*A\}t^*,$$

$$c = 2tDm^*\delta(t^2+m^2)(m^{*2}-L)+2Am^*\{t^2+m(cm^*+m)\}+2Am(t^2-1+\delta)$$

$$+2mD^*t\{\delta(1+m^{*2})+t^2-1\}+2mDBt\{t^2-1+\delta(1+m^{*2})\},$$

$$d = -2m^*\{t^2-1+\delta(1-t^{*2})\}\{D\delta t(L-m^{*2})-A\},$$

$$e = -2t^*\{t^2-1+\delta(1+m^{*2})\}\{D\delta t(tt^*+L)-A\},$$

$$f = m\delta tm^*\{D^*+D\delta(L+1)+D(B+mm^*-1)\}-\delta mtm^*\{D^*+D(B-tt^*+mm^*)\}$$

$$+\delta tD[m^{*2}\{\delta(1-t^{*2})+tt^*-1\}+(L+t^{*2})(1-\delta+m^2)]-A\{m(\delta m^*+m)+1-\delta\},$$

$$g = D^*m\{1-\delta+t(\delta t^*-t)\}+At^*\delta(m+m^*)+Bm\{D(1-t^2-\delta)+\delta tt^*\}+m^{*2}m\delta t^2D$$

$$+m^*t^*D\delta\{t(1+m^2)-\delta(Lt+mm^*t^*)-t(\delta+tt^*)\}-Dm\delta\{t^{*2}(t^2+mm^*+\delta-1)+L(t^2+\delta-1)\},$$

$$h = -m^*\{2t^*(t^2-1)+\delta t^{*2}(t-t^*)+m^{*2}\delta(t+t^*)+2t^*\delta\},$$

$$I = (t^{*2}-m^{*2})(1-t^2)-\delta t^{*2}(tt^*+1)+\delta m^{*2}(1-2t^{*2}-tt^*),$$

$$c' = m^*D^*\{1-t^2-\delta(1+tt^*)\}-m^*t^*tD\delta\{1+m^2+tt^*-\delta(1+L)\}+mD\delta[m^{*2}\{t^2-1+\delta(1-t^{*2})\}$$

$$-B(1+tt^*)+L(1-\delta-t^2)+t^{*2}(1-t^2-mm^*-\delta)]-At^*\delta(m+m^*)+mDB(1-t^2),$$

$$d' = m^*\delta D[m^*t\{\delta(1-t^{*2})-m^2-tt^*-1\}+t^*m\{1-t^2-\delta(1+L)\}-Bm(t+t^*)]$$

$$-A\{m(m+m^*\delta)-\delta+1\}-D^*\delta m^*m(t+t^*)-L\delta Dt(\delta-m^2-1)-t^*\delta D\{tt^*(\delta-1)+m^2(m^{*2}-tt^*)\},$$

$$e' = tt^*(t+\delta t^*)+t^*(\delta-1)+\delta m^{*2}(t+t^*),$$

$$f' = m^*\{1-t^2+\delta(t^{*2}-1)\},$$

where further we have

$$A = t\{D(t^2 + 2\lambda^2 + 1) - D^*\}, \quad B = m^2 - 2\lambda^2 - 1 \quad \text{and} \quad L = 1 + 2\lambda^{*2} - D^*.$$

In Section 4.4.2 the graphical results for the absolute values of R, R', R^* and $R^{*'}$ are given.

4.4 Numerical results

4.4.1 Case A: $2\beta = \alpha + \gamma$, $2\beta^* = \alpha^* + \gamma^*$

For this case the graphical results for different values of d, λ and λ^* are given in Figs 4.3–4.6. Figs 4.3 and 4.4 are for the case with no pre-strain with $d < 1 (> 1)$ respectively. With reference to the slowness curve in Fig. 4.1(a) there exists no transmitted wave in the region $0 \leq \theta \leq 0.685$. We see this fact from Fig. 4.3(a) that $|R| = 1$ in this range. From (4.43) we can find that $|R'|$ is vanishing at $\theta = 0.553$ (as shown in Fig. 4.3(b)). For Fig. 4.3 the graphs are continuous across the regions $0 \leq \theta \leq 0.685$ and $0.685 \leq \theta \leq \pi/2$.

Figs 4.5 and 4.6 are drawn for the case with pre-strain. Fig. 4.5 is drawn with reference to the slowness curve in Fig. 4.1(b) when there exists a transmitted wave for every angle of incidence (this is also the case for the waves in Fig. 4.4). Fig. 4.5 shows that $|R|$ is decreasing but $|R'|$, $|R^*|$ and $|R^{*'}|$ are increasing except $|R'|$ which again decreases in the end. This behaviour is different as compared to Fig. 4.4 (with no pre-strain) where both $|R'|$ and $|R^{*'}|$ decrease after a certain value of θ and $|R|$ increases near the normal incidence.

Here we see from the Section 4.3 from the discussion of the slowness curves in

Fig. 4.1(c) that we have two interfacial waves in $x_2 > 0$ from $0 \leq \theta \leq 0.983$ and then a transmitted wave is accompanied by an interfacial wave in $0.983 \leq \theta \leq \pi/2$. Bearing this in mind we see that $|R| = 1$ for $0 \leq \theta \leq 0.983$ in Fig. 4.6(a). We see in Figs 4.6(b) and 4.6(c) that each of $|R'|$ and $|R^*|$ vanishes at one point. This value of θ can be calculated from (4.43) and (4.44) and is given by 0.75 and 0.763 for $|R'|$ and $|R^*|$ respectively. Notice that the four graphs in Fig. 4.6 are continuous between the two regions.

In all the Figs 4.3–4.6 for the grazing incidence (at $\theta = 0$) there are no non-trivial results as $|R| = 1$ and $|R'| = |R^*| = |R^{*'}| = 0$. In Figs 4.3 and 4.6 for the grazing reflection ($\theta^* = 0$) we have transitional angles $\theta = 0.685$ and 0.983 respectively where one of the interfacial waves changes to a transmitted wave (in $x_2 > 0$). In $x_2 < 0$ there is no such transition because there is only one reflected wave and one interfacial wave for every angle of incidence.

An interesting thing to note is that none of $|R|$, $|R'|$, $|R^*|$ and $|R^{*'}|$ vanishes at $\theta = \pi/2$. To see this in detail we refer to (4.37), (4.38), (4.41) and (4.42). After using (4.35) except (4.37), the other three equations, when $\theta \to \pi/2$ give

$$1 - R = \sqrt{D}R^*, \tag{4.67}$$

$$1 + R = D\delta R^*, \tag{4.68}$$

and

$$R' = -\delta D R^{*'}, \tag{4.69}$$

respectively. Solving simultaneously (4.67), (4.68) and (4.69) alongwith (4.37) we

get

$$R = \frac{\delta\sqrt{D}-1}{\delta\sqrt{D}+1}, \quad R' = \frac{-2\delta\sqrt{D}(\delta D-1)}{(1+\delta\sqrt{D})(1+\delta D)},$$

$$R^* = \frac{2}{\sqrt{D}(\delta\sqrt{D}+1)}, \quad R^{*'} = \frac{2(\delta D-1)}{\sqrt{D}(1+\delta\sqrt{D})(1+\delta D)}. \tag{4.70}$$

Thus we see that none of them is zero since from (4.18) and (4.40) we have $\delta D = \rho^*/\rho$ but it's easily seen that for the two half-spaces to be made up of same material we have $\delta = D = 1$ which gives $R = R' = R^{*'} = 0$ and $R^* = 1$.

For Fig. 4.3 by using (4.18) and (4.40) in (4.70) with $\lambda = \lambda^* = 1, d = 0.6$ and $\mu/\mu^* = a\,(\text{say}) = 1.5$, we see that $|R| = 0.32, |R'| = 0.292, |R^*| = 1.7$ and $|R^{*'}| = 0.73$ at $\theta = \pi/2$. Similarly from (4.70) we see that $|R| = 0.07$, $|R'| = 0.185$, $|R^*| = 0.62$ and $|R^{*'}| = 0.12$ for $\lambda = \lambda^* = 1, d = 3$ and $a = 2$ (as shown in Fig. 4.4) at $\theta = \pi/2$. With $d = 10, \lambda = 2, \lambda^* = 1.2$ and $a = 2$, we get $|R| = 0.45, |R'| = 0.97, |R^*| = 0.289$ and $|R^{*'}| = 0.193$ (as shown in Fig. 4.5) at $\theta = \pi/2$. Similarly for $d = 3, \lambda = 1.2, \lambda^* = 3$ and $a = 2$ we have $|R| = 0.48, |R'| = 0.103, |R^*| = 0.34$ and $|R^{*'}| = 0.07$ as we see in Fig. 4.6 at the normal incidence.

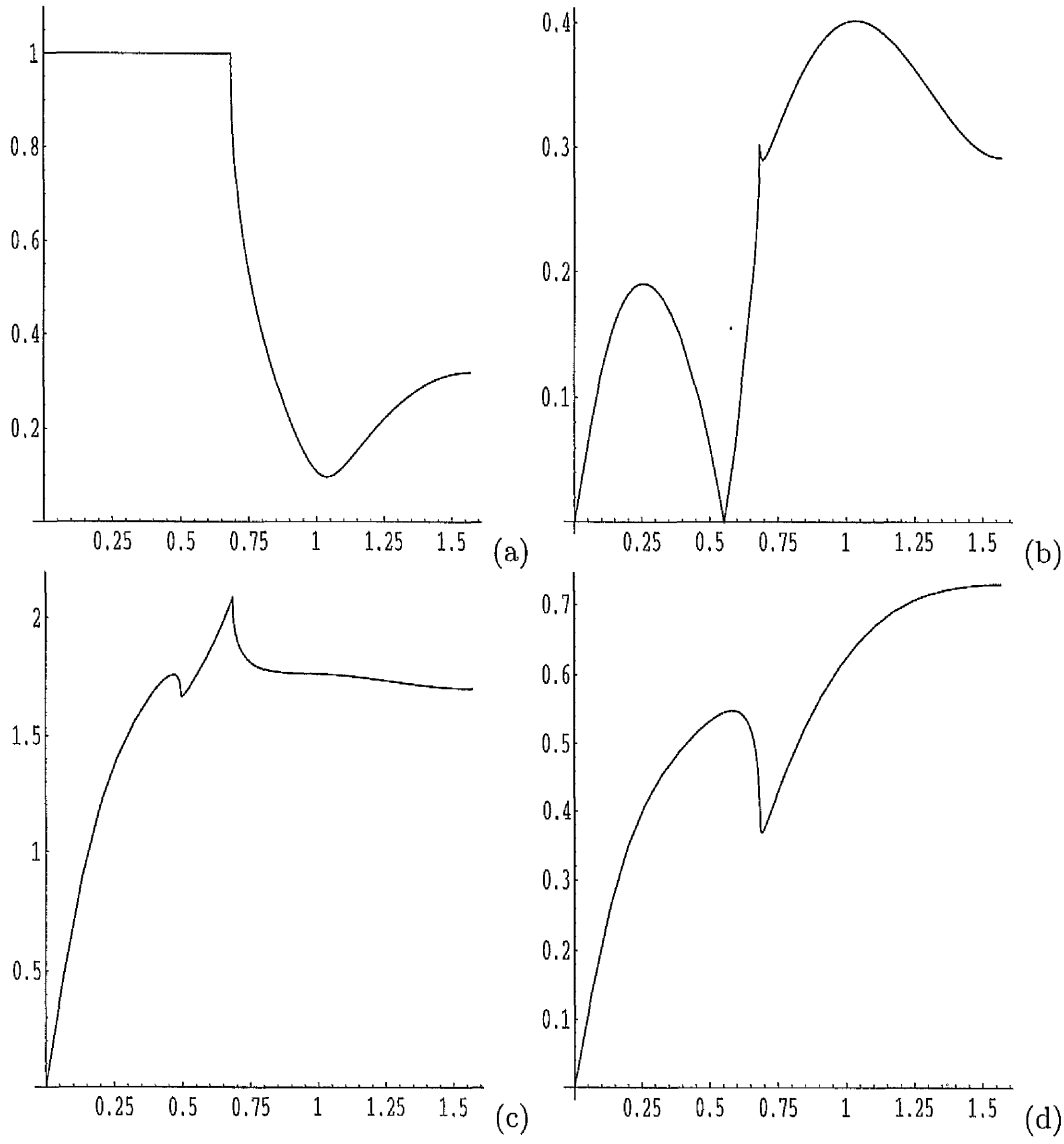

Figure 4.3: Plots of $|R|$, $|R'|$, $|R^*|$ and $|R^{*'}|$ in (a), (b), (c) and (d) respectively against $\theta\,(0 \leq \theta \leq \pi/2)$ for $2\beta = \alpha + \gamma$, $2\beta^* = \alpha^* + \gamma^*$ with $\{d,\, \lambda,\, \lambda^*\} = \{0.6,\, 1,\, 1\}$.

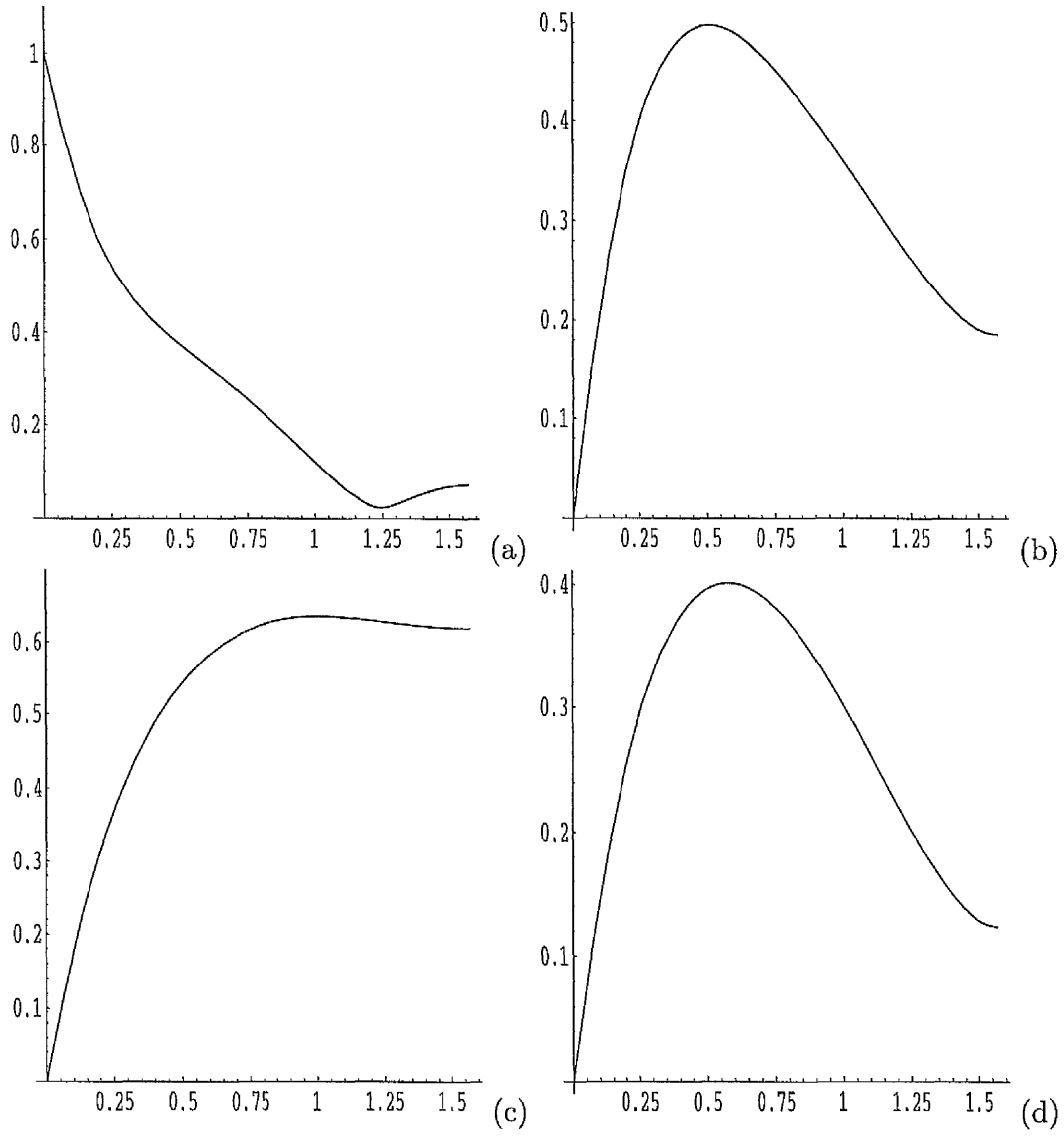

Figure 4.4: Plots of $|R|$, $|R'|$, $|R^*|$ and $|R^{*'}|$ in (a), (b), (c) and (d) respectively against $\theta\,(\,0 \leq \theta \leq \pi/2\,)$ for $2\beta = \alpha + \gamma$, $2\beta^* = \alpha^* + \gamma^*$ with $\{d,\, \lambda,\, \lambda^*\} = \{3,\, 1,\, 1\}$.

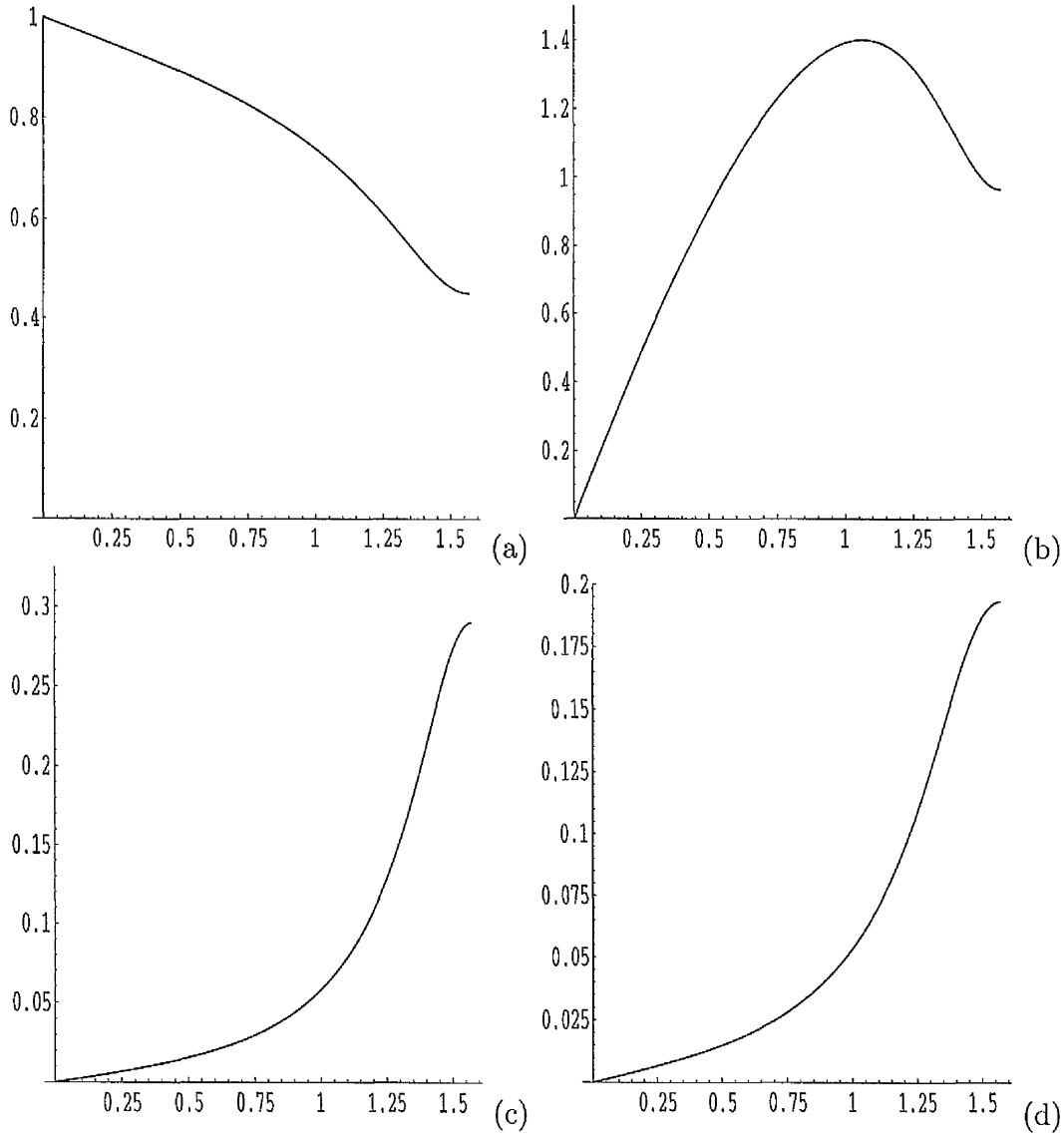

Figure 4.5: Plots of $|R|$, $|R'|$, $|R^*|$ and $|R^{*'}|$ in (a), (b), (c) and (d) respectively against $\theta\,(\,0 \leq \theta \leq \pi/2\,)$ for $2\beta = \alpha + \gamma$, $2\beta^* = \alpha^* + \gamma^*$ with $\{d,\, \lambda,\, \lambda^*\} = \{10,\, 2,\, 1.2\}$.

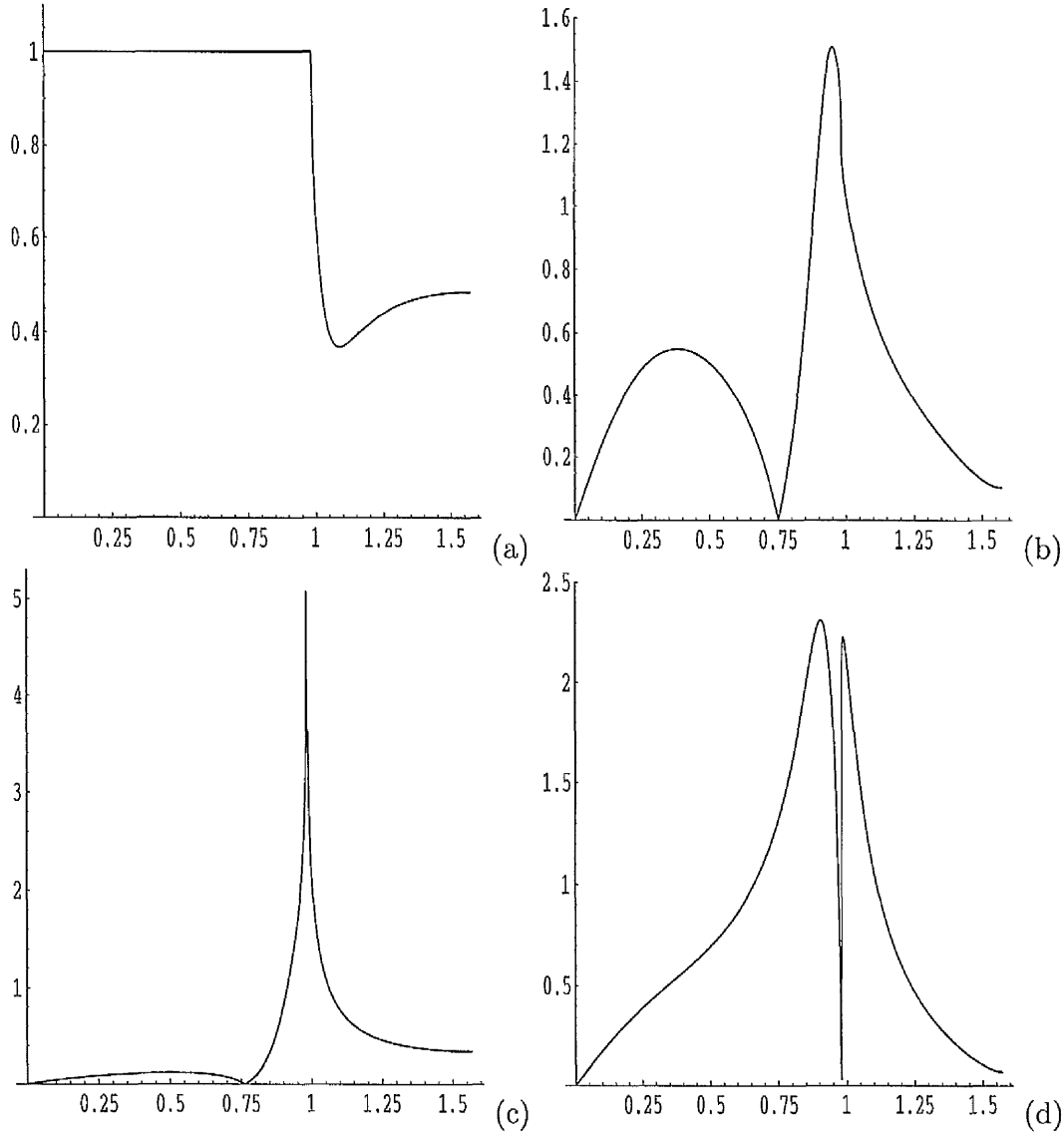

Figure 4.6: Plots of $|R|$, $|R'|$, $|R^*|$ and $|R^{*'}|$ in (a), (b), (c) and (d) respectively against $\theta\,(0 \leq \theta \leq \pi/2)$ for $2\beta = \alpha + \gamma$, $2\beta^* = \alpha^* + \gamma^*$ with $\{d,\, \lambda,\, \lambda^*\} = \{3,\, 1.2,\, 3\}$.

4.4.2 Case B: $\beta = \sqrt{\alpha\gamma}$, $\beta^* = \sqrt{\alpha^*\gamma^*}$

For this case the graphical results are given in Figs 4.7–4.9. In Fig. 4.7 results are drawn (for $a = 3$) with reference to the slowness curves in Fig. 4.2(a) in which we have one reflected wave accompanied by an interfacial wave in $x_2 < 0$ and one transmitted wave accompanied by an interfacial wave in $x_2 > 0$ for every angle of incidence. As in Case A, $|R|$ starts from 1 but $|R'|$, $|R^*|$, and $|R^{*'}|$ starts from 0 so there are no non-trivial results for grazing incidence. Both $|R'|$ and $|R^{*'}|$ are increasing in the start and then decreasing after a certain value of θ. $|R^*|$ increases throughout but $|R|$ decreases in the start and then increase after a certain value of θ. These results are of similar nature to those in Fig. 4.4 (in Case A).

In Fig. 4.8 (for $a = 1.5$) with reference to the slowness curves in Fig. 4.2(b) there are three separate regions for $0 \leq \theta \leq 0.743$, $0.743 \leq \theta \leq 1.06$ and $1.06 \leq \theta \leq \pi/2$ in which waves change their nature in $x_2 > 0$. In $x_2 < 0$ we have one reflected wave accompanied by an interfacial wave for every value of θ since $\lambda = 0.7 < \sqrt{2}$, as discussed in Section 4.3.2.

For $0 \leq \theta \leq 0.743$ we have *two interfacial* waves in $x_2 > 0$, for $0.743 \leq \theta \leq 1.06$ we have two *transmitted* waves in $x_2 > 0$ and finally for $1.06 \leq \theta \leq \pi/2$ one transmitted wave is accompanied by an interfacial wave.

Again as in Figs 4.3(a) and 4.6(a) (in Case A) we see that in Fig. 4.8(a) $|R| = 1$ in $0 \leq \theta \leq 0.743$ as long as there is no transmitted wave. The graphs of $|R|$, $|R'|$, $|R^*|$ and $|R^{*'}|$ are continuous between the three regions.

In Fig. 4.9 (for $a = 2$), with reference to the slowness curves in Fig. 4.2(c) for $x_2 > 0$, we have one transmitted wave with an interfacial wave in $0 \leq \theta \leq \pi/2$ but

for $x_2 < 0$ we have two intervals for $0 \leq \theta \leq 1.38$ with two reflected waves and $1.38 \leq \theta \leq \pi/2$ with one reflected wave accompanied by an interfacial wave.

Graphs of $|R|$, $|R'|$, $|R^*|$ and $|R^{*'}|$ are continuous between two regions. Since $\lambda = 2.5 > \sqrt{2}$, it follows from Section 4.3.2 that we have a critical angle $\theta_c = 1.38$.

Again, as in Case A at $\theta = \pi/2$, none of $|R|$, $|R'|, |R^*|$ and $|R^{*'}|$ vanish. To check this behaviour we refer to (4.62)–(4.65). When $\theta \to \pi/2$ (4.55) becomes $D^* \simeq Dt^2$ and using this in (4.65) gives

$$Dt^2 = t^{*2}, \tag{4.71}$$

for $t = \tan\theta$, $t^* = \tan\theta^*$ and D is given by (4.24). Equations (4.63) and (4.64) become

$$t(1 - R) = t^* R^*, \tag{4.72}$$

$$t^2(1 + R) = \delta t^{*2} R^* \tag{4.73}$$

and (4.62) is unchanged. In order to see the values of $|R'|$ and $|R^{*'}|$ as $\theta \to \pi/2$ let us assume

$$1 + R - R^* = K \text{ (say)}, \tag{4.74}$$

So that from (4.62) we have

$$K + R' = R^{*'}. \tag{4.75}$$

On solving (4.72) and (4.73) (by using (4.71) for $t^* > 0$) we get

$$R^* = \frac{2}{\sqrt{D}(1 + \delta\sqrt{D})} \tag{4.76}$$

and

$$R = \frac{\delta\sqrt{D} - 1}{\delta\sqrt{D} + 1}. \tag{4.77}$$

From (4.24) the values of D for the Figs 4.7–4.9 are given by 14.48, 46.686 and 0.2 respectively. Similarly from (4.61) the corresponding values of δ are given by 0.138, 0.015 and 3.1. Using these values of D and δ in (4.76) and (4.77) we get $R = -0.311$, -0.814 and 0.366 and $R^* = 0.345$, 0.2655 and 0.911 for the Figs 4.7–4.9 respectively. It's easily seen that these values tally with their absolute values as shown in the Figs 4.7–4.9 respectively. Therefore K from (4.74) for the Figs 4.7–4.9 is given by 0.344, -0.795 and 0.455 respectively. Further from the graphical results we have $|R^{*'}| \simeq 0.12$, 0.05 and 0.18 for the Figs 4.7–4.9 respectively. By using the corresponding values of K and $R^{*'}$ as $0.12, -0.05$ and 0.18 in (4.75), the values of R' are given by -0.23, -0.03 and -0.275 respectively which tally with the absolute values as shown in the Figs 4.7–4.9.

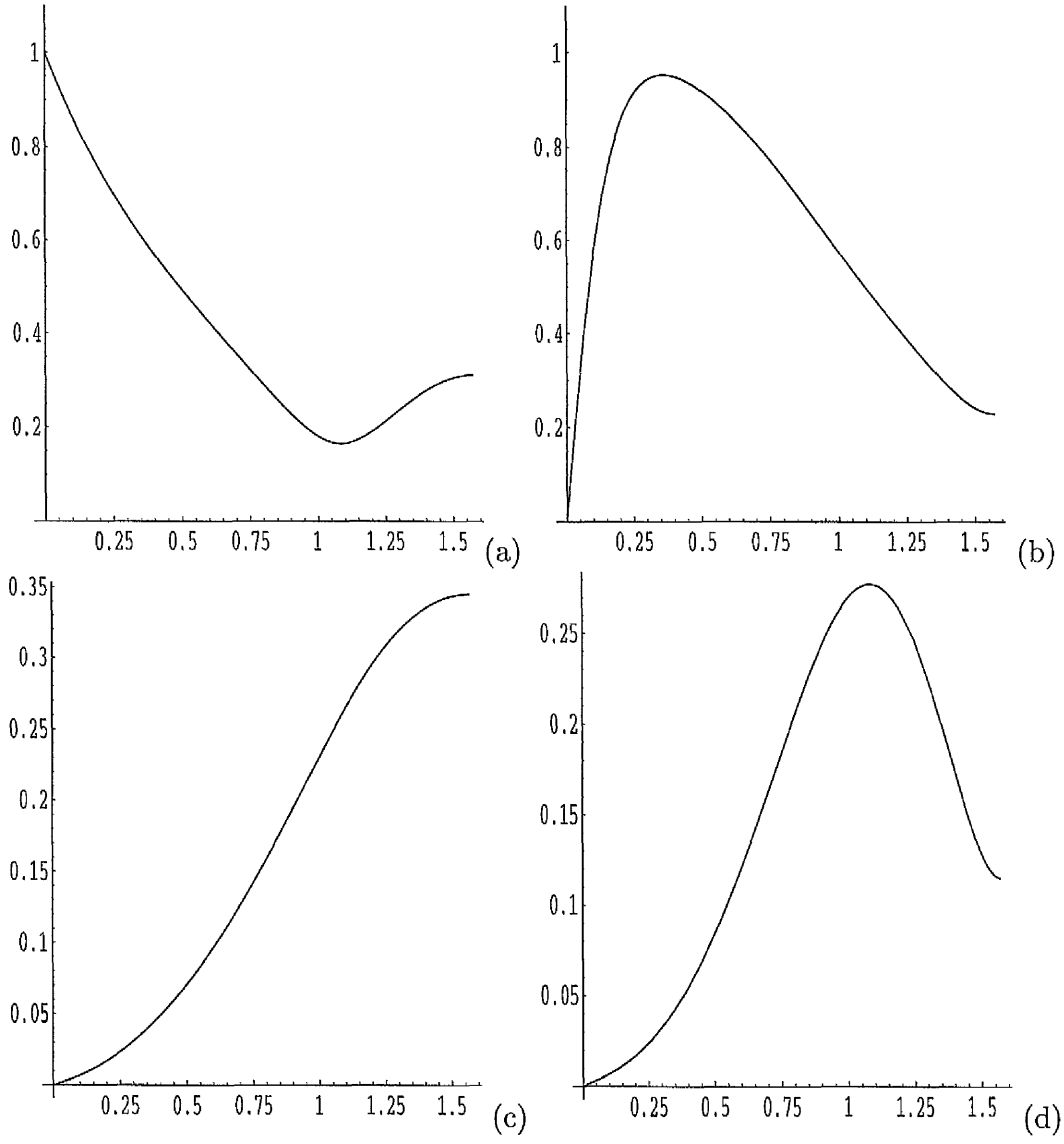

Figure 4.7: Plots of $|R|$, $|R'|$, $|R^*|$ and $|R^{*'}|$ in (a), (b), (c) and (d) respectively against $\theta\,(\,0 \leq \theta \leq \pi/2\,)$ for $\beta = \sqrt{\alpha\gamma}$, $\beta^* = \sqrt{\alpha^*\gamma^*}$ with $\{d,\, \lambda,\, \lambda^*\} = \{6,\, 1.4,\, 2\}$.

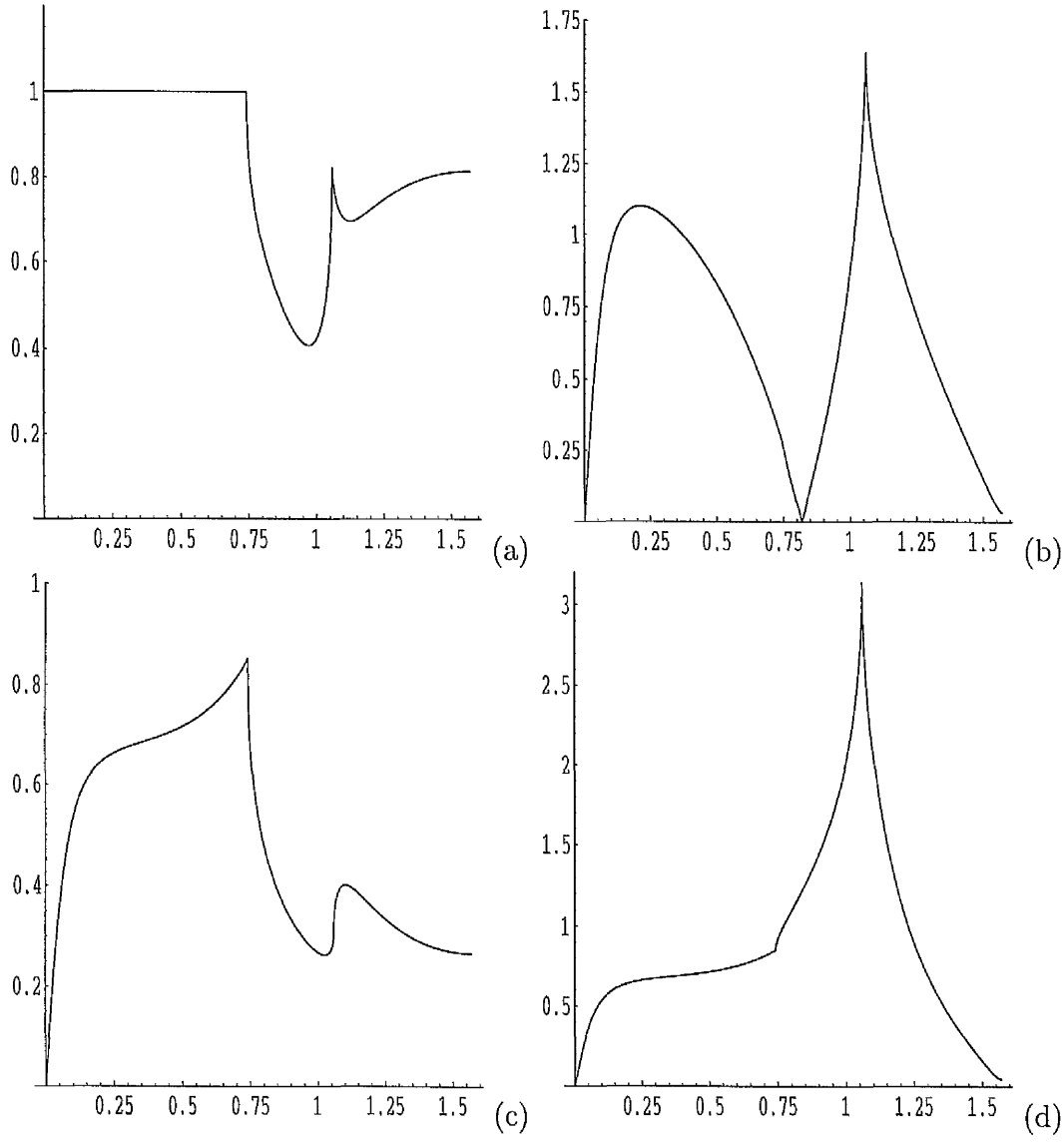

Figure 4.8: Plots of $|R|$, $|R'|$, $|R^*|$ and $|R^{*'}|$ in (a), (b), (c) and (d) respectively against $\theta\,(0 \leq \theta \leq \pi/2)$ for $\beta = \sqrt{\alpha\gamma}$, $\beta^* = \sqrt{\alpha^*\gamma^*}$ with $\{d,\, \lambda,\, \lambda^*\} = \{1.1,\, 0.7,\, 3.5\}$.

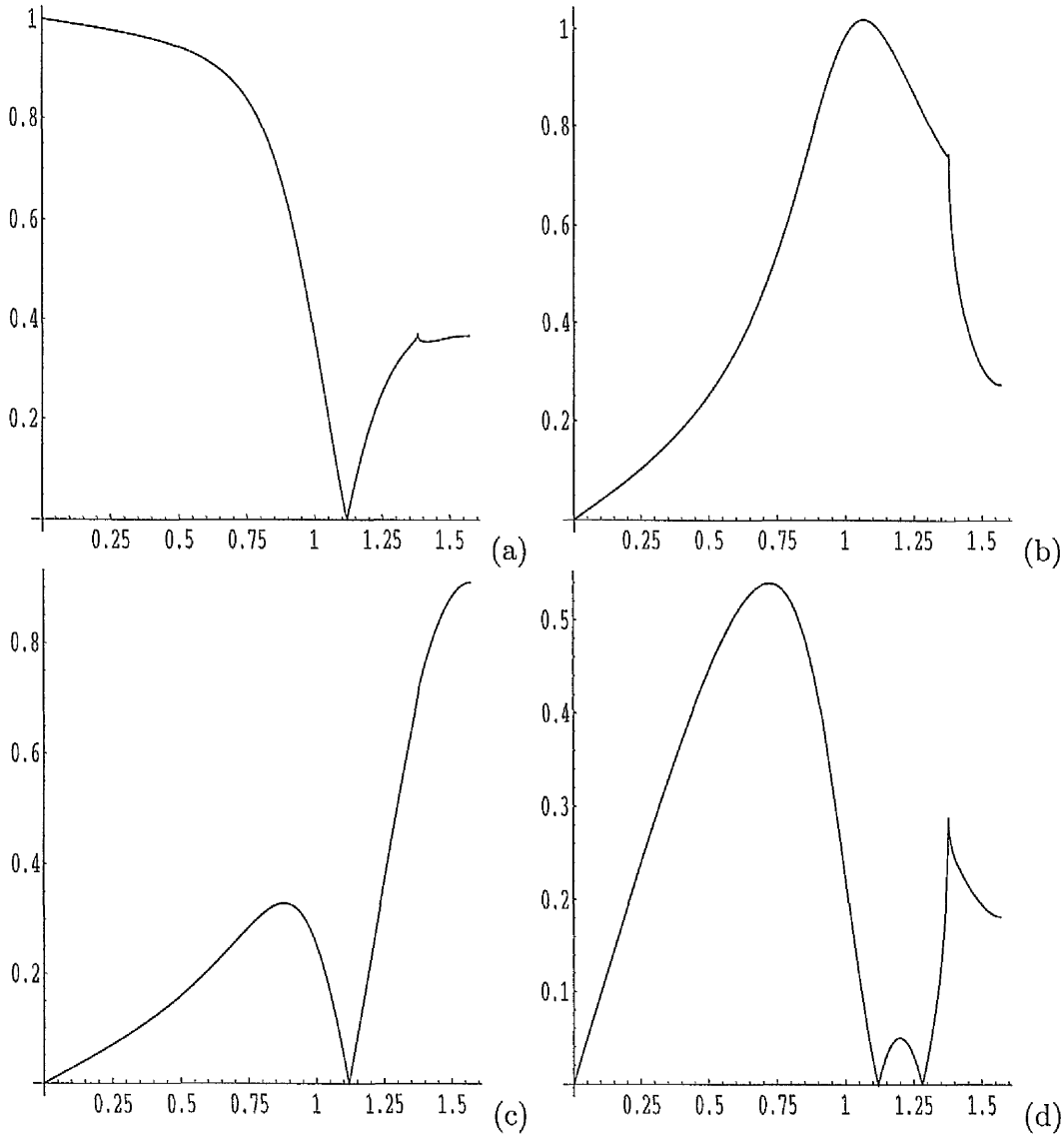

Figure 4.9: Plots of $|R|$, $|R'|$, $|R^*|$ and $|R^{*'}|$ in (a), (b), (c) and (d) respectively against $\theta\,(0 \leq \theta \leq \pi/2)$ for $\beta = \sqrt{\alpha\gamma}$, $\beta^* = \sqrt{\alpha^*\gamma^*}$ with $\{d,\, \lambda,\, \lambda^*\} = \{3,\, 2.5,\, 1.2\}$.

Chapter 5

Reflection of plane waves at the boundary of an elastic half-space subject to simple shear

In this chapter we will discuss the effect of finite strain principal axis orientation on the reflection from a plane boundary of infinitesimal plane waves propagating in a half-space of incompressible isotropic elastic material. Attention is focussed on waves propagating in a principal plane of the deformation corresponding to simple shear.

5.1 Basic equations

For a *simple shear* deformation, from Section 2.2, the Eulerian principal axes $\mathbf{v}^{(1)}$ and $\mathbf{v}^{(2)}$ are given by

$$\mathbf{v}^{(1)} = \cos\phi\,\mathbf{e}_1 + \sin\phi\,\mathbf{e}_2,$$

$$\mathbf{v}^{(2)} = -\sin\phi\,\mathbf{e}_1 + \cos\phi\,\mathbf{e}_2, \tag{5.1}$$

where ϕ is given by (2.28). Since the material is isotropic we must have equation (2.30) to hold with $\mathbf{v}^{(3)} = \mathbf{e}_3$, so that the Cartesian components of $\boldsymbol{\sigma}$ are given by

$$\sigma_{11} = \sigma_1 \cos^2\phi + \sigma_2 \sin^2\phi,$$

$$\sigma_{12} = (\sigma_1 - \sigma_2)\sin\phi\cos\phi,$$

$$\sigma_{22} = \sigma_1 \sin^2\phi + \sigma_2 \cos^2\phi. \tag{5.2}$$

It is convenient to re-cast (2.71) in terms of components relative to the Eulerian axes with coordinates (x_1', x_2'). Let u_i' and $\mathcal{A}_{0jilk}'$ be the components in this case, with u_i' regarded as functions of (x_1', x_2', t). From the incompressibility condition (2.64) in terms of these components we deduce the existence of a function $\psi' = \psi'(x_1', x_2', t)$ such that

$$u_1' = \psi_{,2}', \quad u_2' = -\psi_{,1}', \tag{5.3}$$

wherein the indicated differentiations are with respect to (x_1', x_2').

When referred to the Eulerian axes equation (2.71), after substitution from (5.3), yields an equation for ψ', namely

$$\alpha\psi_{,1111}' + 2\beta\psi_{,1122}' + \gamma\psi_{,2222}' = \rho(\ddot{\psi}_{,11}' + \ddot{\psi}_{,22}'), \tag{5.4}$$

as in [5,6], where the material parameters α, β, γ are now defined by

$$\alpha = \mathcal{A}'_{01212}, \quad \gamma = \mathcal{A}'_{02121}, \quad 2\beta = \mathcal{A}'_{01111} + \mathcal{A}'_{02222} - 2\mathcal{A}'_{01122} - 2\mathcal{A}'_{01221}. \tag{5.5}$$

Here, the components $\mathcal{A}'_{0jilk}$ are constants since the underlying deformation is homogeneous. For future reference we note that the components $\mathcal{A}_{0jilk}$ (mentioned in (2.63) and (2.69)) are related to $\mathcal{A}'_{0jilk}$ through

$$\mathcal{A}_{0ijkl} = l_{pi} l_{qj} l_{rk} l_{sl} \mathcal{A}'_{0pqrs}, \tag{5.6}$$

where

$$(l_{ij}) = \begin{pmatrix} \cos\phi & \sin\phi \\ -\sin\phi & \cos\phi \end{pmatrix} \tag{5.7}$$

$(i, j, k, l = 1, 2)$ and we recall (2.29) in case of simple shear. Equation (5.4) may also be expressed in terms of derivatives with respect to (x_1, x_2) by use of (2.23) and the notational change $\psi(x_1, x_2, t) \equiv \psi'(x'_1, x'_2, t)$. Explicitly, we then have

$$(\alpha\cos^4\phi + 2\beta\sin^2\phi\cos^2\phi + \gamma\sin^4\phi)\psi_{,1111} + 2\sin 2\phi(\alpha\cos^2\phi - \beta\cos 2\phi - \gamma\sin^2\phi)\psi_{,1112}$$

$$+ [2\beta + 6(\alpha + \gamma - 2\beta)\sin^2\phi\cos^2\phi]\psi_{,1122} + 2\sin 2\phi(\alpha\sin^2\phi + \beta\cos 2\phi - \gamma\cos^2\phi)\psi_{,1222}$$

$$+ (\alpha\sin^4\phi + 2\beta\sin^2\phi\cos^2\phi + \gamma\cos^4\phi)\psi_{,2222} = \rho(\ddot{\psi}_{,11} + \ddot{\psi}_{,22}). \tag{5.8}$$

Stress boundary conditions on the half-space boundary $x_2 = 0$ are expressed in terms of the shear and normal components of the incremental nominal traction, namely Σ_{21} and Σ_{22} respectively. From (2.63), by using (5.6), we obtain expressions for Σ_{21} and $\Sigma_{22,1}$ in terms of ψ in the form

$$\Sigma_{21} = -\sin 2\phi[\beta - \alpha + \cos^2\phi(\alpha + \gamma - 2\beta)]\psi_{,12} + [\sin^4\phi(\alpha + \gamma - 2\beta)$$

$$+ 2\sin^2\phi(\beta - \gamma) + \gamma]\psi_{,22} + [\sin^2\phi\cos^2\phi(\alpha + \gamma - 2\beta) + \sigma_2 - \gamma]\psi_{,11}, \qquad (5.9)$$

$$-\Sigma_{22,1} = [2\beta(\cos^4\phi + \sin^4\phi) + 3(\alpha + \gamma - 2\beta)\sin^2\phi\cos^2\phi + 2(\alpha + \gamma)\sin^2\phi\cos^2\phi$$

$$+ \gamma - \sigma_2]\psi_{,112} + 2\sin 2\phi[\alpha - \beta - (\alpha + \gamma - 2\beta)\cos^2\phi]\psi_{,122} + [2\beta\sin^2\phi\cos^2\phi$$

$$+ \gamma\cos^4\phi + \alpha\sin^4\phi]\psi_{,222} - \rho\ddot{\psi}_{,2} - \sin 2\phi[(\gamma - \beta)\sin^2\phi + (\beta - \alpha)\cos^2\phi]\psi_{,111}. \qquad (5.10)$$

In equation (5.10) we have again eliminated π from Σ_{22} by differentiating with respect to x_1 and use of (2.69). (5.9) and (5.10) will be used in Section 5.3.

5.2 Plane waves

We consider time-harmonic homogeneous planes waves of the form (2.75). Substitution of (2.75) into (5.8) leads to

$$\alpha\cos^4(\theta - \phi) + 2\beta\sin^2(\theta - \phi)\cos^2(\theta - \phi) + \gamma\sin^4(\theta - \phi) = \rho c^2. \qquad (5.11)$$

Equation (5.11) is the *propagation condition* which determines the wave speed for any given direction of propagation in the (x_1, x_2)-plane. We note that $\rho c^2 > 0$ for all such directions if and only if the *strong ellipticity* inequalities given by (2.77) hold. Further (5.11) reduces to (2.76) for $\phi = 0$.

Similarly, for an *inhomogeneous* plane wave of the form

$$\psi = A^* \exp[ik^*(x_1 - imx_2 - c^*t)] \qquad (5.12)$$

we obtain

$$\alpha\cos^4\phi + 2\beta\sin^2\phi\cos^2\phi + \gamma\sin^4\phi - 2i\sin 2\phi(\alpha\cos^2\phi - \beta\cos 2\phi - \gamma\sin^2\phi)m$$

$$- [2\beta + 6(\alpha+\gamma-2\beta)\sin^2\phi\cos^2\phi]m^2 + 2i\sin 2\phi(\alpha\sin^2\phi + \beta\cos 2\phi - \gamma\cos^2\phi)m^3$$

$$+ (\alpha\sin^4\phi + 2\beta\sin^2\phi\cos^2\phi + \gamma\cos^4\phi)m^4 = \rho(1-m^2)c^{*2}, \qquad (5.13)$$

and for the wave to decay as $x_2 \to -\infty$ we require that m has positive real part. (5.13) reduces to (4.4) for $\phi = 0$ and $c^* = c'$.

Note that the above applies for any isochoric plane deformation in the (1,2)-plane and that results for simple shear are obtained by appropriate specialization.

We consider two distinct cases corresponding to different relative values of the material parameters α, β, γ.

Case A: $2\beta = \alpha + \gamma$

With this specialization equations (5.11) and (5.13) reduce to

$$\alpha\cos^2(\theta-\phi) + \gamma\sin^2(\theta-\phi) = \rho c^2 \qquad (5.14)$$

and

$$(m^2-1)[(\alpha\sin^2\phi + \gamma\cos^2\phi)m^2 + im(\alpha-\gamma)\sin 2\phi + \rho c^{*2} - (\alpha\cos^2\phi + \gamma\sin^2\phi)] = 0 \qquad (5.15)$$

respectively.

In terms of the *slowness vector* (s_1, s_2) defined by (4.8) equation (5.14) may be written as

$$\overline{\alpha}(s_1\cos\phi + s_2\sin\phi)^2 + \overline{\gamma}(s_1\sin\phi - s_2\cos\phi)^2 = 1,$$

where $\overline{\alpha}$ and $\overline{\gamma}$ are defined by (3.15).

By using the dimensionless slowness vector $(\overline{s}_1, \overline{s}_2)$ defined by (4.11) and again, on noting that $\alpha/\gamma = \lambda^4$, we obtain

$$\lambda^4(\overline{s}_1 \cos\phi + \overline{s}_2 \sin\phi)^2 + (\overline{s}_1 \sin\phi - \overline{s}_2 \cos\phi)^2 = 1. \tag{5.16}$$

Equation (5.16) is a dimensionless form of the equation of the *slowness curve* in the (1,2)-plane, which has an important role in connection with the interpretation of wave reflections and it reduces to (4.12) for $\phi = 0$.

When the deformation is specialized to simple shear use of (2.29) enables (5.16) to be simplified to

$$(\lambda^4 - \lambda^2 + 1)\overline{s}_1{}^2 + 2\lambda(\lambda^2 - 1)\overline{s}_1\overline{s}_2 + \lambda^2\overline{s}_2{}^2 = 1. \tag{5.17}$$

Note that this is the equation of an ellipse and its principal axes can be shown to coincide with the Eulerian principal axes. For the Mooney-Rivlin strain-energy function this fact was pointed out in [2].

Case B: $2\beta \neq \alpha + \gamma$

In this case we illustrate the possible differences from Case A by considering a strain-energy function for which

$$\beta = \sqrt{\alpha\gamma}, \tag{5.18}$$

as discussed in Section 4.2.2.

For (5.18) equation (5.11) simplifies to

$$[\sqrt{\alpha}\cos^2(\theta - \phi) + \sqrt{\gamma}\sin^2(\theta - \phi)]^2 = \rho c^2, \tag{5.19}$$

and, in terms of the notation defined in (4.11) with $\alpha/\gamma = \lambda^4$, the corresponding slowness curve has equation

$$[\lambda^2(\overline{s}_1 \cos\phi + \overline{s}_2 \sin\phi)^2 + (\overline{s}_1 \sin\phi - \overline{s}_2 \cos\phi)^2]^2 = \overline{s}_1{}^2 + \overline{s}_2{}^2. \tag{5.20}$$

Note that (5.19) and (5.20) reduce to (4.20) and (4.22) respectively for $\phi = 0$. For simple shear (5.20) gives

$$[(\lambda^4 + 1)\overline{s}_1{}^2 + 2\lambda(\lambda^2 - 1)\overline{s}_1\overline{s}_2 + 2\lambda^2\overline{s}_2{}^2]^2 = (\lambda^2 + 1)^2(\overline{s}_1{}^2 + \overline{s}_2{}^2). \tag{5.21}$$

The specialization of (5.13) for this case is obtained similarly, and, in particular, for simple shear, yields

$$(\lambda^4 + 1)^2 - 4i\lambda m(\lambda^4 + 1)(\lambda^2 - 1) - 8\lambda^2 m^2(\lambda^4 - \lambda^2 + 1) + 8i\lambda^3 m^3(\lambda^2 - 1)$$

$$+ 4\lambda^4 m^4 = (1 - m^2)(\lambda^2 + 1)^2 c^{*2}/\overline{\gamma}, \tag{5.22}$$

but, unlike (5.15), this does not yield a simple factorization.

We now illustrate the dependence of the slowness curves on λ in respect of both classes of materials by plotting the curves in $(\overline{s}_1, \overline{s}_2)$-space on the basis of (5.17) and (5.21). Note that (5.21) includes the degenerate solution $\overline{s}_1 = \overline{s}_2 = 0$ corresponding to a P wave with infinite speed. This solution has effectively been factored out from (5.17) by the specialization $2\beta = \alpha + \gamma$.

Figure 5.1 shows the slowness curves for the case $2\beta = \alpha + \gamma$ for a selection of values of $\lambda > 1$. The curves for $\lambda < 1$ have the same shape and are essentially reflections of those in Fig. 5.1 in the vertical axis.

Figure 5.2 shows the corresponding slowness curves for the case $\beta = \sqrt{\alpha\gamma}$, again for a selection of values of $\lambda > 1$. As in Case A, the curves for $\lambda < 1$ are essentially

obtained by reflection in the vertical axis. We observe, in particular, than unlike in Fig. 5.1, if λ is sufficiently large a vertical line may cut the curve in more than two points.

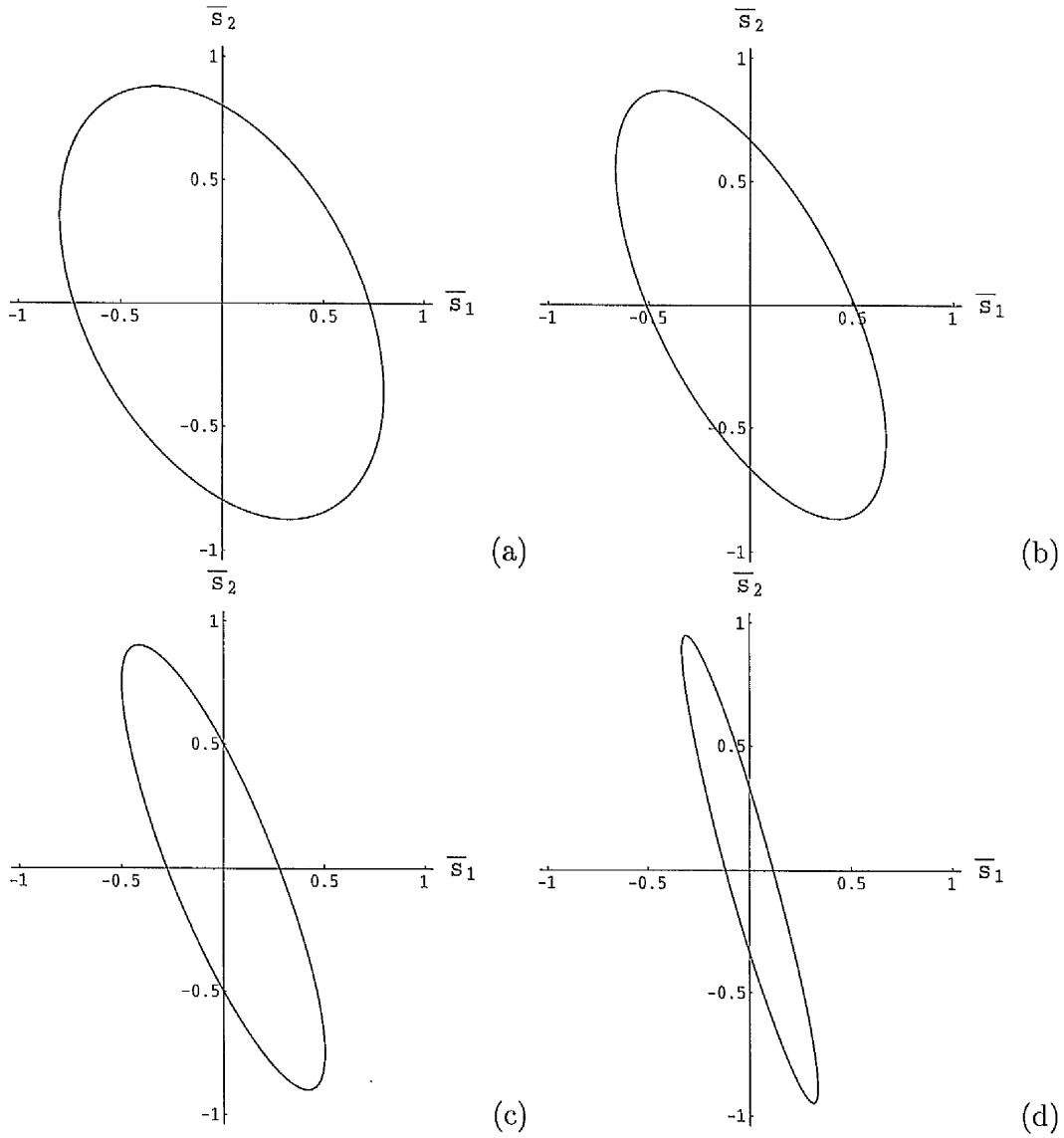

Figure 5.1: Slowness curves in $(\overline{s}_1, \overline{s}_2)$-space for $2\beta = \alpha + \gamma$ with the following values of λ: (a) 1.25, (b) 1.5, (c) 2, (d) 3.

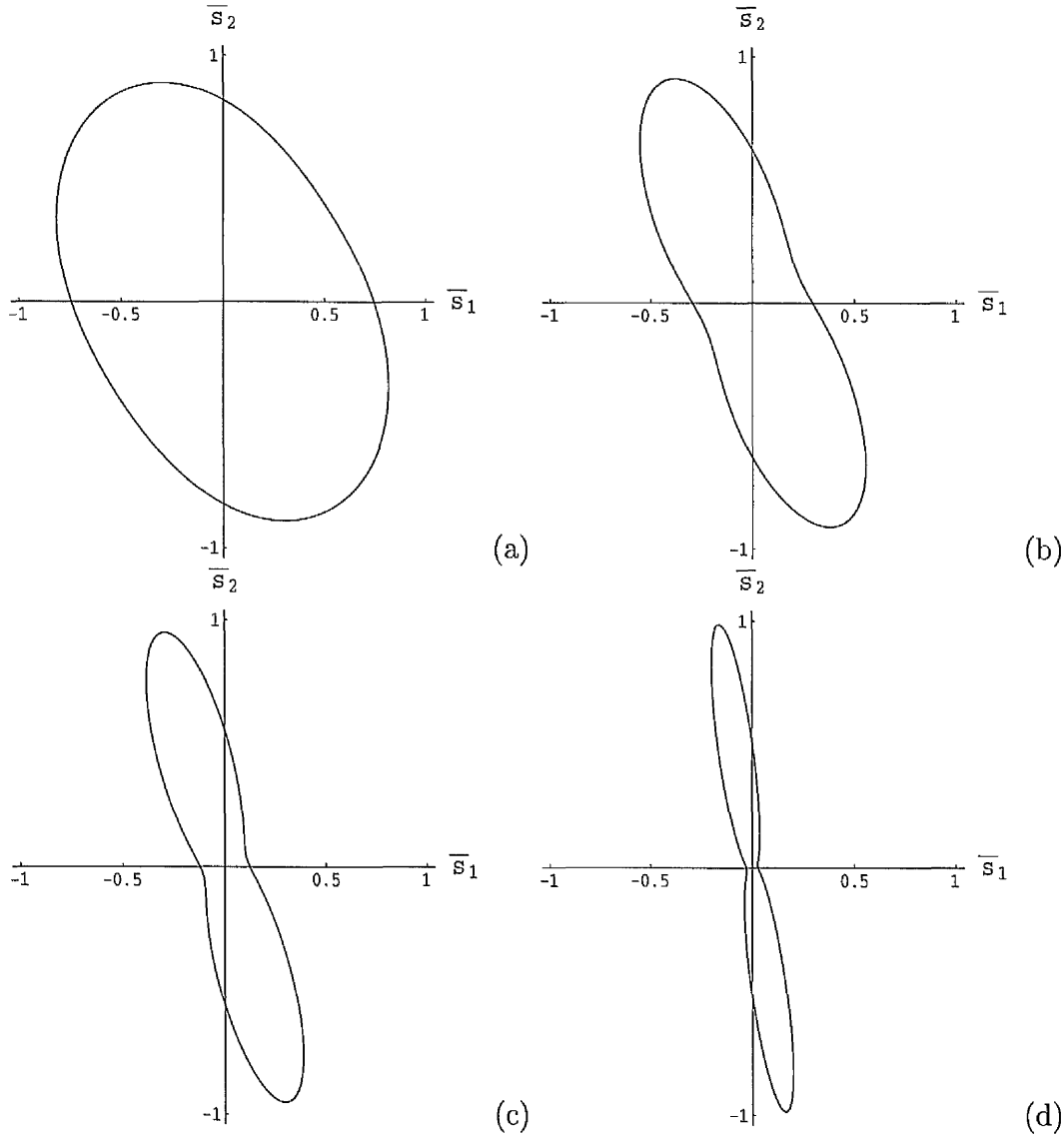

Figure 5.2: Slowness curves in $(\overline{s}_1, \overline{s}_2)$-space for $\beta = \sqrt{\alpha\gamma}$ with the following values of λ: (a) 1.25, (b) 2, (c) 3, (d) 6.

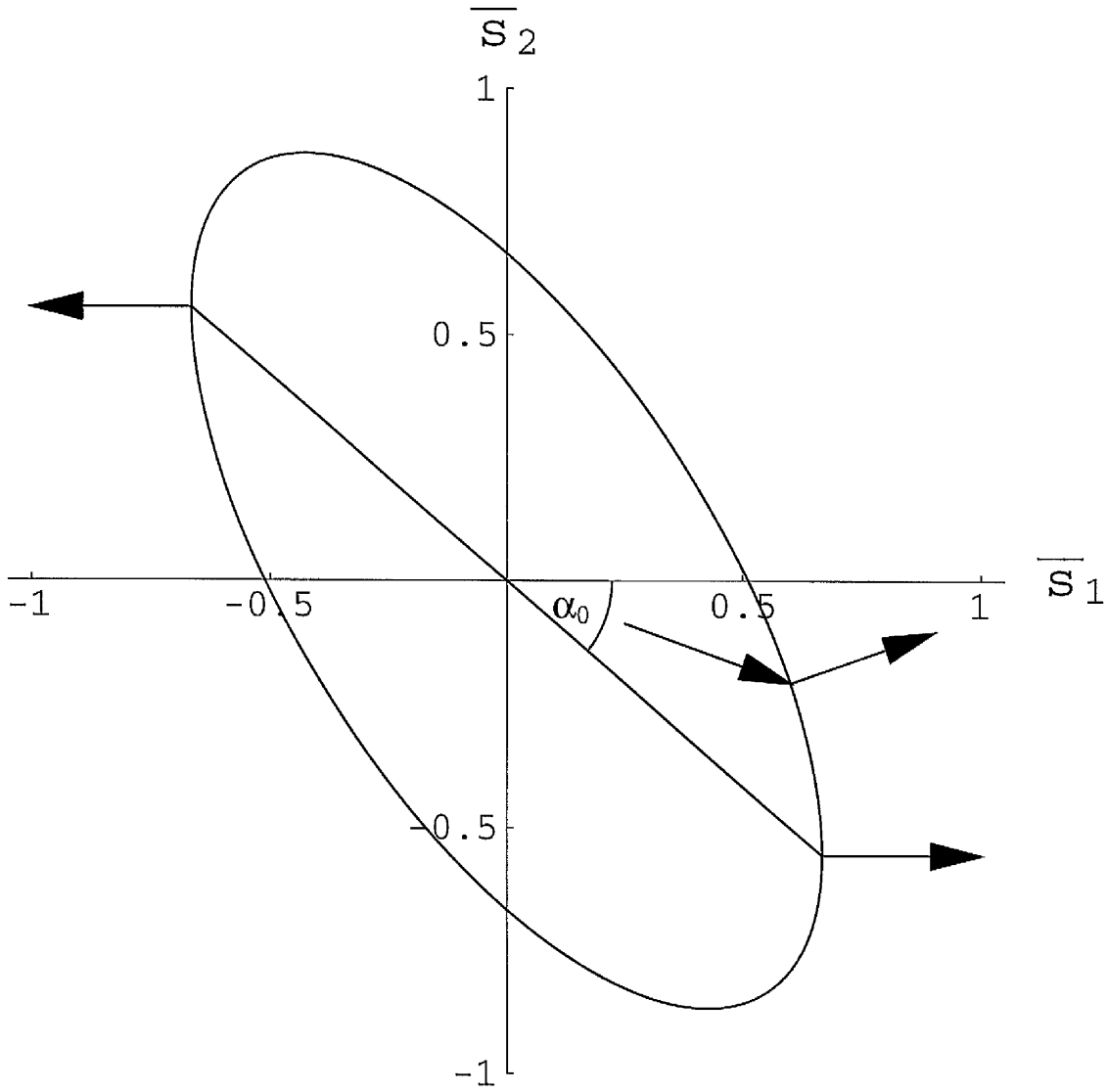

Figure 5.3: Slowness curve in the $(\overline{s}_1, \overline{s}_2)$-plane for $\lambda = 1.5$ for a material with $2\beta = \alpha + \gamma$. The arrows normal to the curve show the direction of the time-averaged energy flux.

Figure 5.3 shows a typical slowness curve for Case A. There are two points at which the tangent to the curve is vertical. Let α_0 (> 0), as shown in Fig. 5.3, be the angle that a line joining these points to the origin makes with the $\overline{s}_1$ axis. This is a *critical angle* in the sense that the normals to the curve at these points are parallel to the horizontal axis. In general, the normal to the slowness curve identifies the direction of the (incremental) time-averaged energy flux. This flux is parallel to the $\overline{s}_1$ axis for a plane wave whose direction of propagation $(\cos\theta, \sin\theta)$ is such that either $\theta = -\alpha_0$ or $\theta = \pi - \alpha_0$. An incident wave from $x_2 < 0$ must have energy flux directed *towards* the boundary $x_2 = 0$ and hence its angle of propagation θ must be such that

$$-\alpha_0 \leq \theta \leq \pi - \alpha_0 \tag{5.23}$$

with $\alpha_0 > 0$ for $\lambda > 1$ and the extreme values in (5.23) corresponding to grazing incidence.

Using the slowness equation (5.16) it is easy to calculate that

$$\tan\alpha_0 = \frac{(\lambda^4 - 1)\cot\phi}{(\lambda^4 + \cot^2\phi)}. \tag{5.24}$$

For simple shear equation (5.24) simplifies to

$$\tan\alpha_0 = \epsilon, \tag{5.25}$$

where ϵ is defined by (2.26).

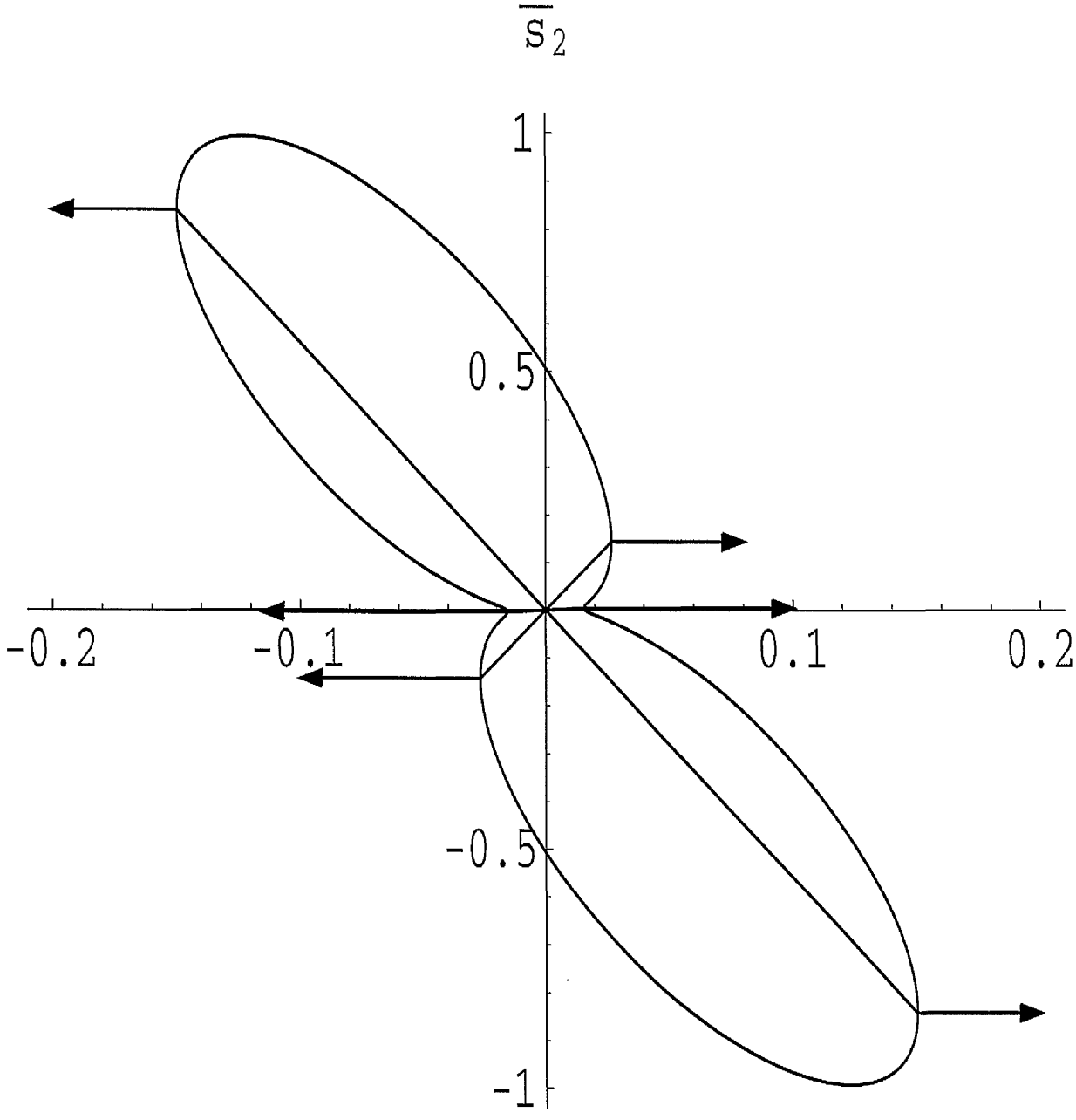

Figure 5.4: Slowness curve in the $(\overline{s}_1, \overline{s}_2)$-plane for $\lambda = 8$ for a material with $\beta = \sqrt{\alpha\gamma}$. The arrows show the points on the curve at which the direction of the time-averaged energy flux is parallel to the $\overline{s}_1$ direction. Note that the horizontal and vertical scales are different.

Figure 5.4 shows the analogue of Fig. 5.3 for Case B with $\lambda = 8$. In this case, there are six points where the tangent to the curve is vertical, although two of these are barely distinguishable since they are very close to the $\overline{s}_1$ axis. In Fig. 5.4 there is point symmetry about the origin, as is also the case in Fig. 5.3.

Let α_0 be defined as previously as the angle (below the $\overline{s}_1$ axis) that a line from the origin to a point where the tangent to the slowness curve is vertical makes with the $\overline{s}_1$ axis, and let $t_0 = \tan\alpha_0$. Then, by seeking points where equation (5.20) has a vertical tangent, it can be shown that t_0 satisfies the cubic equation

$$(\lambda^2 \sin^2\phi + \cos^2\phi)t_0^3 - [2(\lambda^2 - 1)\cos 2\phi - (\lambda^2\cos^2\phi + \sin^2\phi)]t_0 - (\lambda^2 - 1)\sin 2\phi = 0, \tag{5.26}$$

which, for simple shear, reduces to

$$2t_0^3 - (\epsilon^2 - 2)t_0 - 2\epsilon = 0. \tag{5.27}$$

For $\epsilon > 0\,(\lambda > 1)$ equation (5.27) always has a positive solution for t_0, while if ϵ is sufficiently large it has, additionally, two negative solutions. Figure 5.4 illustrates the latter case.

5.3 Reflection from a plane boundary

Let an incident wave impinging on the boundary $x_2 = 0$ from the region $x_2 < 0$ have direction of propagation $(\cos\theta, \sin\theta)$ and speed c. Let $(\cos\theta', -\sin\theta')$ and c' (> 0) be the corresponding values for a reflected wave and let c^* be the speed of a surface wave generated. Then, according to Snell's law we must have

$$\cos\theta/c = cos\theta'/c' = 1/c^*. \tag{5.28}$$

We can take $c > 0$, $c' > 0$ without loss of generality since, by reference to Fig. 5.3 or Fig. 5.4, it is clear that $\cos\theta' > 0$ whenever $\cos\theta > 0$ and $\cos\theta' < 0$ whenever $\cos\theta < 0$. On the other hand, $c^* > 0$ and $c^* < 0$ respectively in these two cases. Similarly, $k > 0$, $k' > 0$ and k^* has the sign of c^*. There is now in general not a reflected wave with the same speed as the incident wave.

For the situation in which a single reflected wave is accompanied by a surface wave we have

$$\psi = A\exp[ik(x_1\cos\theta + x_2\sin\theta - ct)] + AR'\exp[ik'(x_1\cos\theta' - x_2\sin\theta' - c't)]$$

$$+ AR^*\exp[ik^*(x_1 - imx_2 - c^*t)], \tag{5.29}$$

with

$$k\cos\theta = k'\cos\theta' = k^*, \tag{5.30}$$

where R' is the reflection coefficient and R^* a measure of the relative amplitude of the surface wave.

For the situation in which there are two reflected waves (5.29) is replaced by

$$\psi = A\exp[ik(x_1\cos\theta + x_2\sin\theta - ct)] + AR'\exp[ik'(x_1\cos\theta' - x_2\sin\theta' - c't)]$$

$$+AR^*\exp[ik''(x_1\cos\theta'' - x_2\sin\theta'' - c''t)] \tag{5.31}$$

with

$$\cos\theta/c = \cos\theta'/c' = \cos\theta''/c'' \tag{5.32}$$

and

$$k\cos\theta = k'\cos\theta' = k''\cos\theta'' \tag{5.33}$$

and we may take $c'' > 0$ and $k'' > 0$. The transformations $k^* = k'' \cos\theta''$, $c^* = c''/\cos\theta''$, $im = \tan\theta''$ take (5.29) to (5.31).

The coefficients R', R^* will be determined by application of the boundary conditions $\Sigma_{21} = 0$ and $\Sigma_{22,1} = 0$ on $x_2 = 0$, where expressions for Σ_{21} and $\Sigma_{22,1}$ are given by (5.9) and (5.10). Again we consider Cases A and B separately.

5.3.1 Case A: $2\beta = \alpha + \gamma$

From the propagation condition (5.14) and its counterpart for the reflected wave together with the first equation in (5.28) we obtain an expression for the angle of reflection θ' in the form

$$\tan\theta' = \tan\theta + 2\tan\alpha_0, \tag{5.34}$$

where $\tan\alpha_0$ is given by (5.24) or, for simple shear, by (5.25). We recall that for an incident wave θ is restricted according to (5.23). It follows that θ' is similarly restricted according to

$$\alpha_0 \leq \theta' \leq \pi + \alpha_0. \tag{5.35}$$

With reference to (5.24) we see that (5.34) shows that the angles of reflection and incidence are equal if and only if either $\lambda = 1$ or $\phi = 0$ (or $\pi/2$).

With the specialization $2\beta = \alpha + \gamma$, for the case of simple shear, use of (5.9) and (5.10) enables the boundary conditions $\Sigma_{21} = 0$ and $\Sigma_{22,1} = 0$ on $x_2 = 0$ to be expressed in the form

$$\epsilon\psi_{,21} + \psi_{,22} - \sigma\psi_{,11} = 0 \quad \text{on } x_2 = 0, \tag{5.36}$$

$$\epsilon\,\psi_{,111} + (\epsilon^2 + 2 + \sigma)\psi_{,112} + 2\epsilon\psi_{,122} + \psi_{,222} - \overline{\rho}\lambda^{-2}\ddot{\psi}_{,2} = 0 \quad \text{on } x_2 = 0, \tag{5.37}$$

where $\overline{p}$ is given by (4.10) and σ is defined by

$$\sigma = \lambda^{-2}(1 - \overline{\sigma}_2), \tag{5.38}$$

and $\overline{\sigma}_2$ by

$$\overline{\sigma}_2 = \sigma_2/\gamma, \tag{5.39}$$

as given in Section 3.4.1.

Let $\overline{\sigma}_{22} = \sigma_{22}/\gamma$, where σ_{22} is the normal stress on the boundary $x_2 = 0$ associated with the underlying deformation. Then, from (2.46), (5.2) and (2.29) for simple shear, we obtain

$$\overline{\sigma}_{22} = \lambda^2(1 - \sigma) = \overline{\sigma}_2 + \lambda^2 - 1. \tag{5.40}$$

Thus, σ, or equivalently $\overline{\sigma}_2$, is a measure of the normal stress for given λ.

In this case the solution for ψ has the form (5.29), and, recalling (5.15) and the requirement that m should have positive real part, we have $m = 1$, while $\tan\theta'$ is given by (5.34) with (5.25). With this specialization, substitution of (5.29) into (5.36) and (5.37) leads, after some rearrangement, to

$$a'R' + a^*R^* = -d, \quad b'R' + b^*R^* = e, \tag{5.41}$$

where the coefficients are defined by

$$a' = \sigma - (t^2 + 3\epsilon t + 2\epsilon^2), \quad a^* = \sigma + 1 + i\epsilon,$$

$$b' = -(\sigma + 1)(t + 2\epsilon) + \epsilon, \quad b^* = i(t^2 + 2\epsilon t - \sigma) - \epsilon,$$

$$d = \sigma - \epsilon t - t^2, \quad e = -(\sigma + 1)t - \epsilon, \tag{5.42}$$

and the notation

$$t = \tan\theta \tag{5.43}$$

has been introduced. Note that t should be distinguished from the time variable t used earlier.

The expressions for R' and R^* are obtained from (5.41) as

$$R' = \frac{a^*e + b^*d}{a^*b' - b^*a'}, \quad R^* = \frac{a'e + b'd}{a'b^* - b'a^*}. \tag{5.44}$$

By using (5.42) in (5.44) the expressions for $|R'|$ and $|R^*|$ take the forms

$$|R'| = \sqrt{\frac{1+t^2}{1+t'^2}} \tag{5.45}$$

and

$$|R^*| = \frac{|(t+t')[(t+t')^2 - 4\sigma(1-tt') - 4\sigma^2]|}{\sqrt{(1+t'^2)[\{4\sigma^2 + (t+t')^2\}^2 + 4(t+t')^2(2\sigma + 1 - tt')^2]}}, \tag{5.46}$$

where

$$t' \equiv \tan\theta' = t + 2\epsilon. \tag{5.47}$$

Note that $|R'|$ is independent of pre-stress and that, in general, $|R'| \neq 1$. Moreover, $|R'|$ does not vanish for any angle of incidence.

On the other hand, it follows directly from (5.41) and (5.42) that $R^* = 0$ for $\theta = \pi/2$. Also, R^* vanishes where $t = \tan\theta$ satisfies the equation

$$(t+\epsilon)[(\sigma+1)t^2 + 2\epsilon(\sigma+1)t + \epsilon^2 - \sigma(\sigma+1)] = 0. \tag{5.48}$$

The solution $t = -\epsilon = -t'$ corresponds to an angle of incidence for which the time-averaged energy flux is parallel to the boundary $x_2 = 0$.

Equation (5.48) has three distinct real solutions provided

$$\text{either} \quad \sigma > 0 \quad \text{or} \quad -1-\epsilon^2 < \sigma < -1. \tag{5.49}$$

For the special case in which $\lambda = 1$ it is easy to see that $|R'| = 1$, while

$$|R^*| = \frac{2|(\sigma+1)(\sigma-t^2)t|}{\sqrt{(\sigma+1)^4 t^2 + (\sigma-t^2)^4}}. \tag{5.50}$$

Equation (5.50) agrees with a result obtained in [17] for pure homogeneous strain specialized to this case but expressed in different notation.

Graphical results showing the dependence of $|R'|$ and $|R^*|$ on θ for different values of λ and $\overline{\sigma}_2$ are described in Section 5.4.1.

5.3.2 Case B: $\beta = \sqrt{\alpha\gamma}$

For simple shear, on use of (5.28) and the expression (5.19) for ρc^2 corresponding to an incident wave, we obtain from (5.22) a quartic equation for m, one solution of which is $m = it$, which corresponds to the incident wave. On removing the factor $m - it$ and writing $m = i\tau$, we obtain a cubic for τ in the form

$$4(1+t^2)\tau^3 + 4(1+t^2)(2\epsilon+t)\tau^2 + (4t^2 - 4\epsilon^3 t - \epsilon^4 + 4\epsilon^2 + 4)\tau + 4t^3$$

$$+ 8\epsilon t^2 - (\epsilon^4 - 4\,\epsilon^2 - 4)t + 4\epsilon(\epsilon^2+2) = 0, \tag{5.51}$$

in which the coefficients are real. Equation (5.51) has either one or three real solutions for τ. In the first case we may identify $\tau = -\tan\theta'$ as that solution, which corresponds to a single reflected wave. Of the two complex solutions only one yields a value of $m = i\tau$ with positive real part associated with a surface wave. The conjugate root is discounted in this case. In the second case two roots,

$\tau = -\tan\theta'$, $\tau = -\tan\theta''$ (which have opposite signs) are associated with reflected waves, while the third root has energy flux pointing towards the boundary from $x_2 < 0$ and does not correspond to a reflected wave. We refer to Fig. 5.4 for a geometrical interpretation in terms of the slowness curve.

With $\beta = \sqrt{\alpha\gamma}$ and use of (5.9) and (5.10), we re-cast the boundary conditions $\Sigma_{21} = 0$ and $\Sigma_{22,1} = 0$ on $x_2 = 0$ in the forms

$$[\epsilon^2 - (\epsilon^2+4)\sigma]\psi_{,11} + 4\,\epsilon\,\psi_{,12} + 4\psi_{,22} = 0 \quad \text{on } x_2 = 0, \tag{5.52}$$

$$2\,\epsilon\,(\epsilon^2+2)\psi_{,111} + [7\epsilon^2 + 8 + (\epsilon^2+4)\sigma]\psi_{,112} + 8\,\epsilon\,\psi_{,122}$$

$$+ 4\psi_{,222} - \overline{\rho}\lambda^{-2}(\epsilon^2+4)\ddot{\psi}_{,2} = 0 \quad \text{on } x_2 = 0, \tag{5.53}$$

where σ and $\overline{\rho}$ are again defined by (5.38) and (4.10) respectively.

We now substitute (5.29) into (5.52) and (5.53) with $-\tan\theta'$ obtained as the real solution of (5.51) corresponding to a reflected wave and m obtained as $i\tau$, which corresponds either to a second reflected wave with $\tau = -\tan\theta''$, (5.31) being the relevant solution, or to the complex solution associated with a surface wave when m has positive real part, as appropriate. We use (5.29) and note that $\tau = -im$ ranges through real and complex values as θ varies. This results in R' and R^* again being given by (5.41), but the coefficients in this case have the forms

$$a' = \epsilon^2 - \sigma(\epsilon^2+4) - 4\epsilon t' + 4t'^2, \quad a^* = \epsilon^2 - \sigma(\epsilon^2+4) - 4i\epsilon m - 4m^2,$$

$$b' = 2\epsilon(\epsilon^2+2) - [7\epsilon^2 + 8 + \sigma(\epsilon^2+4)]t' + 8\epsilon t'^2 - 4t'^3 + (2t^2 + 2\epsilon t + \epsilon^2 + 2)^2 t'/(1+t^2),$$

$$b^* = 2\epsilon(\epsilon^2+2) - [7\epsilon^2+8+\sigma(\epsilon^2+4)]im - 8\epsilon m^2 + 4im^3 + (2t^2+2\epsilon t+\epsilon^2+2)^2 im/(1+t^2),$$

$$d = \epsilon^2 - \sigma(\epsilon^2+4) + 4\,\epsilon\,t + 4t^2,$$

$$e = -2\epsilon\,(\epsilon^2+2) - [7\epsilon^2+8+\sigma(\epsilon^2+4)]t - 8\epsilon t^2 - 4t^3 + (2t^2+2\epsilon t+\epsilon^2+2)^2 t/(1+t^2), \tag{5.54}$$

instead of (5.42), where again we have set $t' = \tan\theta'$. The solutions for R' and R^* are then given by (5.44) with (5.54). The values of $\tan\theta'$ and m are obtained from the solution of (5.51) but their explicit expressions are too complicated to be given here. For the special case $\epsilon = 0$ $(\lambda = 1)$ the relevant solutions are given by $t' = t$, $m = 1$, and it follows that $|R'| = 1$ and $|R^*|$ is again given by (5.50).

The problem now is to calculate $|R'|$ and $|R^*|$ for a range of values of λ (≥ 1) and σ as functions of θ, taking account of the fact that solutions of (5.51) for τ may be real or complex. The results are described in Section 5.4.2.

5.4 Numerical results

5.4.1 Case A: $2\beta = \alpha + \gamma$

Recalling that θ is subject to (5.23) and that α_0 depends on ϵ, it is convenient to display $|R'|$ and $|R^*|$ as functions of θ for the range $0 \leq \theta \leq \pi$ in each case by superimposing the plot for $-\alpha_0 \leq \theta \leq 0$ to the right of that for $0 \leq \theta \leq \pi - \alpha_0$ and noting the continuity at $\theta = \pi - \alpha_0$. All the figures have been produced using [22].

Since $|R'| = 1$ for $\lambda = 1$ and $|R'|$ is independent of $\overline{\sigma}_2$, we plot, in Fig. 5.5, $|R'|$ as a function of θ for a series of values of $\lambda > 1$. This shows, in particular, that as λ increases the maximum value of $|R'|$ increases but $|R'|$ becomes more and more concentrated in a narrow band of angles close to normal incidence.

The corresponding behaviour of $|R^*|$, which depends on $\overline{\sigma}_2$, is shown in Figs

5.6–5.10, each figure being associated with a fixed value of λ and displaying the effect of varying $\overline{\sigma}_2$. The values of $\overline{\sigma}_2$ are chosen so as to be consistent with the stability inequalities

$$1 - \lambda - \lambda^2 - \lambda^3 < \overline{\sigma}_2 < 1 + \lambda - \lambda^2 + \lambda^3 \tag{5.55}$$

obtained in [5]. In view of (5.40), it is worth noting that (5.55) can be re-cast as the pair of inequalities

$$-\lambda - \lambda^3 < \overline{\sigma}_{22} < \lambda + \lambda^3 \tag{5.56}$$

restricting the normal stress.

Figure 5.6 shows $|R^*|$ for $\lambda = 1$ based on equation (5.50), and this provides a basis for comparison in order to highlight the effect of simple shear on the magnitude of the surface wave. Note that the plot is symmetric about the value $\theta = \pi/2$, while Figs 5.7–5.10 show the departure from this symmetry. The dependence on θ shown in Fig. 5.6 has the same nature as that occurring in the case of pure homogeneous strain in [17].

Figures 5.7–5.10 are for $\lambda = 1.25$, 1.5, 2 and 3 respectively. In each case $|R^*|$ is calculated from (5.46) with (5.47) and is plotted separately for each of a set of values of $\overline{\sigma}_2$ within the range defined by (5.55). These figures illustrate the separate influences of λ and $\overline{\sigma}_2$ on the nature of $|R^*|$. We note that the maximum value of $|R^*|$, like that of $|R'|$, increases with λ, and the strength of the surface wave is focussed more and more in a narrow band of incident angles as λ increases. This latter effect is less marked than for the reflected wave. The changes in the vertical scale in each of Figs 5.5–5.10 should be noted.

The figures confirm that $|R^*|$ vanishes at $\theta = \pi/2$ in each case. Depending on the values of λ and $\overline{\sigma}_2$, it also vanishes at either one or three other values of θ according to whether (5.48) has one or three real solutions.

If the incident wave propagates parallel to the surface, conventionally the situation of the grazing incidence, then $t = 0$ and equations (5.45) and (5.46) reduces to

$$|R'| = 1/\sqrt{1 + 4\epsilon^2} \tag{5.57}$$

and

$$|R^*| = \frac{|2\epsilon(\epsilon^2 - \sigma - \sigma^2)|}{\sqrt{(1 + 4\epsilon^2)[(\sigma^2 + \epsilon^2)^2 + \epsilon^2(2\sigma + 1)^2]}}. \tag{5.58}$$

Likewise, if the reflected wave propagates parallel to the surface (grazing reflection) then $t' = 0$ and we have

$$|R'| = \sqrt{1 + 4\epsilon^2}, \tag{5.59}$$

and

$$|R^*| = \frac{|2\epsilon(\epsilon^2 - \sigma - \sigma^2)|}{\sqrt{(\sigma^2 + \epsilon^2)^2 + \epsilon^2(2\sigma + 1)^2}}. \tag{5.60}$$

An alternative viewpoint is to regard grazing incidence as corresponding to the situation in which the time-averaged energy flux is parallel to the boundary. This, however, leads to $t' = -t = \epsilon$, $c' = c$, $R' = -1, R^* = 0$, and hence, from (5.29), ψ vanishes. Thus, grazing incidence is not supported by the boundary conditions. An exception to this arises in the special case $\epsilon = 0$ with $\overline{\sigma}_2 = 1$ ($\sigma = 0$), as shown in the context of pure homogeneous strain in [17]. In this case a shear body wave may propagate parallel to the boundary, and it may be deduced from (5.41) with (5.42)

that R' is arbitrary. A similar situation arises in respect of grazing reflection when this is defined in terms of the time-averaged energy flux. These results are reflected in Figs 5.7–5.10. In these figures the grazing angles of incidence $(\pi - \alpha_0)$ for which $|R^*| = 0$ are respectively 2.72, 2.44, 2.16, 1.93. Reference to Fig. 5.5 shows that for the first three of these $|R'| = 1$ in (b), (c), (d) respectively, while the fourth has no counterpart in Fig. 5.5.

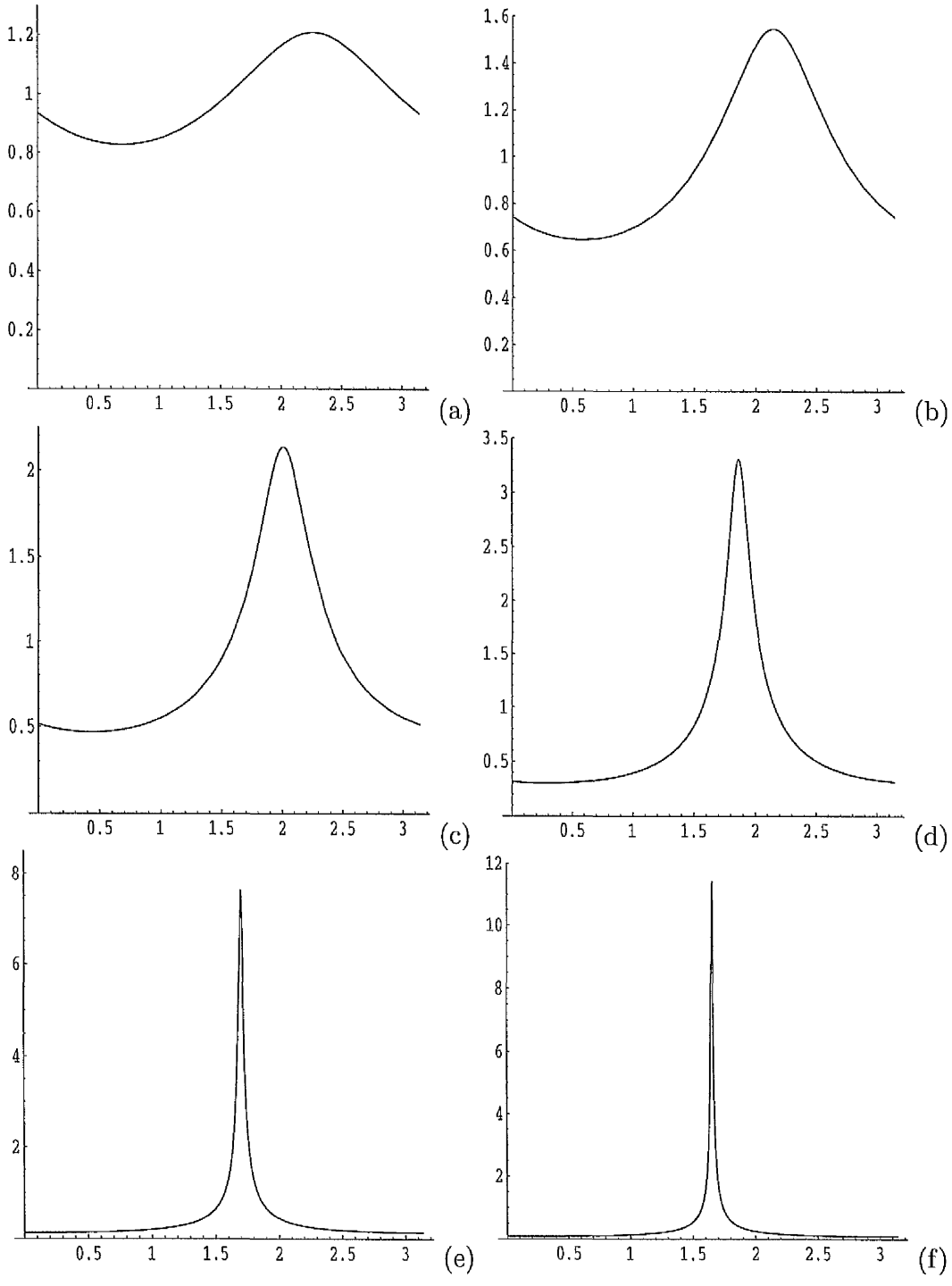

Figure 5.5: Plots of $|R'|$ (independent of $\overline{\sigma}_2$) against θ for the following values of λ: (a) 1.1, (b) 1.25, (c) 1.5, (d) 2, (e) 4, (f) 6.

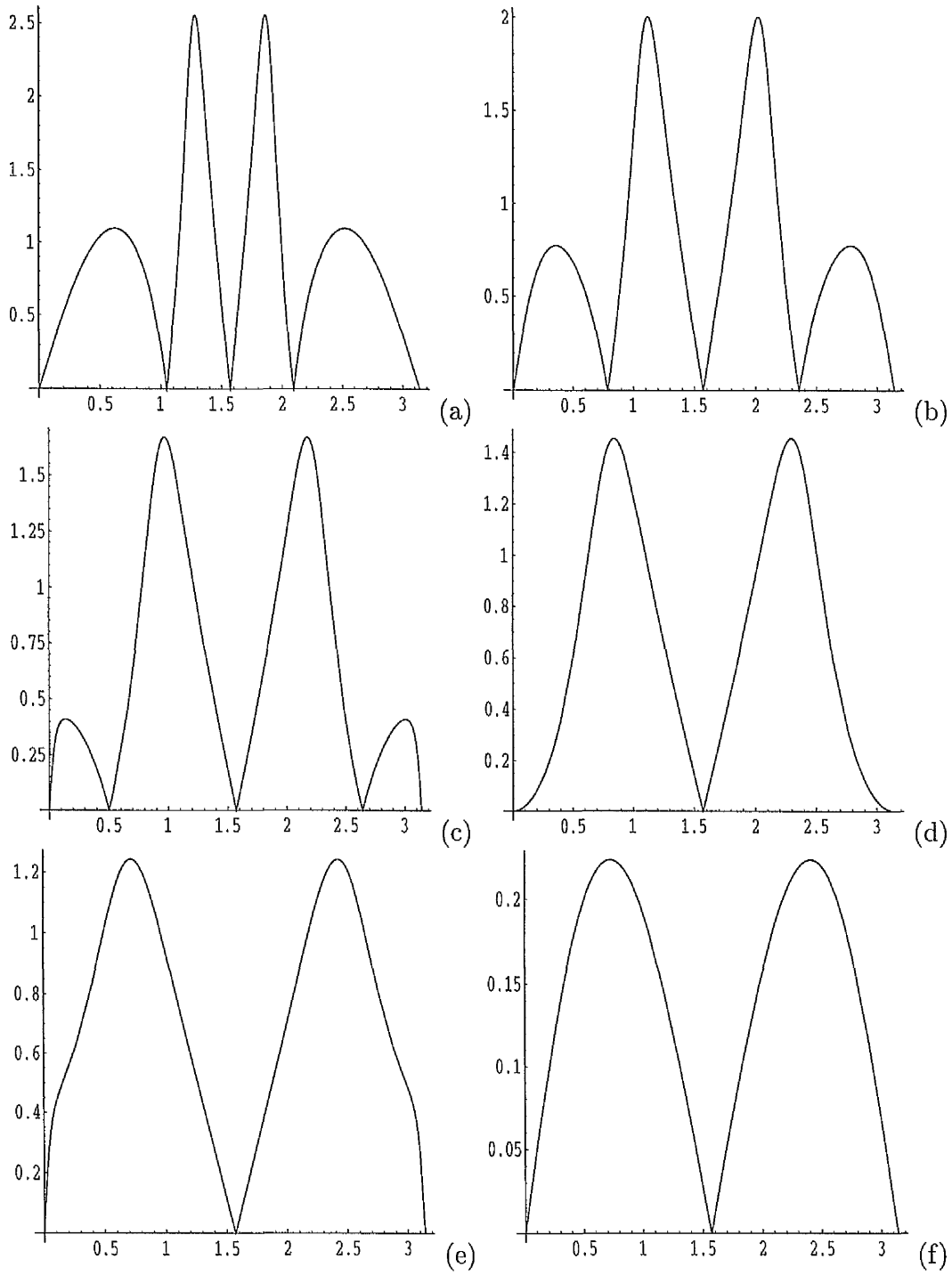

Figure 5.6: Plots of $|R^*|$ against θ for $\lambda = 1$ and the following values of $\overline{\sigma}_2$: (a) -2, (b) 0, (c) 0.7, (d) 1, (e) 1.2, (f) 1.8.

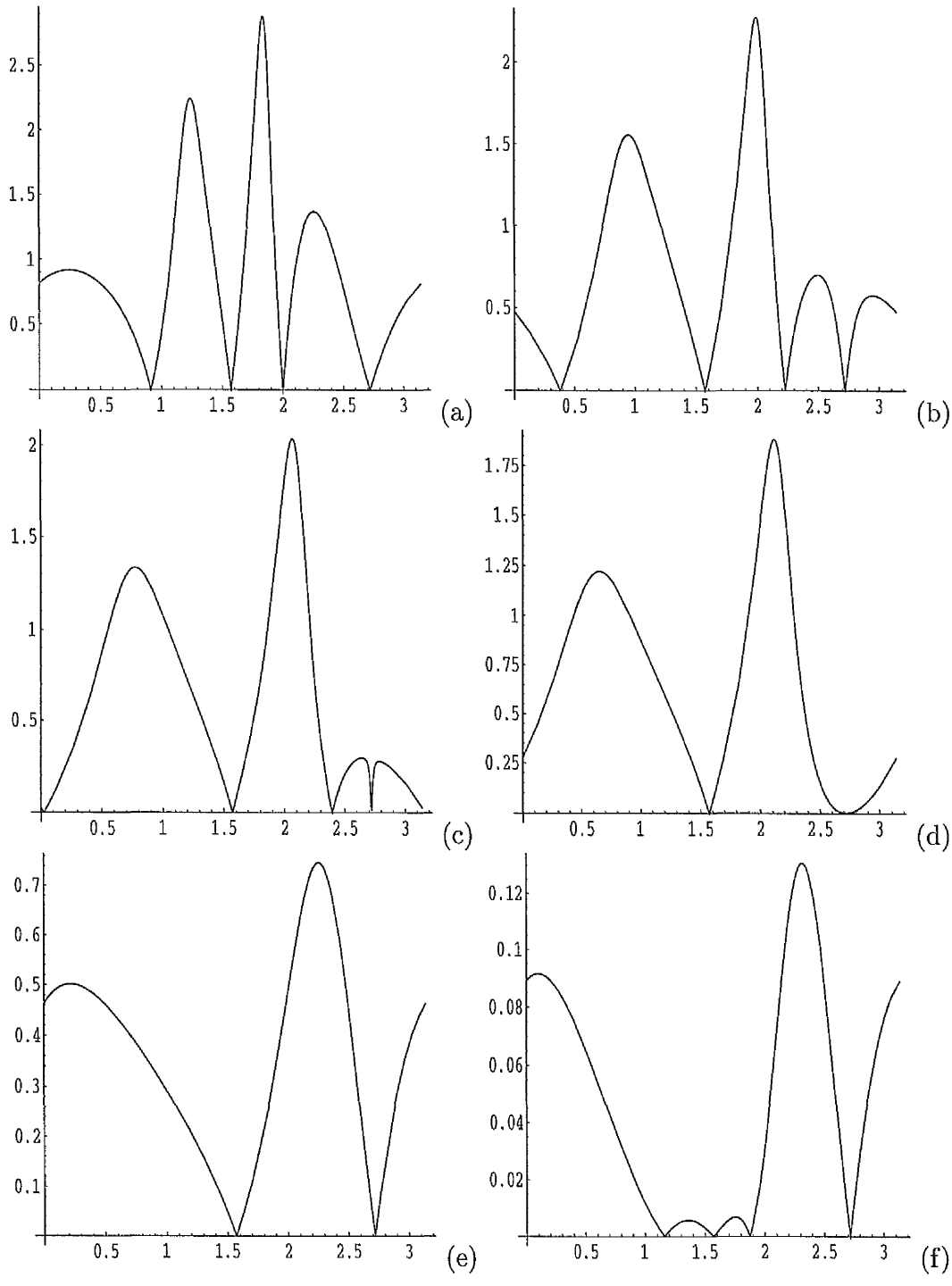

Figure 5.7: Plots of $|R^*|$ against θ for $\lambda = 1.25$ and the following values of $\overline{\sigma}_2$: (a) -3.5, (b) 0, (c) 0.7, (d) 1, (e) 2, (f) 2.6.

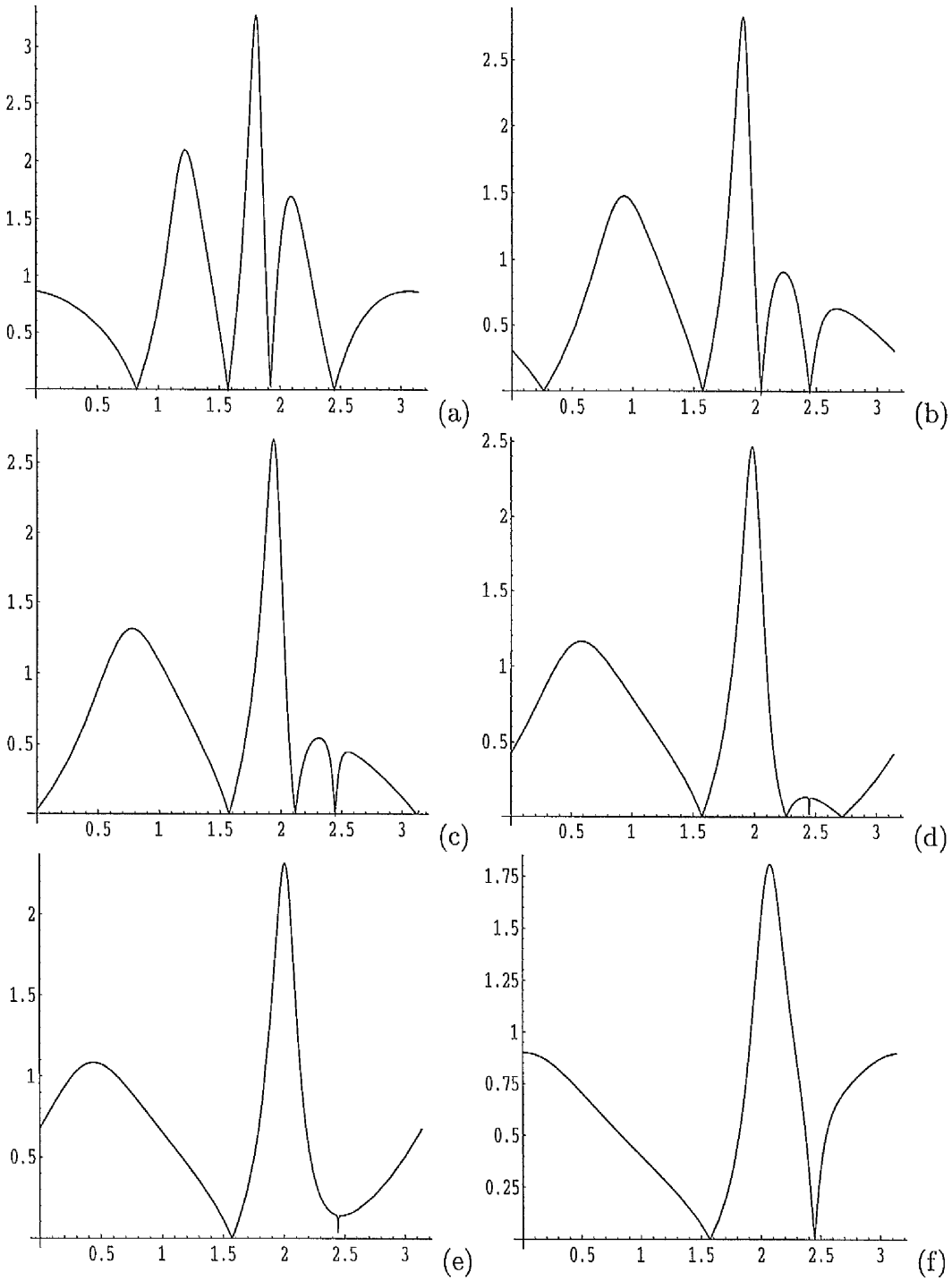

Figure 5.8: Plots of $|R^*|$ against θ for $\lambda = 1.5$ and the following values of $\overline{\sigma}_2$: (a) -6, (b) -1, (c) 0, (d) 0.8, (e) 1.2, (f) 2.

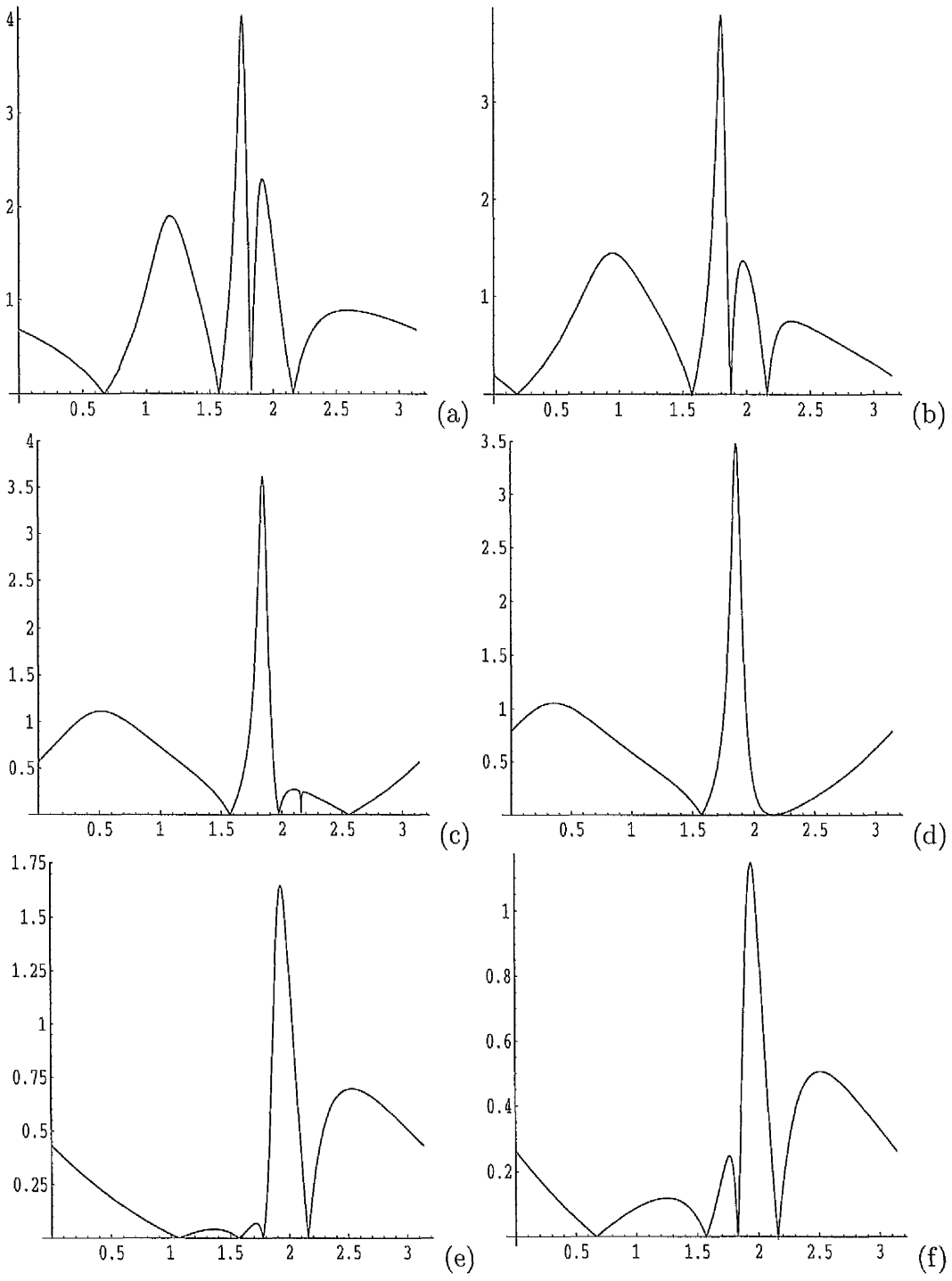

Figure 5.9: Plots of $|R^*|$ against θ for $\lambda = 2$ and the following values of $\overline{\sigma}_2$: (a) -13, (b) -5, (c) 0, (d) 1, (e) 5.9, (f) 7.

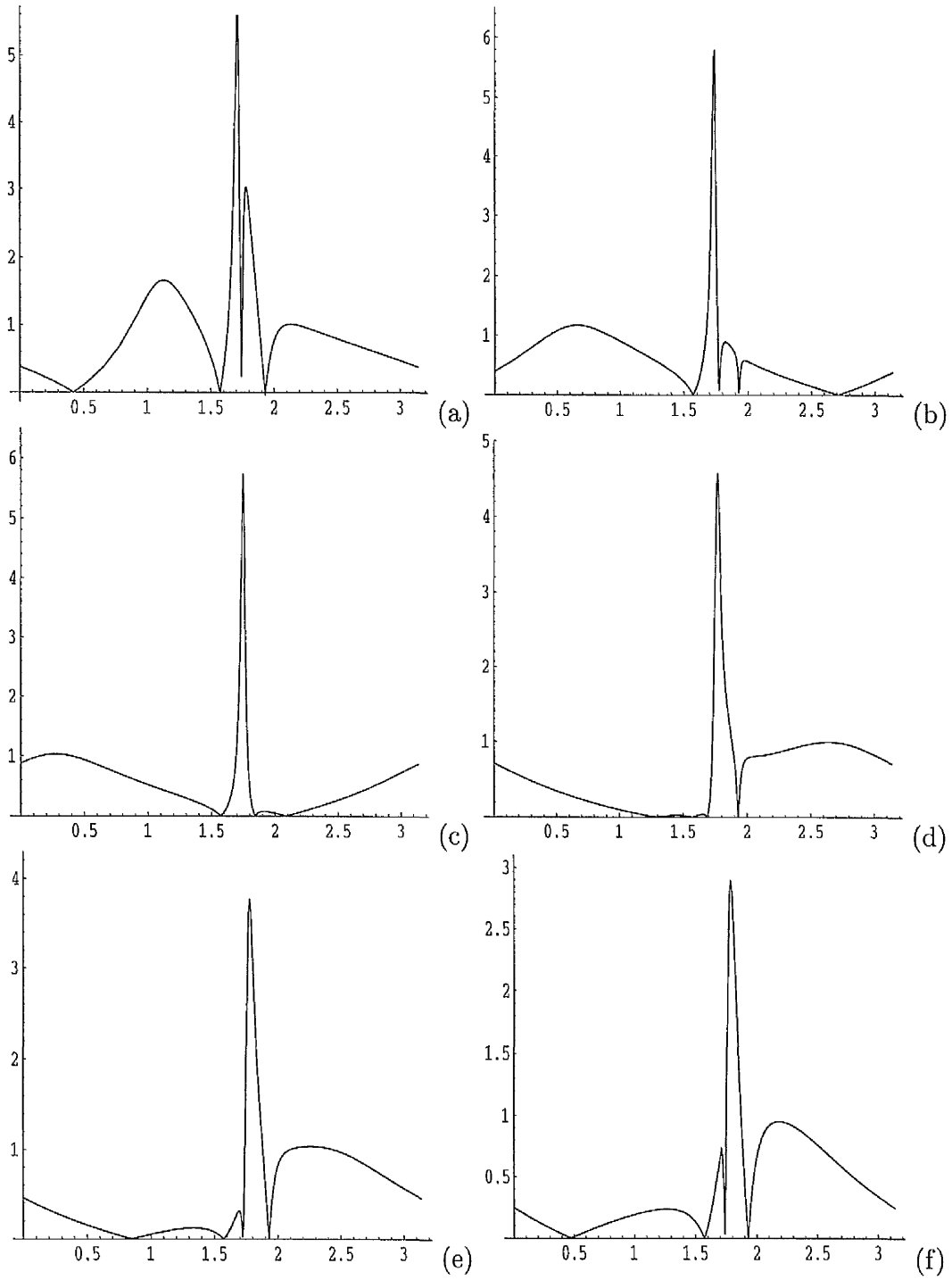

Figure 5.10: Plots of $|R^*|$ against θ for $\lambda = 3$ and the following values of $\overline{\sigma}_2$: (a) -35, (b) -9, (c) 0, (d) 12, (e) 17, (f) 22.

5.4.2 Case B: $\beta = \sqrt{\alpha\gamma}$

Here, we illustrate the results for two separate values of λ. First, for $\lambda = 3$, the slowness curve has the form shown in Fig. 5.2(c) and there is just one reflected wave for each possible angle of incidence. Second, for $\lambda = 8$, the slowness curve is that shown in Fig. 5.4 and there are four separate ranges of incident angles for which two reflected waves are generated.

For $\lambda = 3$ the results are displayed for $0 \leq \theta \leq \pi$ on the same basis as described in Section 5.4.1, and there is a single angle, α_0 say (approximately 1.1), where the time-averaged energy flux is parallel to the positive $\overline{s}_1$ direction. Figure 5.11 shows the plot of $|R'|$ against θ. The expression for $|R'|$ is much more complicated than that given in Section 5.4.1 and is not given explicitly here. Using Mathematica, however, we have shown that it is independent of $\overline{\sigma}_2$. The character of $|R'|$ shown in Fig. 5.11 is very similar to that shown in Fig. 5.5(e), which corresponds to $\lambda = 4$. Just as for the material considered in Section 5.4.1, $|R^*|$ *does* depend on the pre-stress. In Fig. 5.12 we therefore plot $|R^*|$ against θ for a series of values of $\overline{\sigma}_2$ subject to the stability inequalities

$$1 - 3\lambda^2 < \overline{\sigma}_2 < 1 + \lambda^2 \tag{5.61}$$

obtained in [6] for materials with $\beta = \sqrt{\alpha\gamma}$. In terms of the normal stress, the stability inequalities (5.61) may be written

$$-2\lambda^2 < \overline{\sigma}_{22} < 2\lambda^2. \tag{5.62}$$

In general, the behaviour of $|R^*|$ is similar to that shown in Fig. 5.10, and we note that $|R^*|$ always vanishes at $\theta = \pi/2$. Recalling that, for the material

considered in Section 5.4.1, $|R^*|$ vanishes at one or three other values of θ, we find, by contrast, that for the material considered here it can vanish at many more points depending on $\overline{\sigma}_2$, as exemplified in Fig. 5.12 (c). In particular, as can be seen in Fig. 5.12, whatever the value of $\overline{\sigma}_2$, $|R^*|$ vanishes where $\theta = \pi - \alpha_0 \simeq 2.04$, which corresponds to the angle of incidence at which the time-averaged energy flux is parallel to the half-space boundary.

The value $\lambda = 8$, although rather large, has been chosen so that the distinct ranges of angles where two reflected waves exist can be identified clearly.

From Fig. 5.4 we recall that there are six points on the slowness curve at which the time-averaged energy flux vector is parallel to the $\overline{s}_1$ axis. Let the position vectors of the three of these points with positive $\overline{s}_1$ make angles $-\alpha_1$, α_2, α_3 with the positive $\overline{s}_1$ axis, where $\alpha_1 > 0$, $\alpha_3 > \alpha_2 > 0$. Then, for the direction $(\cos\theta, \sin\theta)$ to be associated with an incident wave, θ must lie in one of the three (disjoint) intervals

$$(-\alpha_1, \alpha_2), \ (\alpha_3, \pi - \alpha_1), \ (\pi + \alpha_2, \pi + \alpha_3), \tag{5.63}$$

the total interval length being π. The end points of these intervals are associated with grazing incidence in the energy flux sense. For $\lambda = 8$ the values of α_1, α_2, α_3 are calculated using (5.27) as

$$\alpha_1 \simeq 1.394, \ \alpha_2 \simeq 0.257, \ \alpha_3 \simeq 1.385. \tag{5.64}$$

Let vertical tangents be drawn to the slowness curve at points corresponding to α_2, α_3, $\pi + \alpha_2$, $\pi + \alpha_3$. These tangents cut the slowness curve at two points each. We select one such point for each tangent, namely those whose position vectors make angles $-\theta_1$, θ_2, θ_3, θ_4 respectively with the positive $\overline{s}_1$ direction, where

$\theta_1 > 0,\ \theta_4 > \theta_3 > \theta_2 > 0$. Then,

$$-\alpha_1 < -\theta_1 < 0 < \alpha_2 < \alpha_3 < \theta_2 < \theta_3 < \theta_4 < \pi - \alpha_1$$

and, for each of the four intervals

$$(-\theta_1, \alpha_2),\ (\alpha_3, \theta_2),\ (\theta_3, \theta_4),\ (\pi + \alpha_2, \pi + \alpha_3), \tag{5.65}$$

two reflected waves are possible. For $\lambda = 8$, the values of $\theta_1,\ \theta_2,\ \theta_3,\ \theta_4$ are

$$\theta_1 \simeq 0.742,\ \theta_2 \simeq 1.528,\ \theta_3 \simeq\ 1.596,\ \theta_4 \simeq 1.610. \tag{5.66}$$

A single reflected wave arises together with a surface wave in each of the intervals

$$(-\alpha_1, -\theta_1),\ (\theta_2, \theta_3),\ (\theta_4, \pi - \alpha_1), \tag{5.67}$$

while there are gaps (α_2, α_3) and $(\pi - \alpha_1, \pi + \alpha_2)$, not covered by (5.65) or (5.67), for which there can be no incident wave.

As for the previous examples it is convenient to display results on the interval $(0, \pi)$. For this purpose the results for $(-\alpha_1, 0)$ and $(\pi + \alpha_2, \pi + \alpha_3)$ are inserted into the gaps $(\pi - \alpha_1, \pi)$ and (α_2, α_3) respectively. This ensures continuity of R' and R^* at α_2 and α_3 and of $|R'|$ and $|R^*|$ at $\pi - \alpha_1$. In view of the grazing interpretation at these points, we have $R' = -1,\ R^* = 0$ at $\alpha_2,\ R' = 0,\ R^* = -1$ at α_3 and $|R'| = 1,\ |R^*| = 0$ at $\pi - \alpha_1$. The value of $R'\,(R^*)$ at $\theta = 0$ is the same as that of $R^*\,(R')$ at $\theta = \pi$.

This superposition reduces to three, namely

$$(0, \theta_2),\ (\theta_3, \theta_4),\ (\pi - \theta_1, \pi), \tag{5.68}$$

the number of intervals for which two reflected waves are possible. The two gap intervals

$$(\theta_2, \theta_3),\ (\theta_4, \pi - \theta_1) \tag{5.69}$$

are then associated with a combination of one reflected wave and a surface wave.

When there are two reflected waves, R' and R^* are real. Otherwise, they are complex. We therefore plot the results by showing R' and R^* for the intervals (5.68) and $|R'|$ and $|R^*|$ for (5.69), recalling that $|R'|$ and $|R^*|$ are continuous across the boundaries between intervals.

Our calculations show that $|R'|$ is independent of $\overline{\sigma}_2$ when R' is complex, as in the cases discussed earlier, but, when real, R' shows some slight dependence on $\overline{\sigma}_2$. On the other hand, when R^* is complex $|R^*|$ does depend on $\overline{\sigma}_2$, although its character does not change significantly over a wide range of values of $\overline{\sigma}_2$. Again, $|R^*|$ vanishes at $\theta = \pi/2$. It also vanishes at $\theta = \pi - \alpha_1 \simeq 1.75$, which corresponds to grazing incidence, and at α_2, while R' vanishes at α_3, as noted earlier.

These features are apparent in Figs 5.13–5.15, in each of which (a)–(f) correspond respectively to the intervals $(0, \alpha_3)$, (α_3, θ_2), (θ_2, θ_3), (θ_3, θ_4), $(\theta_4, \pi - \theta_1)$, $(\pi - \theta_1, \pi)$. The values of R' and R^* are plotted in (a), (b), (d) and (f) and those of $|R'|$ and $|R^*|$ in (c) and (e). Figures 5.13 and 5.14 show R^* and $|R^*|$ for $\overline{\sigma}_2 = -120$ and 30 respectively, these two values illustrating the main effects of changes in $\overline{\sigma}_2$, which are evident in (b) and (d)–(f). Figure 5.15 shows R' and $|R'|$ for the representative value $\overline{\sigma}_2 = 30$ of the pre-stress. Changes in $\overline{\sigma}_2$ have no effect on $|R'|$ and very little effect on R'. Note that the horizontal scales in (a)–(f) are very different and, in particular, the intervals corresponding to (c) and (d) are very short. The fine

detail of the behaviour exemplified would not show up clearly on a smaller scale.

The results in Figs 5.13, 5.14 are combined as plots of $|R^*|$ on the single interval $(0, \pi)$ in Figs 5.16 (a), (b) respectively in order to facilitate comparison with the results shown in Fig. 5.12. The main features are seen to be very similar to those in Fig.5.12. Similarly, the results in Fig. 5.15 are combined as a single plot of $|R'|$ in Fig. 5.17. The concentrated spike is akin to that shown in Fig. 5.11 while other features are different from those in Fig. 5.11.

The differences which arise for $\lambda = 8$ as compared with $\lambda = 3$ are due essentially to conversion of a surface wave into a second reflected wave.

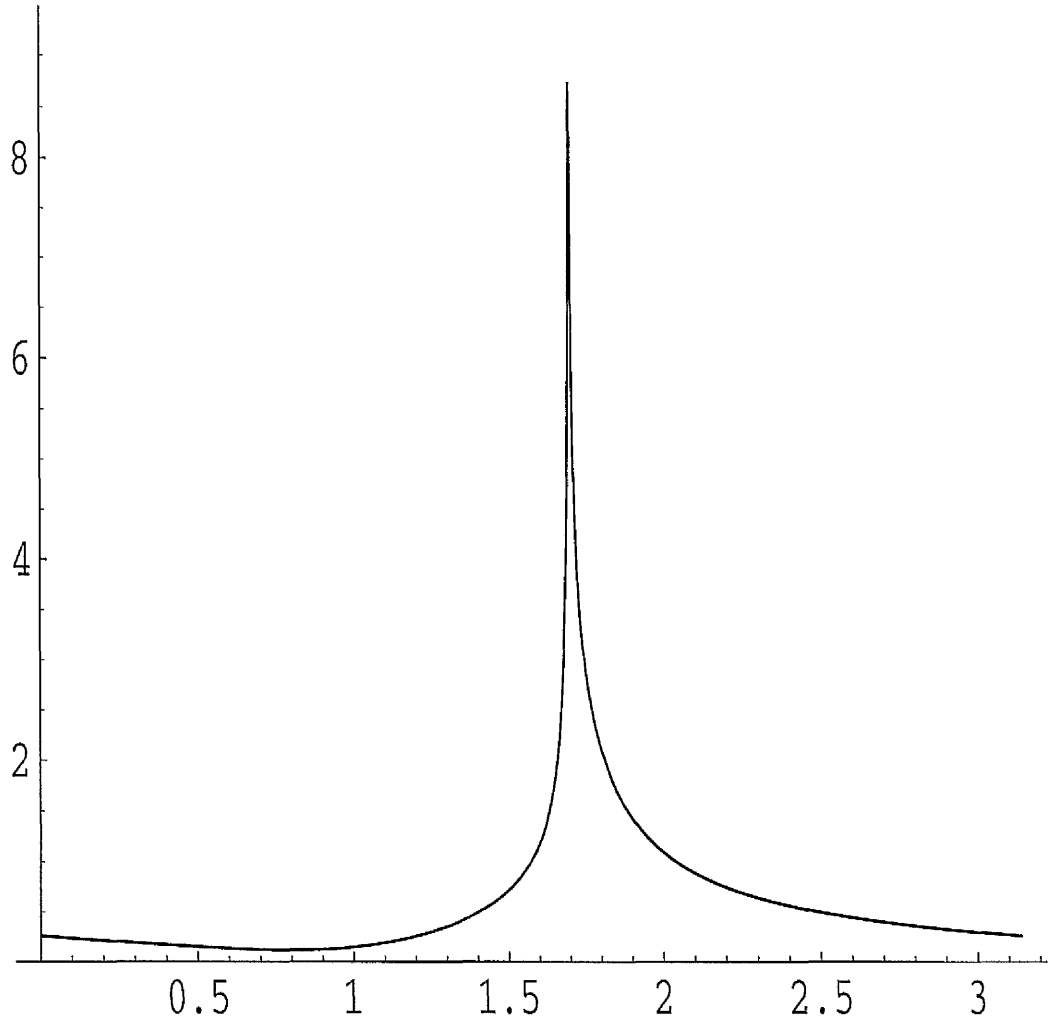

Figure 5.11: Plot of $|R'|$ against θ for $\beta = \sqrt{\alpha\gamma}$ with $\lambda = 3$ (independent of $\overline{\sigma}_2$).

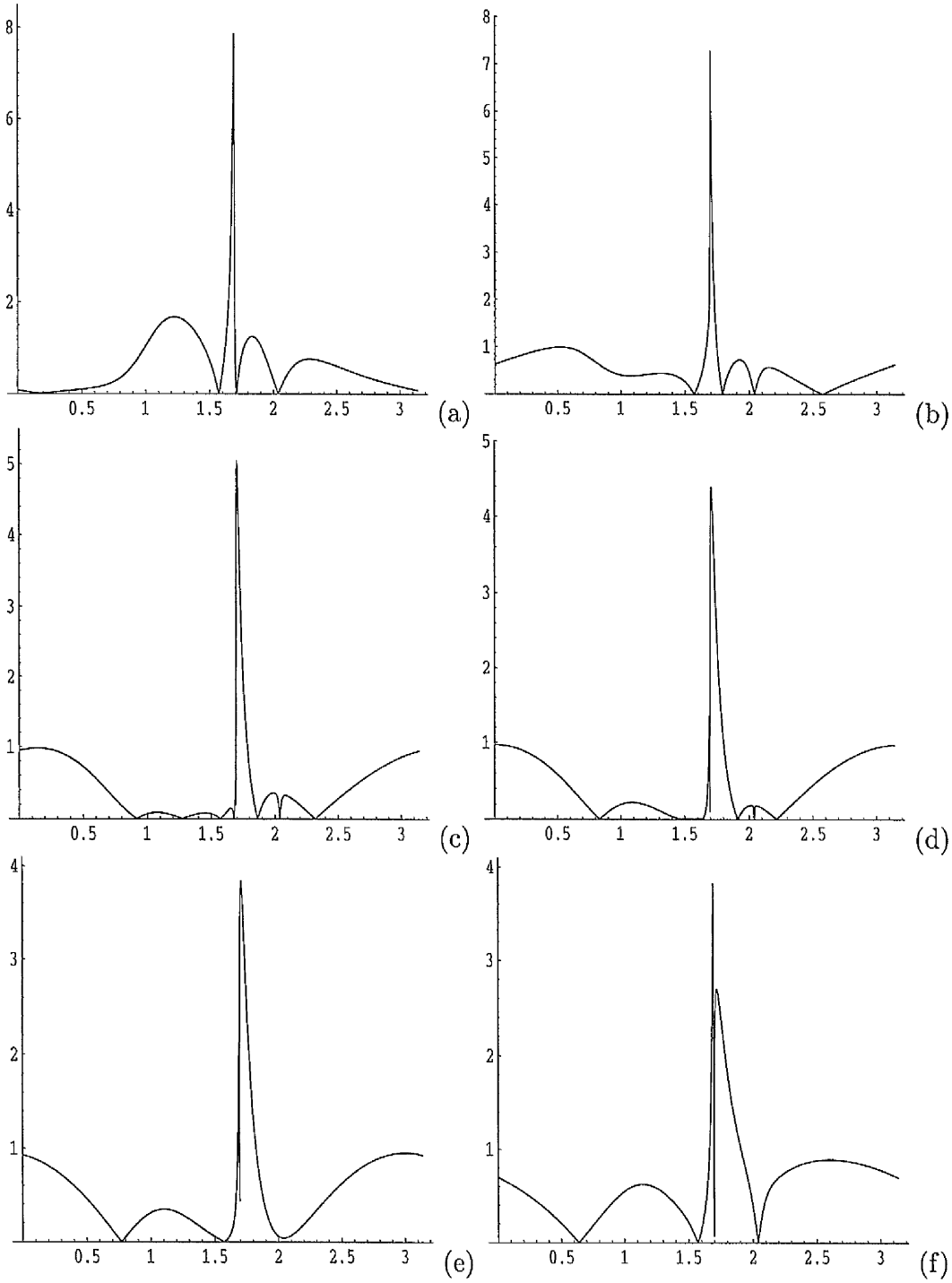

Figure 5.12: Plots of $|R^*|$ against θ for $\beta = \sqrt{\alpha\gamma}$ with $\lambda = 3$ and the following values of $\overline{\sigma}_2$: (a) -24, (b) -10, (c) -4, (d) -2, (e) 0, (f) 5.

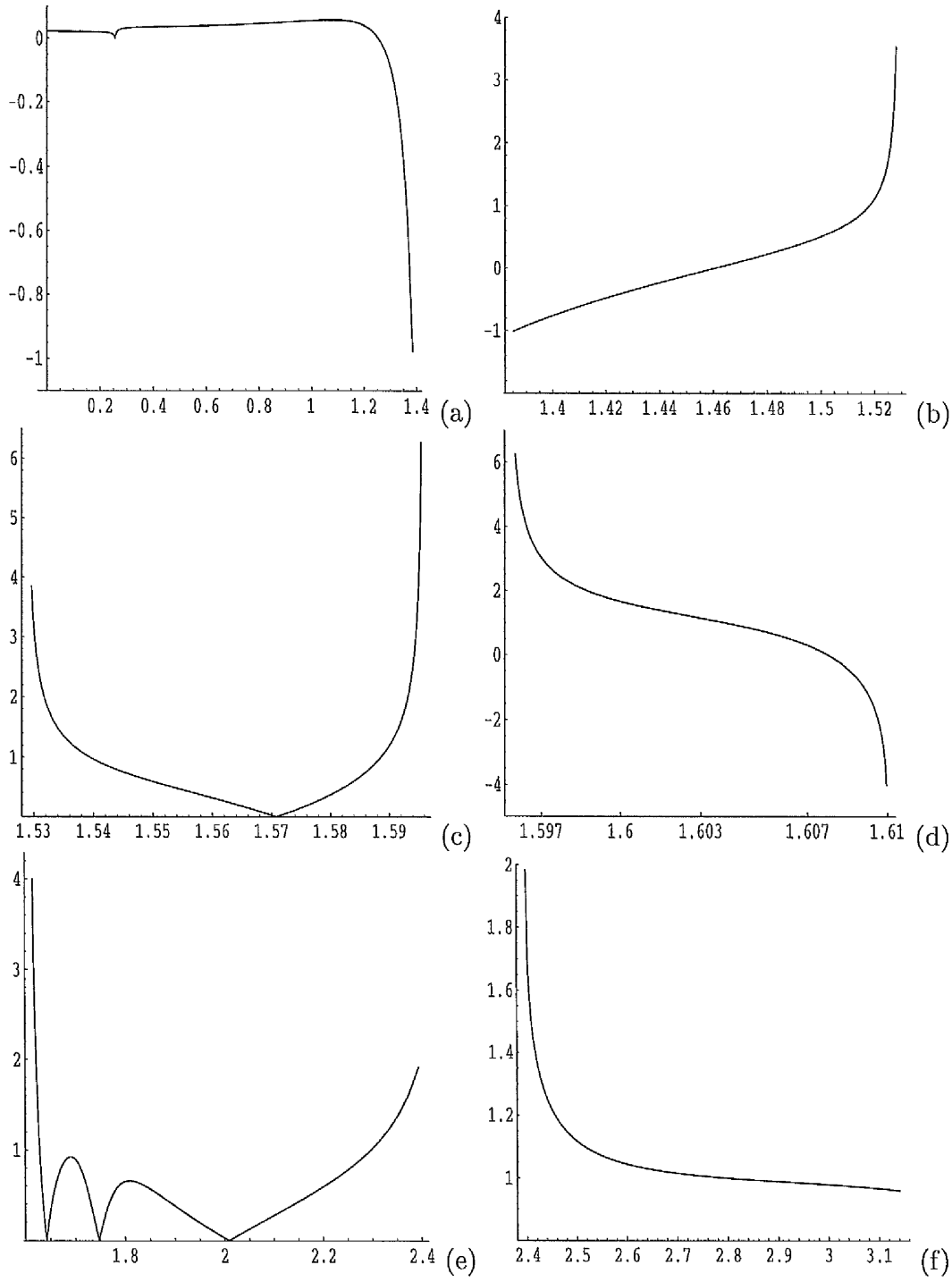

Figure 5.13: Plots of R^* (reflected wave) against θ in (a), (b), (d), (f) and of $|R^*|$ (surface wave amplitude) in (c), (e) for $\beta = \sqrt{\alpha\gamma}$ with $\lambda = 8$ and $\overline{\sigma}_2 = -120$.

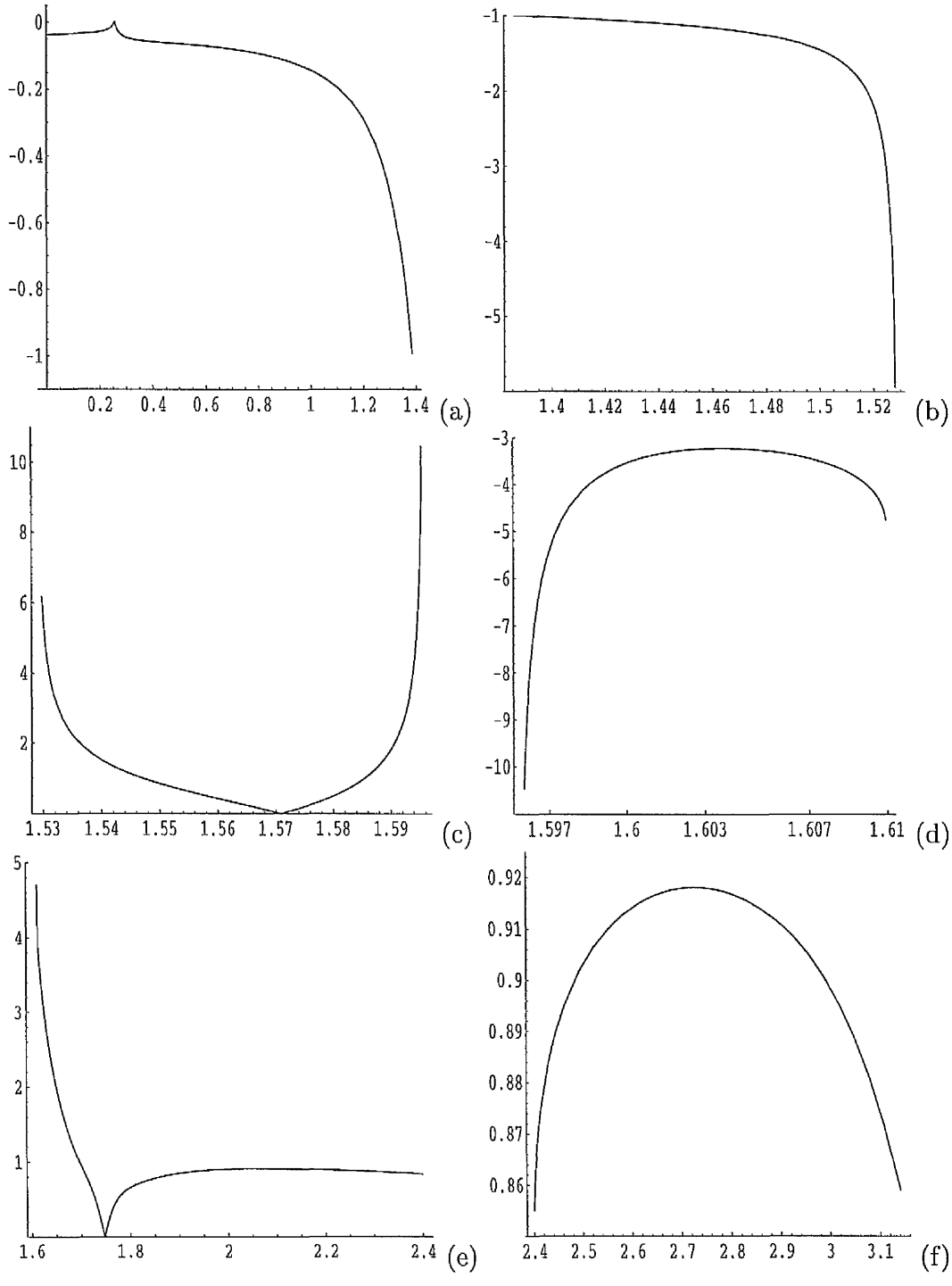

Figure 5.14: Plots of R^* (reflected wave) against θ in (a), (b), (d), (f) and of $|R^*|$ (surface wave amplitude) in (c), (e) for $\beta = \sqrt{\alpha\gamma}$ with $\lambda = 8$ and $\overline{\sigma}_2 = 30$.

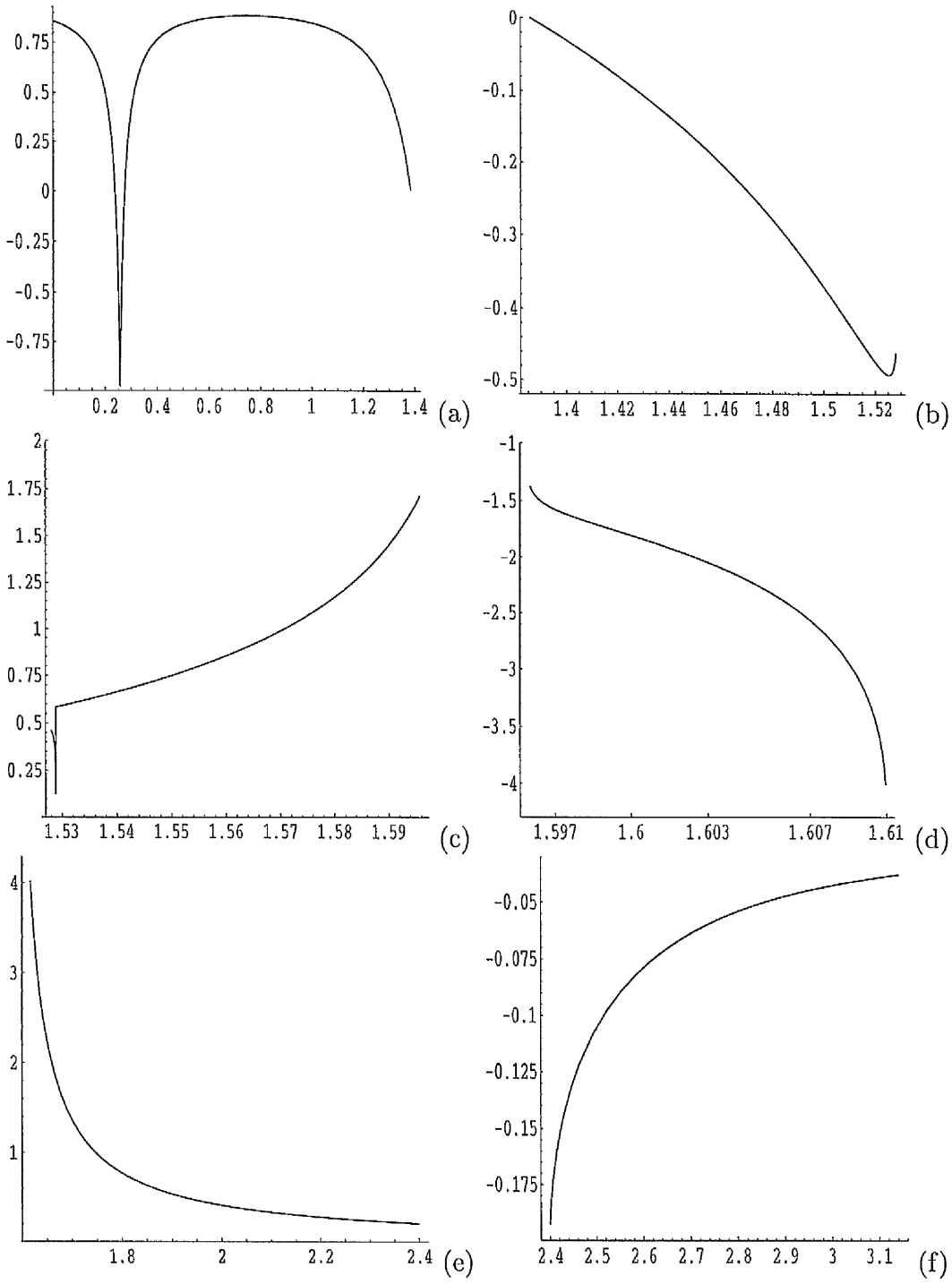

Figure 5.15: Plots of R' (reflected wave) against θ in (a), (b), (d), (f) and of $|R'|$ (reflected wave amplitude) in (c), (e) for $\beta = \sqrt{\alpha\gamma}$ with $\lambda = 8$ and $\overline{\sigma}_2 = 30$.

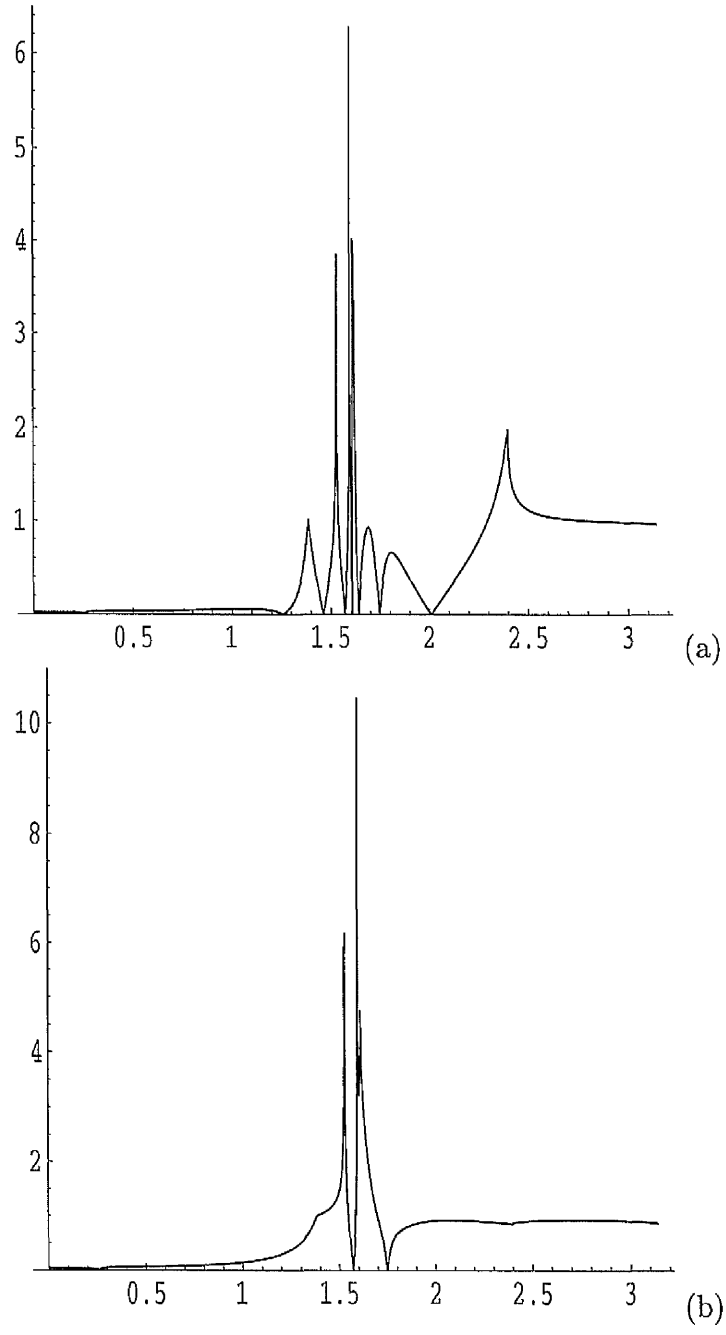

Figure 5.16: Plots of $|R^*|$ against θ $(0 \leq \theta \leq \pi)$ for $\beta = \sqrt{\alpha\gamma}$ with $\lambda = 8$ and the following values of $\overline{\sigma}_2$: (a) -120, (b) 30.

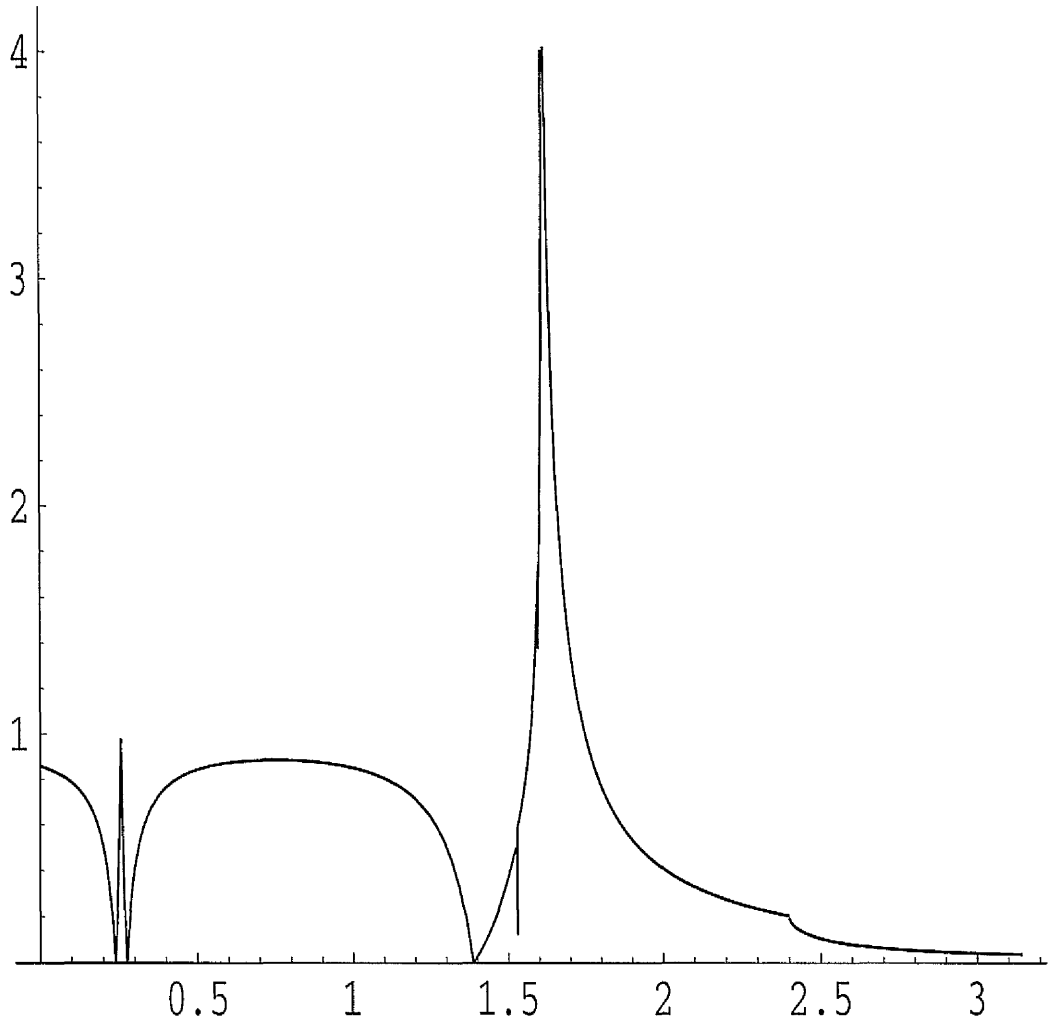

Figure 5.17: Plot of $|R'|$ against θ $(0 \leq \theta \leq \pi)$ for $\beta = \sqrt{\alpha\gamma}$ with $\lambda = 8$ and $\overline{\sigma}_2 = 30$.

Chapter 6

Reflection and transmission of plane waves at a shear-twin interface

In this chapter we shall extend the analysis done in chapter 5 and discuss the effect of *simple shear* on the reflection and transmission of plane waves at the boundary between two half-spaces of incompressible elastic material, and, in particular, two half-spaces which form a twin in the sense that equal and opposite simple shears are applied to the two half-spaces.

6.1 Basic equations

In view of (2.26) and (2.27) it is convenient to define $\hat{W}(\lambda)$ by

$$\hat{W}(\lambda) = W(\lambda, \lambda^{-1}, 1) \equiv \hat{W}(\lambda^{-1}), \tag{6.1}$$

so that from (2.46) it follows that

$$\sigma_1 - \sigma_2 = \lambda_1 W_1 - \lambda_2 W_2 = \lambda \hat{W}'(\lambda), \tag{6.2}$$

where the prime signifies differentiation with respect to argument. With reference to (2.26) and (2.27) we may also regard the strain energy as a function of ϵ, and we write

$$w(\epsilon) = \hat{W}(\lambda), \tag{6.3}$$

and hence

$$\lambda \hat{W}'(\lambda) = \sqrt{4 + \epsilon^2}\, w'(\epsilon). \tag{6.4}$$

The simple shear of a block with $\epsilon > 0$ (given by 2.26) is depicted in Fig. 6.1(a) and the disposition of the principal axes $\mathbf{v}^{(1)}$ and $\mathbf{v}^{(2)}$ in Fig. 6.1(c). Figures 6.1(b), (d) show corresponding results for $\epsilon < 0$.

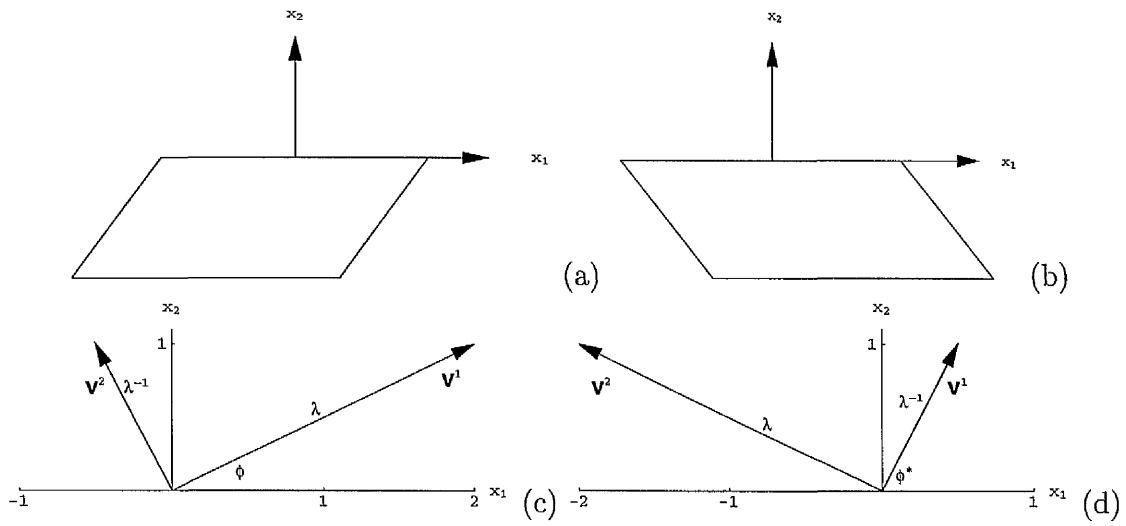

Figure 6.1: Simple shear with (a) $\epsilon > 0$, (b) $\epsilon < 0$. Orientation of the Eulerian principal axes and the associated stretches: (c) $\epsilon > 0$, (d) $\epsilon < 0$.

In order to consider the simple shear depicted in Fig. 6.1(b) we set $\epsilon^* = -\epsilon$, with $\epsilon > 0$ the amount of shear corresponding to Fig. 6.1(a). Let $\phi^* \in [\pi/4, \pi/2)$ be the counterpart of ϕ, so that

$$\phi^* + \phi = \pi/2, \quad \tan 2\phi^* = 2/\epsilon^* = -2/\epsilon \tag{6.5}$$

and

$$\cos\phi^* = \sin\phi, \quad \sin\phi^* = \cos\phi. \tag{6.6}$$

The counterpart of λ is $\lambda^* = \lambda^{-1}$. It follows from (6.1) and (6.3) that

$$w(\epsilon^*) = w(-\epsilon) = w(\epsilon), \tag{6.7}$$

while from (2.46) we may deduce that

$$\sigma_1^* = \sigma_2, \quad \sigma_2^* = \sigma_1 \tag{6.8}$$

since p is independent of the direction of shear. It follows from (5.2) that

$$\sigma_{11}^* = \sigma_{11}, \quad \sigma_{12}^* = -\sigma_{12}, \quad \sigma_{22}^* = \sigma_{22}. \tag{6.9}$$

6.2 Superimposed incremental motions

With reference to the Eulerian axes, the equation of motion, for ψ' is given by (5.4). When referred to the Cartesian axes (5.4) can be expressed in terms of ψ and is given by (5.8).

On a surface $x_2 =$ constant the shear and normal components of the incremental nominal traction Σ_{21} and Σ_{22} respectively in the (x_1, x_2)-plane are given by (5.9) and (5.10).

In the case of the simple shear with $\epsilon > 0$ the expressions (5.9) and (5.10) are simplified to

$$(\epsilon^2+4)\frac{\Sigma_{21}}{\sqrt{\alpha\gamma}} = 2\epsilon(\overline{\beta}+1)\psi_{,12} + 2(\overline{\beta}+1)\psi_{,22} + \{\epsilon^2+2-2\overline{\beta}-\sigma(\epsilon^2+4)\}\psi_{,11} \tag{6.10}$$

and

$$-(\epsilon^2+4)\Sigma_{22,1} = \sqrt{\alpha\gamma}[\{2\overline{\beta}(\epsilon^2-1)+5(\epsilon^2+2)+\sigma(\epsilon^2+4)\}\psi_{,112} + 4\epsilon(\overline{\beta}+1)\psi_{,122}$$

$$+2(\overline{\beta}+1)\psi_{,222} - 2\epsilon\{\overline{\beta}-(\epsilon^2+3)\}\psi_{,111}] - \rho\ddot{\psi}_{,2}(\epsilon^2+4), \tag{6.11}$$

where

$$\overline{\beta} = \beta/\sqrt{\alpha\gamma} \tag{6.12}$$

and σ is given by (5.38).

From (2.65), (5.5) and (6.2) we see that

$$\lambda^{-2}\alpha = \lambda^2\gamma = \frac{\lambda^3\hat{W}'(\lambda)}{\lambda^4-1} = \frac{w'(\epsilon)}{\epsilon}, \quad 2\beta+2\gamma = \lambda^2\hat{W}''(\lambda) \tag{6.13}$$

and hence

$$2\beta = (4+\epsilon^2)w''(\epsilon) - \frac{2w'(\epsilon)}{\epsilon}. \tag{6.14}$$

Also

$$\sigma_1 - \sigma_2 = \alpha - \gamma = \lambda \hat{W}'(\lambda). \tag{6.15}$$

Hence, by (6.13),

$$\gamma^* = \alpha, \quad \alpha^* = \gamma, \quad \beta^* = \beta, \tag{6.16}$$

where α^*, β^*, γ^* are analogues of α, β, γ for $\epsilon^* = -\epsilon$.

6.3 Plane waves

We consider time-harmonic homogeneous plane waves of the form (2.75) with propagation condition given by (5.11). For the wave speed c to be real, the *strong ellipticity* condition, given by (2.77) is also assumed to hold.

Similarly, for an inhomogeneous plane wave of the form (5.12), the propagation condition is given by (5.13).

We consider two distinct cases corresponding to different relative values of the material parameters α, β, γ, which depend on W through (2.65) with (5.5).

Case A: $2\beta = \alpha + \gamma$

For this case the propagation conditions for homogeneous and inhomogeneous plane waves are given by (5.14) and (5.15) respectively.

In terms of the *slowness vector* (s_1, s_2) defined by (4.8) equation (5.14) becomes

$$\alpha(s_1 \cos\phi + s_2 \sin\phi)^2 + \gamma(s_1 \sin\phi - s_2 \cos\phi)^2 = \rho. \tag{6.17}$$

When the deformation is specialized to simple shear use of (2.29) enables (6.17) to be simplified to

$$(\epsilon^2+1)\overline{s}_1^2+2\epsilon\overline{s}_1\overline{s}_2+\overline{s}_2^2=1, \tag{6.18}$$

where the dimensionless slowness vector $(\overline{s}_1,\overline{s}_2)$ is defined by

$$(\overline{s}_1,\overline{s}_2)\equiv(s_1,s_2)\frac{1}{\sqrt{\overline{\rho}}}, \tag{6.19}$$

with

$$\overline{\rho}=\rho/\sqrt{\alpha\gamma}. \tag{6.20}$$

It is clear from (6.16) that (6.19) is unaffected by the change $\epsilon\to-\epsilon$. For this reason the definition (6.19) differs from (4.11).

Case B: $2\beta\neq\alpha+\gamma$

This case is exemplified by a strain-energy function satisfying (5.18). The propagation condition in this case is given by (5.19). In terms of the notation (6.19), the slowness curve has equation

$$[\lambda^2(\overline{s}_1\cos\phi+\overline{s}_2\sin\phi)^2+(\overline{s}_1\sin\phi-\overline{s}_2\cos\phi)^2]^2=\lambda^2({\overline{s}_1}^2+{\overline{s}_2}^2) \tag{6.21}$$

and for simple shear reduces to

$$[(\epsilon^2+2){\overline{s}_1}^2+2\epsilon\overline{s}_1\overline{s}_2+2{\overline{s}_2}^2]^2=(\epsilon^2+4)({\overline{s}_1}^2+{\overline{s}_2}^2). \tag{6.22}$$

Similarly, for this case, equation (5.13) becomes

$$\lambda^2\{(\epsilon^2+2)^2-4im(\epsilon^2+2)\epsilon-8m^2(\epsilon^2+1)+8im^3\epsilon+4m^4\}=(1-m^2)(\epsilon^2+4)\rho c^{*2}/\gamma. \tag{6.23}$$

We now show graphically the dependence of the slowness curves on λ for both classes of materials in $(\overline{s}_1,\overline{s}_2)$-space with reference to (6.18) and (6.22).

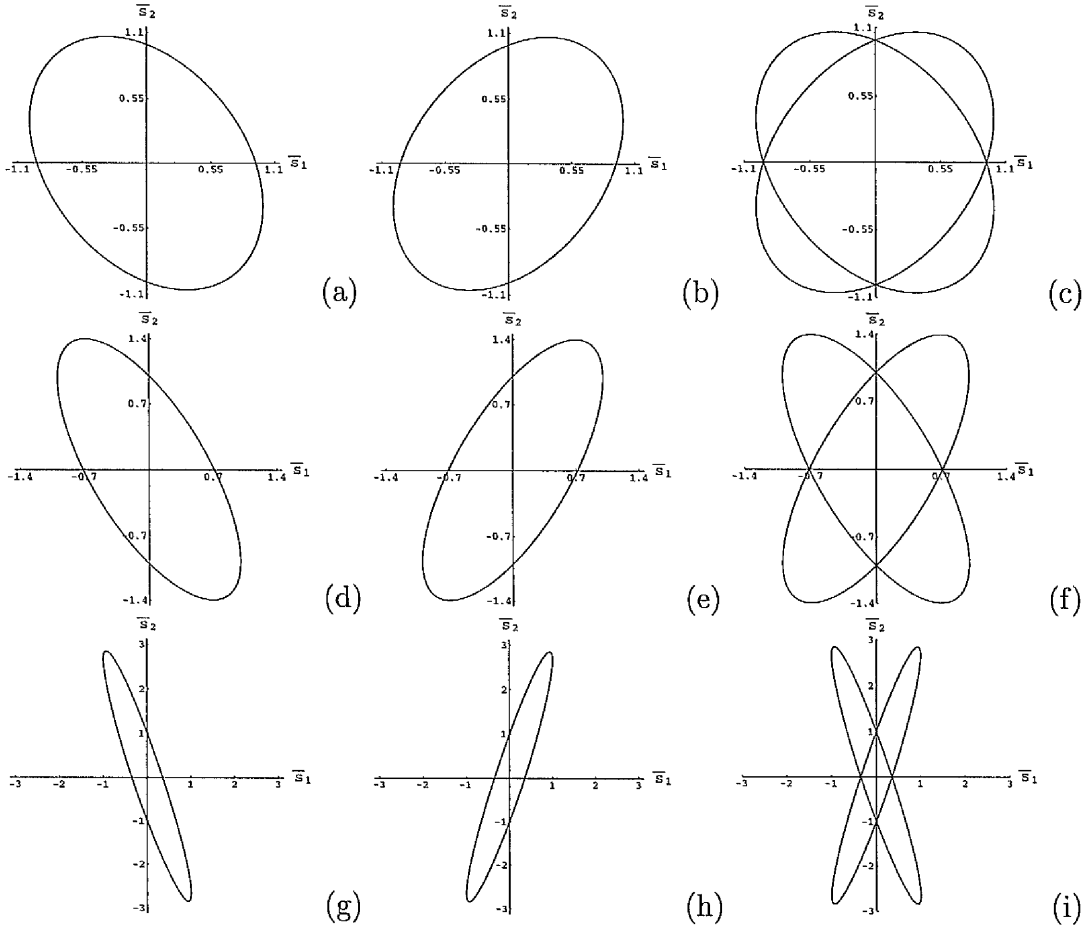

Figure 6.2: Slowness curves in $(\overline{s}_1, \overline{s}_2)$-space for $2\beta = \alpha + \gamma$ with the following values of λ: (a)–(c), 1.2; (d)–(f), 1.6; (g)–(i), 3. The left-hand (centre) column of plots is for $\epsilon > 0$ ($\epsilon < 0$); the right-hand column shows their superposition.

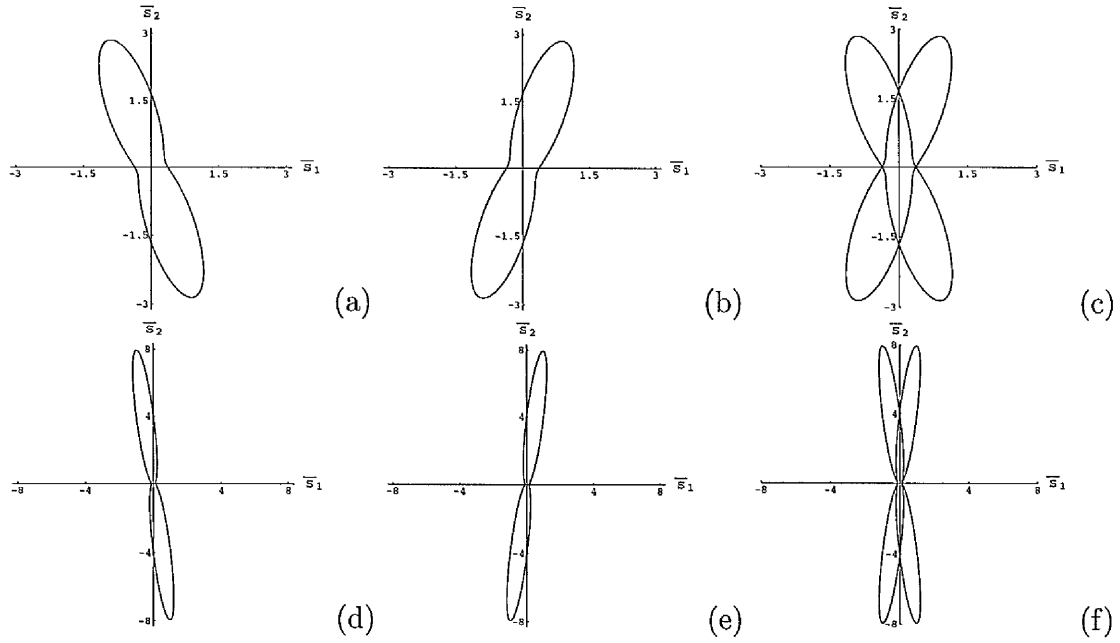

Figure 6.3: Slowness curves in $(\overline{s}_1, \overline{s}_2)$-space for $\beta = \sqrt{\alpha\gamma}$ with $\lambda = 3$ in (a)–(c) and for $\lambda = 8$ in (d)–(f). The left-hand (centre) column of plots is for $\epsilon > 0$ ($\epsilon < 0$); the right-hand column shows their superposition.

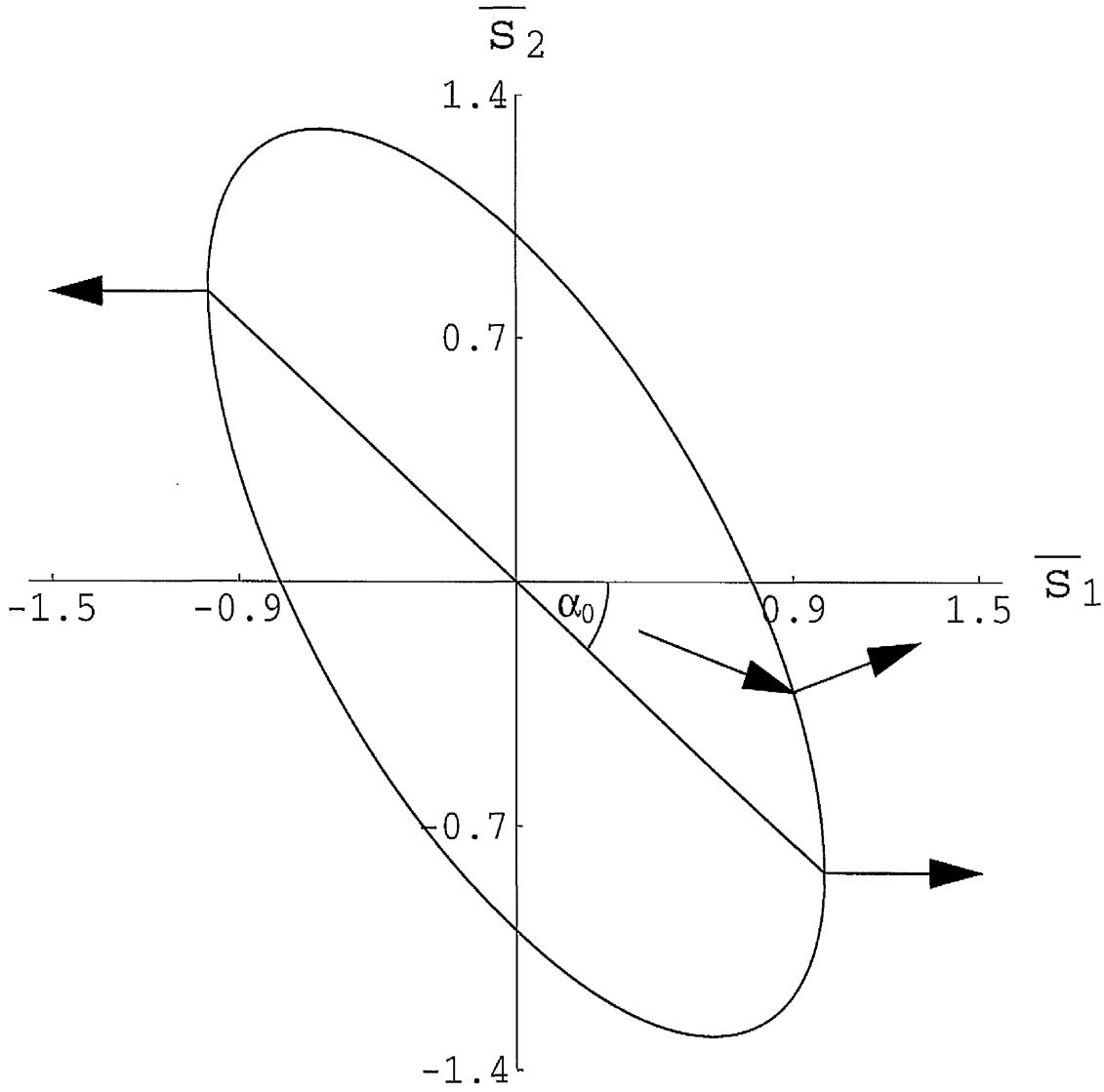

Figure 6.4: Slowness curve in the $(\overline{s}_1, \overline{s}_2)$-plane for $\lambda = 1.5$ $(\epsilon > 0)$ for a material with $2\beta = \alpha + \gamma$. The arrows normal to the curve show the direction of the time-averaged energy flux.

6.4 Reflection and transmission at the interface

We now consider the case in which a half-space defined by $x_2 < 0$ and subject to the simple shear described in Section 2.2 and Section 6.1 is joined to a half-space $x_2 > 0$ with the opposite shear, thereby forming twinned half-spaces.

From (6.9) we can see that for a twin there is a continuity of normal traction σ_{22} across the interface but the shear traction σ_{12} is discontinuous since the direction of shear is reversed at the interface, as shown in Fig. 6.5.

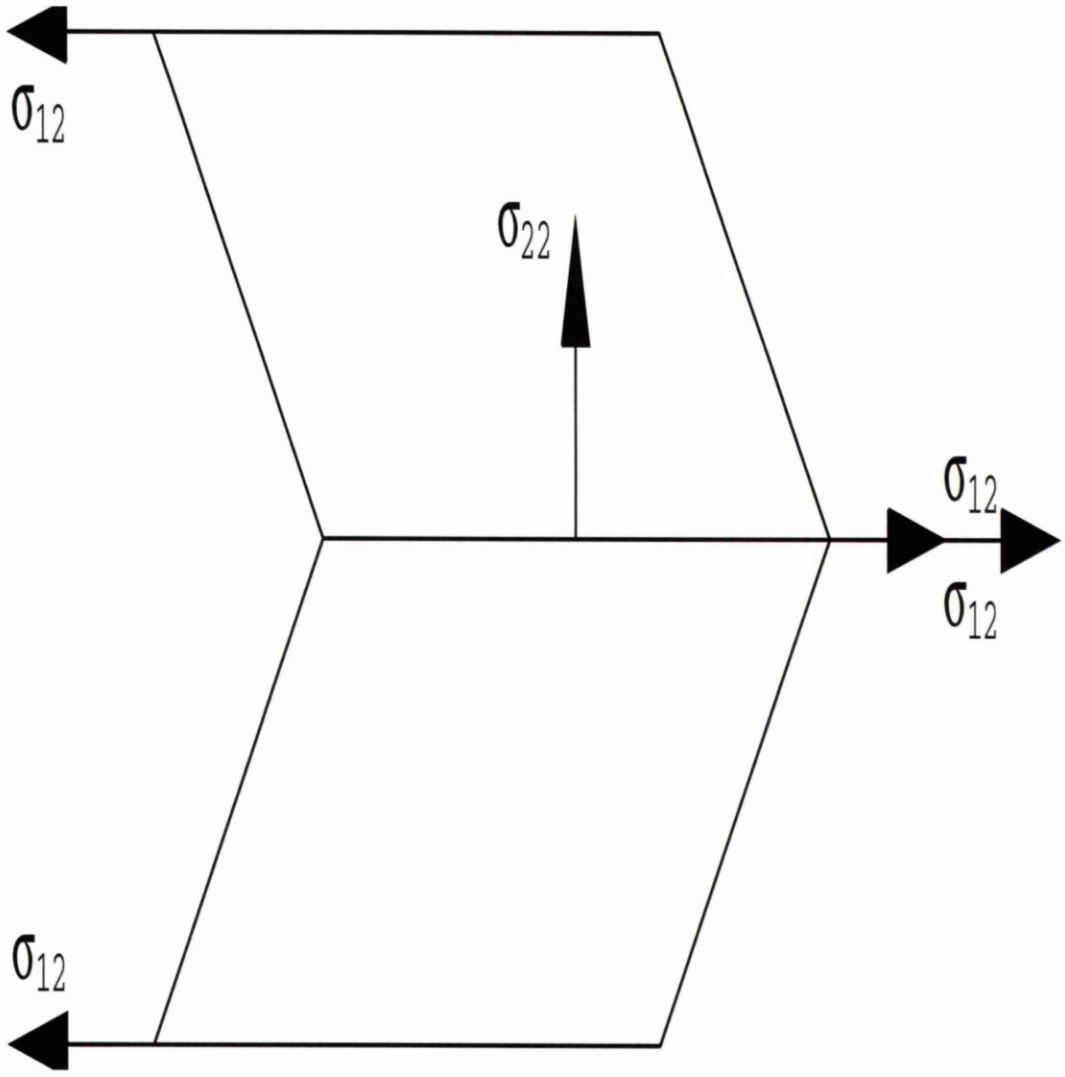

Figure 6.5: The normal (σ_{22}) and shear (σ_{12}) tractions in the twinned half-spaces.

From (5.40) the value of normal stress, σ_{22}, on the boundary $x_2 = 0$ associated with the underlying deformation is given by

$$\sigma_{22} = \gamma\lambda^2 - (\gamma - \sigma_2), \tag{6.24}$$

which is continuous across $x_2 = 0$. So also is $\gamma - \sigma_2$ since from (6.15), (6.16) and (6.8) it is easily seen that

$$\gamma^* - \sigma_2^* = \alpha - \sigma_1 = \gamma - \sigma_2. \tag{6.25}$$

Hence, σ, as defined by (5.38), is continuous.

The boundary conditions corresponding to continuous incremental displacement across the interface $x_2 = 0$ in terms of the scalar functions ψ and ψ^* are given by (4.25).

In terms of ψ, boundary conditions corresponding to continuous incremental traction across the interface $x_2 = 0$ are recast through

$$\Sigma_{21} = \Sigma_{21}^*, \qquad \Sigma_{22,1} = \Sigma_{22,1}^*, \tag{6.26}$$

on use of (6.10), (6.11) and the continuity properties (6.24) and (6.25), in the forms

$$\epsilon\psi_{,12} + \psi_{,22} = -\epsilon\psi_{,12}^* + \psi_{,22}^*, \tag{6.27}$$

$$2\epsilon\psi_{,122} + \psi_{,222} + \epsilon(2\delta + 1)\psi_{,111} = -2\epsilon\psi_{,122}^* + \psi_{,222}^* - \epsilon(2\delta + 1)\psi_{,111}^*, \tag{6.28}$$

in the latter of which the notation

$$\delta = \frac{\alpha + \gamma - 2\beta}{2(\beta + \sqrt{\alpha\gamma})} \tag{6.29}$$

has been used.

Notice that the boundary condition (6.27) is independent of the material parameters α, β, γ, and the stress σ_2, and (6.28) is independent of σ_2 and depends on the material parameters only through δ. Again in general there will be no reflected wave with the same speed as the incident wave as mentioned in Section 5.3 .

We now consider separately the cases in which $2\beta = \alpha + \gamma$ and $\beta = \sqrt{\alpha\gamma}$.

6.4.1 Case A: $2\beta = \alpha + \gamma$

Figure 6.4 shows a typical slowness curve for Case A in $x_2 < 0$. There are two points where the tangent to the curve is vertical. Let α_0 (> 0), as shown in Fig. 6.4, be the angle that a line joining these points to the origin makes with the positive $\overline{s}_1$ axis. This is a *critical angle* as described in Section 5.2. Since, for a wave incident from $x_2 < 0$, the energy flux is directed *towards* the boundary $x_2 = 0$ the angle θ must satisfy the inequality (5.23) (with $\alpha_0 > 0$ for $\lambda > 1$), the extreme values in (5.23) corresponding to grazing incidence. For simple shear the angle α_0 is given by (5.25).

With reference to the slowness curve we see, as discussed in Section 5.3.1, that for an incident wave in $x_2 < 0$ there exists only one reflected wave, coupled, in general, with an interfacial wave.

We therefore write the solution comprising the incident wave, the reflected wave and the interfacial wave in $x_2 < 0$ as

$$\psi = A\exp[ik(x_1\cos\theta + x_2\sin\theta - ct)] + AR\exp[ik_1(x_1\cos\theta_1 - x_2\sin\theta_1 - c_1t)]$$

$$+ AR'\exp[ik_2(x_1 - ix_2 - c_2t)], \tag{6.30}$$

where θ_1 is the angle that the direction of propagation of the reflected wave makes with the horizontal in the fourth quadrant. The interfacial wave corresponds to $m = 1$, which is the relevant solution of (5.15) in this case, as discussed in Section 5.3.1. In (6.30), R is the reflection coefficient, R' is a measure of the amplitude of the interfacial wave in $x_2 < 0$, c_1, c_2 are their speeds and k_1, k_2 their wave numbers respectively.

In order to determine θ_1 we consider a wave propagating in $x_2 < 0$ with dimensionless slowness vector $(s_1', s_2') = (\cos\theta', \sin\theta')/c'\sqrt{\overline{\rho}}$. Then, from (6.18)

$$(\epsilon^2 + 1)s_1'^2 + 2\epsilon s_1' s_2' + s_2'^2 = 1. \tag{6.31}$$

But, by Snell's law, we have $s_1' = \overline{s}_1$ and so, for $s_2' \neq \overline{s}_2$, it follows, by combining (6.18) and (6.31), that $\overline{s}_2 + s_2' = -2\epsilon\overline{s}_1$, and hence

$$\tau + \tau' = -2\epsilon, \tag{6.32}$$

where

$$\tau = \tan\theta, \ \tau' = \tan\theta'. \tag{6.33}$$

For the reflected wave we take $\theta' = -\theta_1$ so that

$$\tau_1 = \tau + 2\epsilon, \quad \tau_1 = \tan\theta_1. \tag{6.34}$$

From (6.18) it can be seen that, for a given value of $\overline{s}_1$, the equation is unaltered by the simultaneous changes $\epsilon \to -\epsilon$, $\overline{s}_2 \to -\overline{s}_2$. This implies that *the angle of transmission for a wave transmitted into $x_2 > 0$ is equal to the angle of reflection of the wave reflected into $x_2 < 0$*. Accordingly, in $x_2 > 0$, the wave

solution may be written

$$\psi^* = AR^* \exp[ik_1(x_1 \cos\theta_1 + x_2 \sin\theta_1 - c_1 t)] + AR^{*'} \exp[ik_2(x_1 + ix_2 - c_2 t)], \tag{6.35}$$

comprising a transmitted and an interfacial wave. The interfacial wave corresponds to $m = -1$ which again is the relevant solution of (5.15). In (6.35), R^* is the transmission coefficient, $R^{*'}$ measures the amplitude of the interfacial wave in $x_2 > 0$.

Here Snell's law takes the form

$$k \cos\theta = k_1 \cos\theta_1 = k_2, \tag{6.36}$$

and the wave speeds are connected through

$$c_1 / \cos\theta_1 = c_2 = c / \cos\theta. \tag{6.37}$$

By substituting the values of ψ and ψ^* from (6.30) and (6.35) in the boundary conditions (4.25) we obtain

$$(R + R^*)\tau_1 + i(R' + R^{*'}) = \tau, \tag{6.38}$$

$$R - R^* + R' - R^{*'} = -1. \tag{6.39}$$

Similarly, from (6.27) and (6.28) with $\delta = 0$ (which follows from (6.29)) we have

$$(R - R^*)(\epsilon - \tau_1)\tau_1 + (R' - R^{*'})(1 + i\epsilon) = \tau(\epsilon + \tau), \tag{6.40}$$

$$i(R + R^*)\{\tau_1^3 - \epsilon(2\tau_1^2 + 1)\} + (R' + R^{*'})(1 + i\epsilon) = i\{\tau^3 + \epsilon(1 + 2\tau^2)\}. \tag{6.41}$$

Equations (6.38)–(6.41) are solved to give

$$R = -i\epsilon^2(\tau + i)/\triangle, \quad R' = -\epsilon(\tau + \epsilon)(\tau\tau_1 + 1)/\triangle,$$

$$R^* = (\tau + \epsilon)(\tau + i)(\tau\tau_1 + 1)/\triangle, \quad R^{*'} = \epsilon(\tau + \epsilon)(\tau + i)(\tau_1 + i)/\triangle, \tag{6.42}$$

where

$$\triangle = (\tau_1 - i)(\tau + \epsilon + i)[\tau\tau_1 + i(\tau + \epsilon)], \tag{6.43}$$

and τ_1 is given by (6.34).

Notice that the solutions in (6.42) are independent of the material parameters.

From (6.42), on use of (6.34), it can be seen that R', R^* and $R^{*'}$ vanish when τ is given by

$$\tau = -\epsilon. \tag{6.44}$$

This corresponds to the special case of grazing incidence. Further, R' and R^* vanish for angles of incidence such that

$$\tau^2 + 2\epsilon\tau + 1 = 0, \tag{6.45}$$

which yields real solutions only for $\epsilon^2 \geq 1$. Since $\tau \to \infty$ as $\theta \to \pi/2$ it follows from (6.42) and (6.43) that $R = R' = R^{*'} = 0$ and $R^* = 1$ in the limit of normal incidence, so that there is total transmission in this case.

Graphical results showing the dependence of $|R|$, $|R'|$, $|R^*|$ and $|R^{*'}|$ on θ for different values of λ are described in Section 6.5.1.

6.4.2 Case B: $\beta = \sqrt{\alpha\gamma}$

With $\beta = \sqrt{\alpha\gamma}$ we shall again use the boundary conditions (6.27) and (6.28)

but now with

$$\delta = \epsilon^2/4, \tag{6.46}$$

obtained from (6.29), in (6.28).

Also, from Section 5.4.2, we know that for $\lambda = 3$ there exists one reflected wave accompanied by an interfacial wave in $x_2 < 0$, so the relevant solutions in $x_2 < 0$ and $x_2 > 0$ are respectively

$$\psi = A\exp[ik(x_1\cos\theta + x_2\sin\theta - ct)] + AR\exp[ik_1(x_1\cos\theta_1 - x_2\sin\theta_1 - c_1t)]$$

$$+ AR'\exp[ik_2(x_1 - im_1x_2 - c_2t)] \tag{6.47}$$

and

$$\psi^* = AR^*\exp[ik_1(x_1\cos\theta_1 + x_2\sin\theta_1 - c_1t)] + AR^{*'}\exp[ik_2(x_1 - im_2x_2 - c_2t)], \tag{6.48}$$

where, as in Case A, the angle of transmission is equal to the angle of reflection (this follows by noting the invariance of (6.22) under the simultaneous transformations $\epsilon \to -\epsilon$, $\overline{s}_2 \to -\overline{s}_2$). Here, m_1 and m_2 are the complex solutions of (6.23) in $x_2 < 0$ and $x_2 > 0$ respectively, and equations (6.36) and (6.37) hold again.

Since $\rho c^{*2}/\lambda^2\gamma$ is the same for each half-space, it follows from (6.23) that if $m = i\tau$ is a solution for $x_2 < 0$ then $-m$ is a solution for $x_2 > 0$ since changing ϵ to $-\epsilon$ and m to $-m$ does not change (6.23). Hence $m_2 = -m_1$.

Substitution of (6.47) and (6.48) in (6.27) leads to

$$\tau_1(\epsilon - \tau_1)(R - R^*) + m_1(m_1 + i\epsilon)(R' - R^{*'}) = \tau(\epsilon + \tau). \tag{6.49}$$

Similarly, by using (6.47), (6.48) and (6.46) in (6.28), we obtain

$$\{\tau_1^2(\tau_1 - 2\epsilon) - \epsilon(\epsilon^2/2 + 1)\}(R + R^*) + \{m_1^2(2\epsilon - im_1) - \epsilon(\epsilon^2/2 + 1)\}(R' + R^{*'})$$

$$= \tau^2(2\epsilon + \tau) + \epsilon(\epsilon^2/2 + 1). \tag{6.50}$$

In this case the second boundary condition in (4.25) takes the form

$$\tau_1(R + R^*) + im_1(R' + R^{*'}) = \tau, \tag{6.51}$$

but the form (6.39) still holds.

For simple shear, by using (6.37) and the expression (5.19) for ρc^2 corresponding to an incident wave in (6.23) with $c^* = c_2$ we obtain a quartic equation for m, which may be expressed in the form

$$(\epsilon^2 + 2 - 2i\epsilon m - 2m^2)^2(1 + \tau^2) = (1 - m^2)(\epsilon^2 + 2 + 2\epsilon\tau + 2\tau^2)^2. \tag{6.52}$$

By removing the factor $m - i\tau$ which corresponds to an incident wave and writing $m = i\tau^*$, we then obtain the following cubic equation for τ^*

$$4(1 + \tau^2)\tau^{*3} + 4(1 + \tau^2)(2\epsilon + \tau)\tau^{*2} + (4\tau^2 - 4\epsilon^3\tau - \epsilon^4 + 4\epsilon^2 + 4)\tau^* + 4\tau^3$$

$$+ 8\epsilon\tau^2 - (\epsilon^4 - 4\,\epsilon^2 - 4)\tau + 4\epsilon(\epsilon^2 + 2) = 0, \tag{6.53}$$

in which the coefficients are real. Equation (6.53) is same as (5.51) for $\tau = t$ and $\tau^* = \tau$ and has either one or three real solutions for τ^*. In the first case we may write $\tau^* = -\tau_1 = -\tan\theta_1$ as that solution, which identifies the reflected wave in $x_2 < 0$ (and the transmitted wave in $x_2 > 0$). One of the two complex solutions yields a value of $m = i\tau^*$ with positive real part associated with an interfacial wave in $x_2 < 0$, m_1 say, while $-m_1$ is associated with an interfacial wave in $x_2 > 0$.

The solutions for R, R', R^* and $R^{*'}$ in equations (6.39) and (6.49)–(6.51) are given by

$$R = (im_1 + \tau)(a + ib)/\triangle, \quad R' = -i(\tau_1 + \tau)(c + id)/\triangle,$$

$$R^* = (m_1 - i\tau)(e + if)/\triangle, \quad R^{*'} = i(\tau_1 + \tau)(g + ih)/\triangle, \tag{6.54}$$

where the coefficients are defined by

$$a = 2\epsilon m_1(2+\epsilon^2) + 2m_1(2\epsilon^2 - m_1^2)(\tau_1 - \tau) - 2\epsilon m_1\tau^2 - 2m_1\tau_1^2(\epsilon+\tau) + 2m_1\tau_1\tau(4\epsilon+\tau),$$

$$b = 2\epsilon^2(2+\epsilon^2) + \epsilon(2+\epsilon^2+6m_1^2)\tau + 2m_1^2(\tau^2+\tau_1^2) - \tau_1\{\epsilon(2+\epsilon^2) + 2m_1^2(3\epsilon+2\tau)\},$$

$$c = \epsilon(2+\epsilon^2)(2\epsilon+\tau) - 2\tau_1^2\tau(3\epsilon+\tau) + 2\tau_1^2(m_1^2+\tau_1\tau) + 2\tau_1\{\epsilon\tau^2 - (m_1^2-2\epsilon^2)\tau - \epsilon(2+\epsilon^2+m_1^2)\},$$

$$d = -m_1\epsilon(2+\epsilon^2) + 2\tau_1^2 m_1(2\tau + 3\epsilon - \tau_1) - 2\tau_1(2\epsilon^2 + 4\epsilon\tau + \tau^2)m_1,$$

$$e = (\tau_1 + \tau)\{\epsilon(2+\epsilon^2-6m_1^2) + 2m_1^2(\tau_1 - \tau)\},$$

$$f = (\tau_1 + \tau)\{\tau_1\tau + \epsilon(\tau_1 - \tau) + 2m_1(m_1^2 - 2\epsilon^2)\},$$

$$g = -2\tau\tau_1\{\tau_1^2 + \epsilon(\tau+2\epsilon)\} + \epsilon(2+\epsilon^2)\tau - 2\tau_1 m_1^2(\epsilon+\tau) + 2\tau_1^2(m_1^2 + 3\epsilon\tau + \tau^2),$$

$$h = -2m_1\tau_1^3 + m_1\epsilon(2+\epsilon^2) - 2\tau_1 m_1\epsilon(2\epsilon+\tau) + 2\tau_1\tau m_1(\epsilon+\tau) + 6\tau_1^2 m_1\epsilon, \tag{6.55}$$

but the definition of $\triangle$ in this case is

$$\triangle = 2(\epsilon - im_1 - \tau_1)(m_1 + i\tau_1)\{2\epsilon + \epsilon^3 - 2m_1^2\tau_1 + 2im_1\tau_1(\tau_1 + 2\epsilon)\}, \tag{6.56}$$

with the notations $\tau = \tan\theta$ and $\tau_1 = \tan\theta_1$. It should be emphasized that m_1 is in general complex.

From equations (6.54)–(6.56) it is clear that the expressions for R, R', R^* and $R^{*'}$ are not as simple as in Case A, but use of [22] to solve

(6.53) for τ_1 and m_1 enables R, R', R^* and $R^{*'}$ to be expressed explicitly in terms of τ and ϵ. The resulting expressions are too cumbersome to be given here, but they are used to obtain graphical results showing the dependence of $|R|$, $|R'|$, $|R^*|$ and $|R^{*'}|$ on θ. Results for $\lambda = 3$ are described in Section 6.5.2. From Section 5.4.2 we know that for this case there is only one real solution of (6.53), so that there are accordingly one reflected, one transmitted and two interfacial waves (one in each half-space).

For $\lambda = 8$, there are six points on the slowness curve at which the tangent is vertical. This was illustrated in Section 5.2 in Fig. 5.4 but it is not clear from Fig. 6.3(d) on the scale used here. A consequence of this is that there are certain ranges of angles of incidence for which two reflected and two transmitted plane waves are generated. The qualitative character of the behaviour of $|R|$, $|R'|$, $|R^*|$ and $|R^{*'}|$ for $\lambda = 8$, however, is very similar to that for $\lambda = 3$ so that detailed discussion is not included here.

6.5 Numerical results

6.5.1 Case A: $2\beta = \alpha + \gamma$

Recalling that θ is subject to (5.23) and that α_0 depends on ϵ, it is convenient to display $|R|$, $|R'|$, $|R^*|$ and $|R^{*'}|$ as functions of θ for the range $0 \leq \theta \leq \pi$

in each case by superimposing the plot for $-\alpha_0 \leq \theta \leq 0$ to the right of that for $0 \leq \theta \leq \pi - \alpha_0$ and noting the continuity at $\theta = \pi - \alpha_0$. All the figures have been produced using [22].

In Figs 6.6–6.9, $|R|$, $|R'|$, $|R^*|$, $|R^{*'}|$ respectively are plotted as functions of θ for a series of values of $\lambda > 1$. (Note that $\lambda = 1$ corresponds to the trivial situation in which the two half-spaces are not distinguished and $R = R' = R^{*'} = 0$, $R^* = 1$.) These show, in particular, that as λ increases the maximum values of the interfacial wave amplitudes $|R'|$ and $|R^{*'}|$ increase but both $|R'|$ and $|R^{*'}|$ become more and more concentrated in a narrow band of angles to the right of normal incidence, as shown in Fig. 6.7 and Fig. 6.9 respectively. A similar effect is evident in Figs 6.6 and 6.8 in respect of the reflected and transmitted waves. As shown in Fig. 6.8 the behaviour of $|R^*|$ is also similar to that of $|R^{*'}|$ and $|R'|$ but $|R^*| \neq 0$ at $\theta = \pi/2$, where $|R|$, $|R'|$ and $|R^{*'}|$ each vanish, as mentioned at the end of Section 6.4.1. The vanishing points of $|R'|$, $|R^*|$ and $|R^{*'}|$ vary with the amount of shear in accordance with (6.44)—specifically, at θ approximately 2.95, 2.79, 2.54, 2.37, 2.06 and 1.93 for $\lambda =$ 1.1, 1.2, 1.4, 1.6, 2.3 and 3 respectively.

Similarly, from (6.45) (which is a quadratic in τ) and Figs 6.7 and 6.8 it can be seen that $|R'|$ and $|R^*|$ also vanish where the quadratic yields real angles, that is for $\epsilon^2 \geq 1$ or

$$\lambda \geq \frac{1+\sqrt{5}}{2} \simeq 1.61.$$

Thus, for $\lambda = 2.3$, $|R'|$ and $|R^*|$ vanish at θ approximately 1.85 and 2.86. Similarly, for $\lambda = 3$, they vanish at θ approximately 1.76 and 2.95.

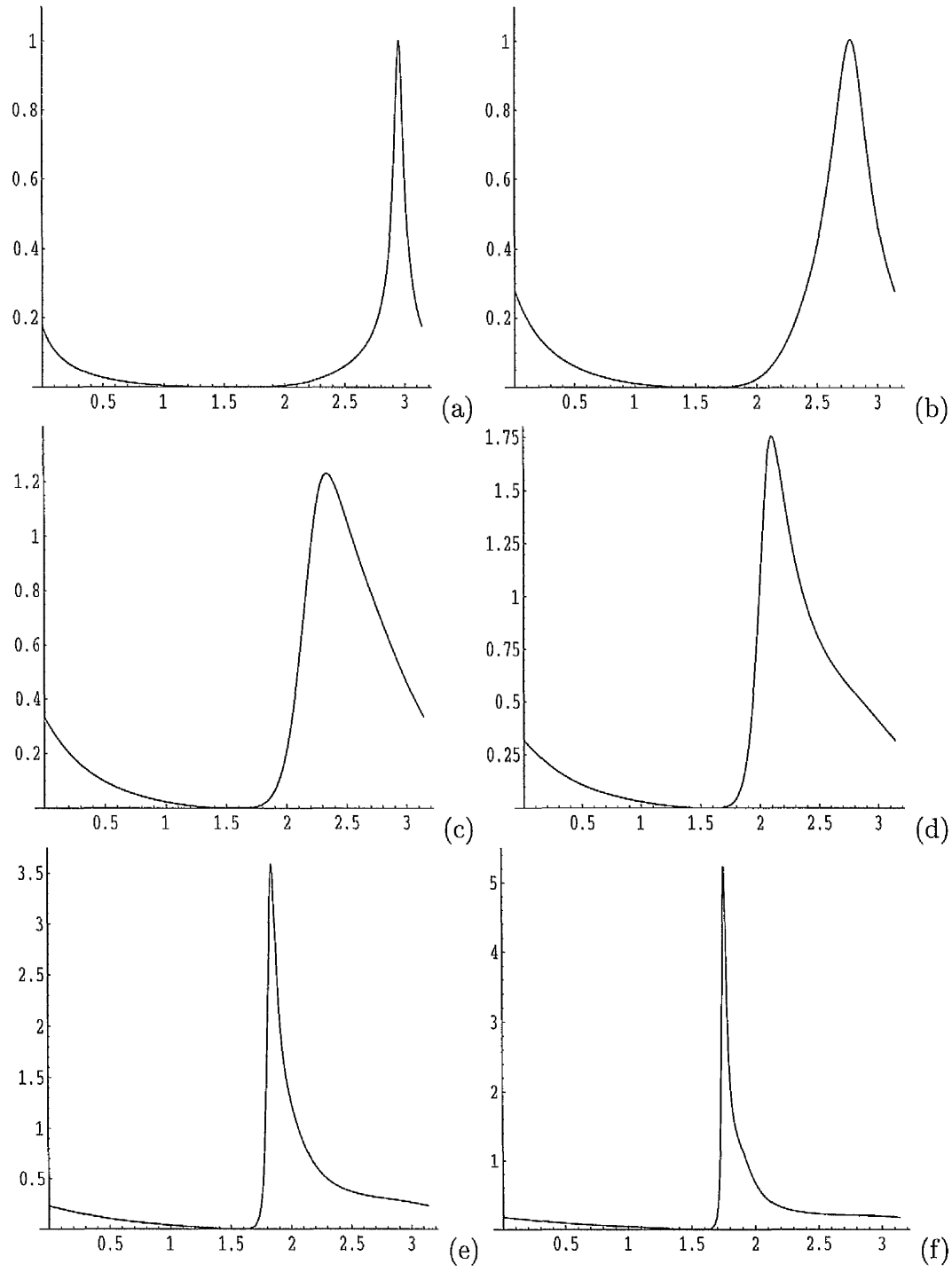

Figure 6.6: Plots of $|R|$ (reflected wave amplitude in $x_2 < 0$) against $\theta\,(0 \leq \theta \leq \pi)$ for $2\beta = \alpha + \gamma$ with the following values of λ: (a) 1.1, (b) 1.2, (c) 1.4, (d) 1.6, (e) 2.3, (f) 3.

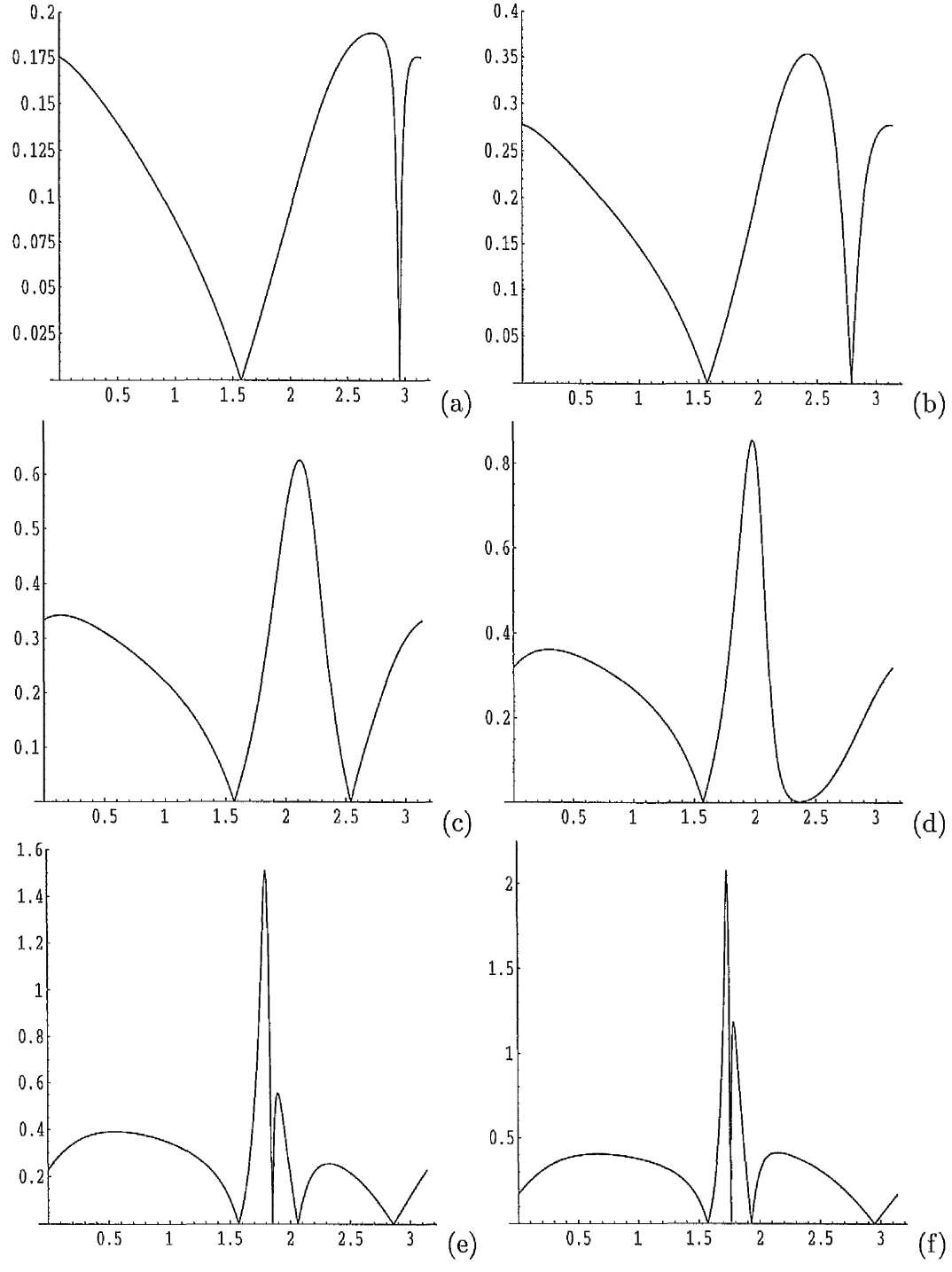

Figure 6.7: Plots of $|R'|$ (interfacial wave amplitude in $x_2 < 0$) against $\theta\,(0 \leq \theta \leq \pi)$ for $2\beta = \alpha + \gamma$ with the following values of λ: (a) 1.1, (b) 1.2, (c) 1.4, (d) 1.6, (e) 2.3, (f) 3.

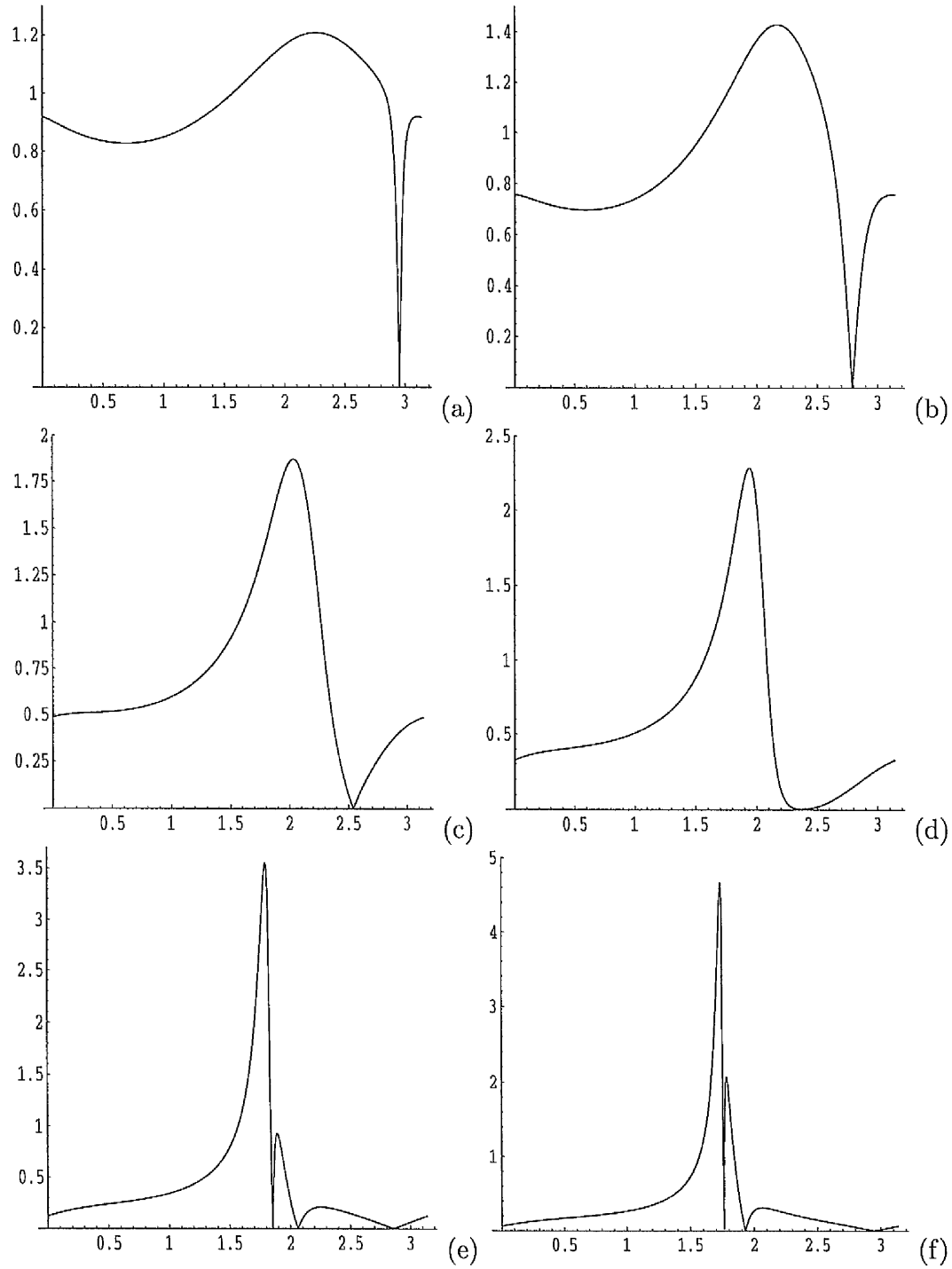

Figure 6.8: Plots of $|R^*|$ (transmitted wave amplitude in $x_2 > 0$) against $\theta\,(0 \leq \theta \leq \pi)$ for $2\beta = \alpha + \gamma$ with the following values of λ: (a) 1.1, (b) 1.2, (c) 1.4, (d) 1.6, (e) 2.3, (f) 3.

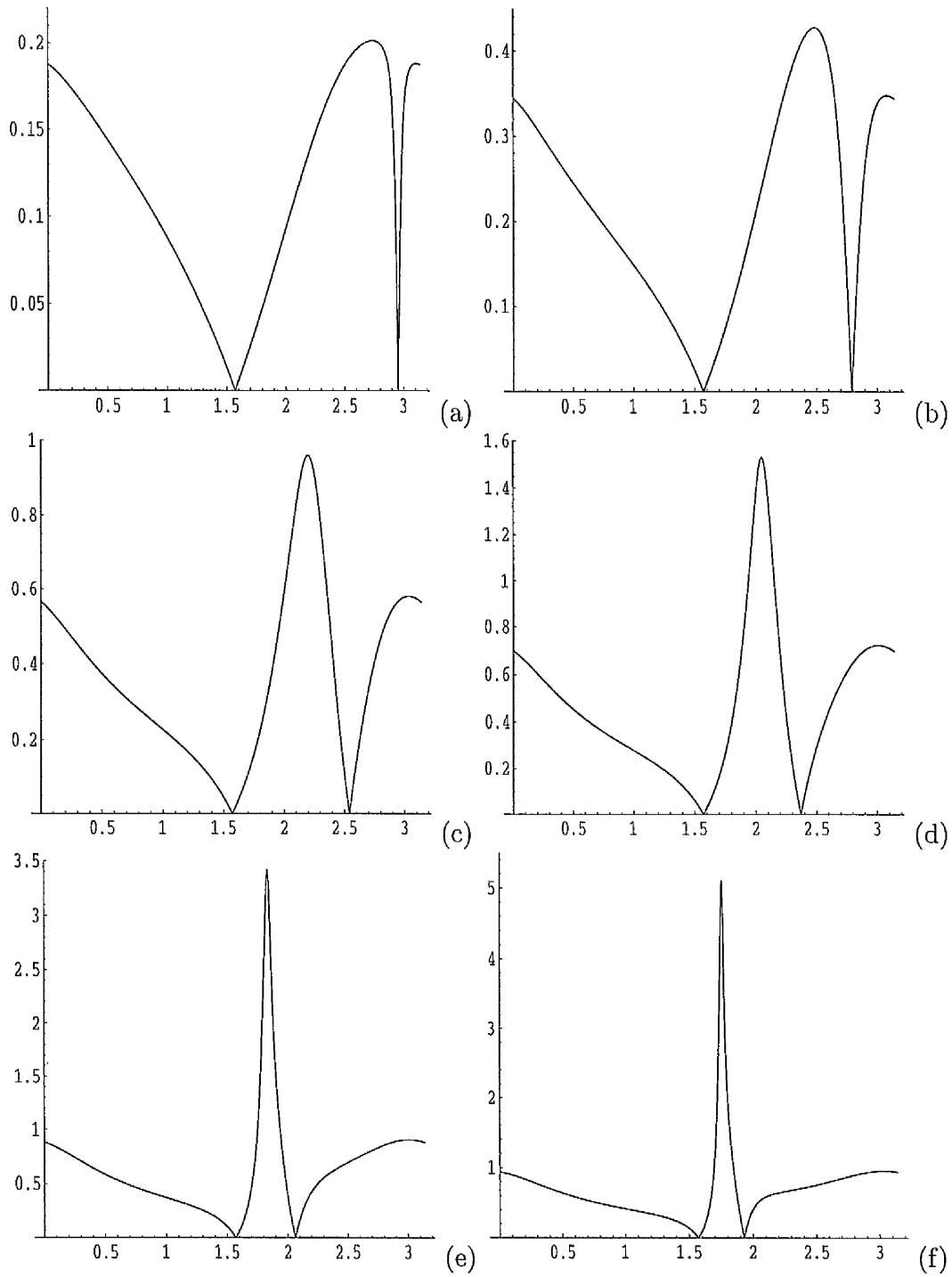

Figure 6.9: Plots of $|R^{*'}|$ (interfacial wave amplitude in $x_2 > 0$) against $\theta\,(0 \leq \theta \leq \pi)$ for $2\beta = \alpha + \gamma$ with the following values of λ: (a) 1.1, (b) 1.2, (c) 1.4, (d) 1.6, (e) 2.3, (f) 3.

6.5.2 Case B: $\beta = \sqrt{\alpha\gamma}$

Here, we illustrate the results for $\lambda = 3$. The slowness curve has the form shown in Fig. 6.3(a) and there is again one reflected wave, one transmitted wave and two interfacial waves for each possible angle of incidence. As in Case A, there is a single angle, α_0, where the time-averaged energy flux is parallel to the positive $\overline{s}_1$ direction.

The results for $|R|$, $|R'|$, $|R^*|$ and $|R^{*'}|$ are displayed against θ for $0 \leq \theta \leq \pi$, on the same basis as for Case A, in Fig. 6.10(a)–(d).

The plot of $|R|$ in Fig. 6.10(a) is quite similar in shape and amplitude to the one in Fig. 6.6(f) for $\lambda = 3$ and the amplitudes of each vanish at $\theta = \pi/2$.

The plots of $|R'|$ and $|R^*|$ shown in Fig. 6.10(b) and (c) have some features in common with Fig. 6.7(f) and Fig. 6.8(f) respectively, which are also for $\lambda = 3$, but also reveal some differences. The maximum amplitudes are larger and there is only a single spike compared with the double spikes in Fig. 6.7(f) and Fig. 6.8(f). The magnitude $|R'|$ vanishes at $\theta = \pi/2$ and at one other value of θ (compared with three other values in Fig. 6.7(f)). Similarly for $|R^*|$ except that it does not vanish at $\theta = \pi/2$ in either case.

Finally Fig. 6.10(d) shows the plot of $|R^{*'}|$ against θ. It is very similar to that in Fig. 6.9(f) for $\lambda = 3$ in both shape and amplitude.

The above results show the general character of the effect of simple shear on the reflection and transmission of plane waves at the boundary of twinned half-spaces. For $\lambda = 3$ the results for the two constitutive laws considered are broadly similar but with some differences in detail. For $\beta = \sqrt{\alpha\gamma}$ the results for $\lambda = 8$

are similar qualitatively to those for $\lambda = 3$, although in general the maximum amplitudes increase with λ and the number of vanishing points of the amplitudes also increases. Moreover, as mentioned at the end of Section 6.4.2, the interfacial wave in $x_2 < 0\,(x_2 > 0)$ converts to a reflected (transmitted) wave for certain ranges of angles of incidence.

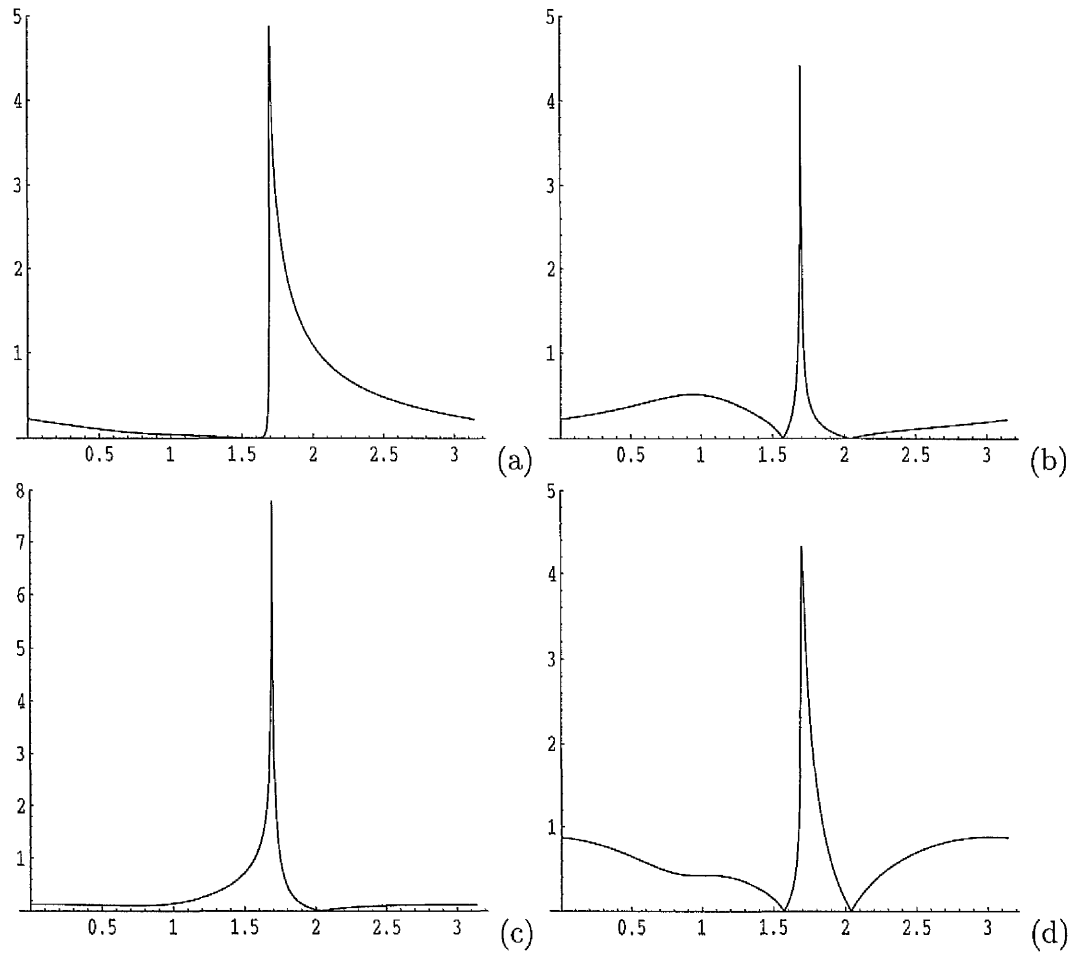

Figure 6.10: Plots of (a) $|R|$ (reflected wave amplitude in $x_2 < 0$), (b) $|R'|$ (interfacial wave amplitude in $x_2 < 0$), (c) $|R^*|$ (transmitted wave amplitude in $x_2 > 0$), (d) $|R^{*'}|$ (interfacial wave amplitude in $x_2 > 0$) against θ $(0 \leq \theta \leq \pi)$ for $\beta = \sqrt{\alpha\gamma}$ with $\lambda = 3$.

Bibliography

[1] BIOT, M. A. 1965 *Mechanics of Incremental Deformations.* New York: Wiley.

[2] BOULANGER, P. and HAYES, M. 1997 Wave propagation in sheared rubber. *Acta Mechanica* **122**, 75-87.

[3] CHADWICK, P. 1995 Interfacial waves in pre-strained isotropic elastic media. *Z. angew. Math. Phys.* **46**, S51-S71.

[4] CHADWICK, P. and JARVIS, D. A. 1979 Surface waves in a pre-stressed elastic body. *Proc. R. Soc. Lond.* A **366**, 517-536.

[5] CONNOR, P. and OGDEN, R. W. 1995 The effect of shear on the propagation of elastic surface waves. *Int. J. Engng Sci.* **33**, 973-982.

[6] CONNOR, P. and OGDEN, R. W. 1996 The influence of shear strain and hydrostatic stress on stability and elastic waves in a layer. *Int. J. Engng Sci.* **34**, 375-397.

[7] DOWAIKH, M. A. and OGDEN, R. W. 1990 On surface waves and deformations in a pre-stressed incompressible elastic solid. *IMA J. Appl. Math.* **44**, 261-284.

[8] DOWAIKH, M. A. and OGDEN, R. W. 1991 On surface waves and deformations in a compressible elastic half-space. *Stability Appl. Anal. Continuous Media* **1**, 27-45.

[9] HAYES, M. A. and RIVLIN, R. S. 1961 Surface waves in deformed elastic materials. *Arch. Rat. Mech. Anal.* **8**, 358-380.

[10] HUSSAIN, W. and OGDEN, R. W. 1999 On the reflection of plane waves at the boundary of an elastic half-space subject to simple shear. *Int. J. Engng Sci.* **37**, 1549-1576.

[11] HUSSAIN, W. and OGDEN, R. W. Reflection and transmission of plane waves at a shear-twin interface. *Int. J. Engng Sci.* (to appear).

[12] OGDEN, R. W. 1984 *Non-linear Elastic Deformations.* Chichester: Ellis Horwood.

[13] OGDEN, R. W. and CONNOR, P. 1995 On the stability of shear bands. In *Proc. IUTAM Symposium on Anisotropy, Inhomogeneity and Nonlinearity in Solid Mechanics* (ed. D. F. Parker and A. H. England). Dordrecht: Kluwer, 217-222.

[14] OGDEN, R. W. and ROXBURGH, D. G. 1993 The effect of pre-stress on the vibration and stability of elastic plates. *Int. J. Engng Sci.* **31**, 1611-1639.

[15] OGDEN, R. W. and SOTIROPOULOS, D. A. 1995 On interfacial waves in pre- stressed layered incompressible elastic solids. *Proc. R. Soc. Lond.* A **450**, 319-341.

[16] OGDEN, R. W. and SOTIROPOULOS, D. A. 1996 The effect of pre-stress on guided ultrasonic waves between a surface layer and a half-space. *Ultrasonics* **34**, 491-494.

[17] OGDEN, R. W. and SOTIROPOULOS, D. A. 1997 The effect of pre-stress on the propagation and reflection of plane waves in incompressible elastic solids. *IMA J. Appl. Math.* **59**, 95-121.

[18] OGDEN, R. W. and SOTIROPOULOS, D. A. 1998 Reflection of plane waves from the boundary of a pre-stressed compressible elastic half-space. *IMA J. Appl. Math.* **61**, 61-90.

[19] ROGERSON, G. A. and SANDIFORD, K. J. 1996 On small amplitude vibrations of pre-stressed laminates. *Int. J. Engng Sci.* **34**, 853-872.

[20] ROGERSON, G. A. and SANDIFORD, K. J. 1997 Flexural waves in incompressible pre-stressed elastic composites. *Q. Jl Mech. Appl. Math.* **50**, 597-624.

[21] ROXBURGH, D. G. and OGDEN, R. W. 1994 Stability and vibration of pre-stressed compressible elastic plates. *Int. J. Engng Sci.* **32**, 427-454.

[22] WOLFRAM, S. 1996 *Mathematica*, version 3. Wolfram Research Inc., Champaign, Illinois.